Aus dem Institut für Medizinische Psychologie der Medizinischen Fakultät

Institut der Universität München

Vorstand: Prof. Martha Merrow, Ph.D.

Ocular light effects on human autonomous function: the role of intrinsically photosensitive retinal ganglion cell sensitivity and time of day

Dissertation
zum Erwerb des Doktorgrades der Humanbiologie
an der Medizinischen Fakultät der
Ludwig-Maximilians-Universität zu München

vorgelegt von

Johannes Zauner

aus

Eggenfelden

Jahr

2022

Mit Genehmigung der Medizinischen Fakultät
der Universität München

Berichterstatter:	Prof. Dr. Hans Strasburger
Mitberichterstatter:	Prof. Dr. Herbert Plischke
	Prof. Dr. Michael Riedel
	Prof. Dr. Angela Schuh
	Prof. Dr. Ingrid Boekhoff
Dekan:	Prof. Dr. med. Thomas Gudermann
Tag der mündlichen Prüfung:	22.06.2022

Affidavit

Eidesstattliche Versicherung

Zauner, Johannes

Name, Vorname

Ich erkläre hiermit an Eides statt, dass ich die vorliegende Dissertation mit dem Titel:

Ocular light effects on human autonomous function: the role of intrinsically photosensitive retinal ganglion cell sensitivity and time of day

selbständig verfasst, mich außer der angegebenen keiner weiteren Hilfsmittel bedient und alle Erkenntnisse, die aus dem Schrifttum ganz oder annähernd übernommen sind, als solche kenntlich gemacht und nach ihrer Herkunft unter Bezeichnung der Fundstelle einzeln nachgewiesen habe.

Ich erkläre des Weiteren, dass die hier vorgelegte Dissertation nicht in gleicher oder in ähnlicher Form bei einer anderen Stelle zur Erlangung eines akademischen Grades eingereicht wurde.

Kolbermoor, 23.06.2022
Ort, Datum

Johannes Zauner
Unterschrift Doktorandin bzw. Doktorand

Table of contents

List of abbreviations

AIC	Akaike's Information Criterion
∆AIC	change in Akaike's Information Criterion
ANS	autonomous nervous system
BF	Bayes Factor
BMI	body mass index
bpm	beats per minute
CCT	correlated color temperature
cd	candela
CI	confidence interval
CIE	Commission Internationale de l'Eclairage (International Commission on illumination)
CIE S	CIE standard
CP	chromatic pupillometry
CSV	Comma-separated values
df	degrees of freedom
D65	standard daylight illuminant with a CCT of 6500 Kelvin
DAP	dark adaptation period
DLMO	dim light melatonin onset
D-MEQ	Morningness-Eveningness Questionnaire (German translation)
E	irradiance / weighted irradiance
ECG	electrocardiogram
EMS	electromechanical systole
∆EMS	change in electromechanical systole
eq	equation
FOV	field of view
GAM	generalized additive model
GAMM	generalized additive mixed model
H	relative humidity
HGAM	hierarchical generalized additive model (see GAMM)
HR	heart rate
∆HR	change in heart rate
ICG	impedance cardiogram
ipRGC	intrinsically photosensitive retinal ganglion cells
K	Kelvin

KSS	Karolinska-Sleepiness Scale
L	luminance
L+M-cone	long (red) and mid-wavelength (green) cones
Lvet	left ventricular cardiac ejection time
∆Lvet	change in left ventricular ejection time
M	group average
MEDI	melanopic equivalent of daylight (D65) illuminance
mel	melanopic
MEQ	Morningness-Eveningness Questionnaire
n	sample size
NIF	non image forming
nm	nanometer
nPC	normalized pupillary constriction
PEBL	The Psychology Experiment Building Language
PEP	left ventricular cardiac pre-ejection time
∆PEP	change in left ventricular cardiac pre-ejection time
PIPR	post-illumination pupil reflex
PLR	pupillary light reflex
ppm	parts per million
RTLX	raw Task Load Index
SCN	suprachiasmatic nucleus
SD	standard deviation
SE	standard error
SEM	standard error of the mean
T	temperature
TLX	Task Load Index
TPS	thin plate regression spline
v	visual
VC	visual cortex
VR	virtual reality
Z	impedance

List of publications

In publication date order:

1. *Plischke H, Linek M,* ***Zauner J*** *(2018) The opportunities of biodynamic lighting in homes for the elderly. Current Directions in Biomedical Engineering. 4(1):123-6. doi: 10.1515/cdbme-2018-0031*
2. ***Zauner J****, Plischke H, Stijnen H, Schwarz UT, Strasburger H (2020) Influence of common lighting conditions and time-of-day on the effort- related cardiac response. PLoS ONE 15(10): e0239553. doi: 10.1371/journal. pone.0239553*
3. ***Zauner J****, Plischke H (2021) Designing Light for Night Shift Workers: Application of Nonvisual Lighting Design Principles in an Industrial Production Line. Applied Sciences. 2021;11(22). doi: 10.3390/app112210896*
4. ***Zauner J****, Plischke H, Strasburger H (2021) Spectral dependency of the human pupillary light reflex. Influences of pre-adaptation and chronotype. PLoS ONE, accepted November 2nd, 2021. doi: 10.1371/journal.pone.0253030*

The publications 2 and 4 are the main papers of this dissertation. The role of the other publications in the context of this dissertation is discussed below in the *Introduction* section. Publication 4 was accepted at the print date of this dissertation, but not yet publicly available.

Contributions to the publications

1.1 Contribution to Paper I

The first paper was a collaborative effort of five authors where I was first author, and Herbert Plischke, Hanna Stijnen, Ulrich Schwarz, and Hans Strasburger were co-authors. Hanna Stijnen was the experimenter performing data collection as part of her bachelor thesis, which I supervised. Ulrich Schwarz, together with Hanna Stijnen, developed the *Mathematica Notebook* tool to calculate the relevant parameters from the impedance cardiogram and the electrocardiogram. These parameters were heart rate, pre-ejection period, and left-ventricular ejection time. Herbert Plischke and Hans Strasburger were joint senior supervisors. Herbert Plischke had the initial idea and further helped with resources. Hans Strasburger contributed to the validation of the results. All authors read, reviewed, and edited the manuscript. I did the conceptualization of the study, as well as the lighting design, and took care of the project funding and administration. For the lighting design, I developed the nonvisual light-simulation process described in section 2.2.2 of this dissertation. I further handled data curation, the formal statistical analysis, visualization, and worked with Hanna Stijnen and Ulrich Schwarz on the methodology of the data analysis. Finally, I wrote the original draft and contributed to review and editing. We had some help from outside the group of authors. Timo Müller contributed with input on the lighting and control system and installed all components. The lighting components were funded by the Lumitech Lighting Solution GmbH, Austria, which also provided funding for disposable materials and participant compensation. The Open Access Publication Fund of the Munich University of Applied Sciences provided financial support for the publication.

1.2 Contribution to Paper II

The second paper was a collaborative effort of three authors where again I was first author, and Herbert Plischke and Hans Strasburger were co-authors. Herbert Plischke and Hans Strasburger were joint senior supervisors. Herbert Plischke had the initial idea and further helped with resources. Hans Strasburger contributed to the validation of the results. All authors read, reviewed, and edited the manuscript. I did the conceptualization of the study and took care of project administration. I further performed all measurements and data collection not otherwise attributed below. I handled data curation, methodology and data preparation, formal statistical analysis, and visualization. Finally, I wrote the original manuscript and contributed to review and editing. We had some help from outside the group of authors. All following theses were supervised by me. Timo Weinert considerably enhanced the light dome with a monochromator, shutter, and automation capabilities as part of his bachelor thesis. Jorge Alberto Gutiérrez Alvarez improved the automation and software-calibrated the monochromator. He also collected 50% of preliminary data and programmed the first of nine experimental protocols as part of his bachelor thesis. Theresa Scherzer collected the data from about 90% of participants in

the first experimental protocol as part of her bachelor thesis. Daniel Philipp Setzensack collected 50% of the preliminary data and about 80% of the data in the second experimental protocol. He also developed the pixel-to-millimetre-conversion method used in the third to ninth protocol. He further programmed the third, fourth, and fifth experimental protocol, where he collected the data from all participants. He did his work as part of his master thesis. Regina Heiß collected the data from all participants in the sixth to the ninth experimental protocol as part of her bachelor thesis. Moritz Faust supported Daniel Setzensack and Regina Heiß with data collection and measurements, and digitalized the paper questionnaires. The Open Access Publication Fund of the Munich University of Applied Sciences provided financial support for the publication.

2. Introduction

2.1 Light and health

2.1.1 Light is more than a means for vision

When we think of light we think of vision. Light lets us perceive our environment. This far exceeds a mere visual representation of our world. Neural processing of visual sensations influences us on a psychological and physiological level. Stated more broadly, from the light reaching our eyes, we extract *what* our environment contains, *where* the things before us are in relation to one another and to us, and *how* we should feel about and react to them (for an accessible overview see Wolfe et al. (1)). As we have learned in the past decades, humans not only gather light information for the central nervous system, but also extract temporal information from the light reaching the eyes and feed it directly into the autonomous nervous system (ANS): *when* it is. Why should we require this, when visual information about temporal states such as day and night is readily available to our conscious mind?

In short, the necessity for *when* predates many higher-level cognitive functions and affects the very building blocks of all living beings. As Roenneberg and Foster (2) argue, there is a strong evolutionary pressure towards adaptation to the specific niche an organism inhabits. This is not limited to a geographical or ecological niche, but also includes the cycle of day and night, as that brings stark changes to the environmental conditions. There are survival benefits to being active at certain times, e.g., dawn or dusk, either to catch prey or to avoid being caught. These times of maximum performance necessitate times of rest at other phases of the nychthemeral cycle. Therefore, organisms with good predictive capabilities about the daily cycle are at an evolutionary advantage. Good prediction allows them to anticipate environmental changes and prepare internally, instead of just reacting to such changes. [2, 3]

2.1.2 Connection between light and the autonomous nervous system

Good temporal prediction requires an internal mechanism for keeping time, and an external signal for adjustment of the mechanism. It has long been known that, for humans as for many other species, (day)light is the main *Zeitgeber*, or external signal [3-6]. The daylight signal is extremely reliable in its period; the difference in illumination between day and night is considerable (between less than 1 lux at night to 10^5 lux during the day); the signal is further very characteristic (daylight is strongest in the upper range of vision, with a blue-enriched light spectrum); and the signal is in phase with environmental changes, not least because variations in solar irradiation cause most of these changes [7].

The internal mechanism (see *Figure 2-1*) is a cascade of internal clocks. Each cell has an internal clock which emerges from transcriptional-translational feedback loops [8]. All

clocks are synchronized by a master clock, located in the suprachiasmatic nucleus (SCN) in the ventral hypothalamus of humans [9]. The master clock communicates with the cell clocks through neural pathways, hormones, and temperature changes, targeting individual organs [10]. While the master clock has its own, endogenous rhythm, with a period of about – but not quite – 24 hours, it needs the photic input to synchronize to the external time [11]. Other inputs to change the internal time include social cues, activity, and food consumption [8]. The photic synchronization is realized through the retinohypothalamic pathway and, ultimately, a specialized group of photoreceptors in the retina. These are called *intrinsically photosensitive retinal ganglion cells*, ipRGCs in short, which are especially sensitive to light that exhibits daylight properties [11, 12]. IpRGCs form a retina-spanning network that is intrinsically photosensitive through its photopigment melanopsin. This nonvisual system is most sensitive to wavelengths of light at and around 480 nm (or 490 nm for a 32-year old standard observer) [13].

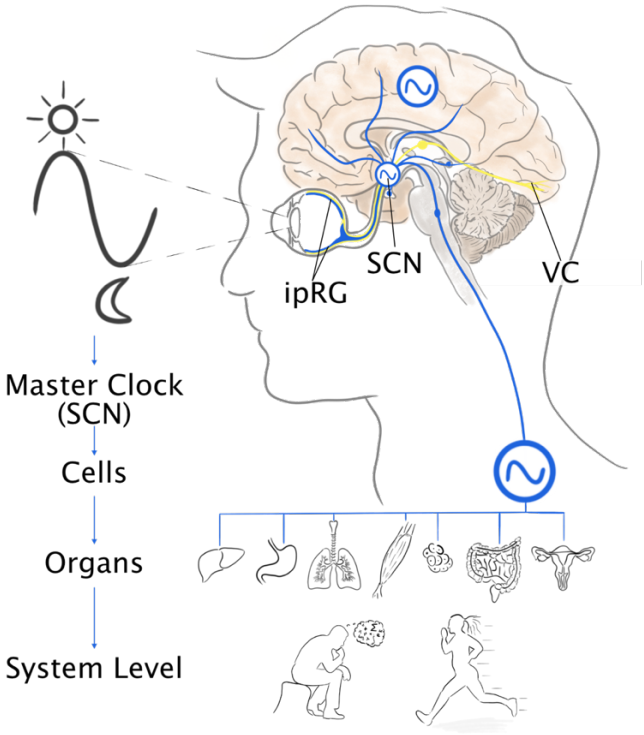

Figure 2-1. External and internal rhythms. External time cues are integrated into the internal master clock. The most potent cue or, more precisely, *Zeitgeber* is light. Visual information (yellow) from rods and cones is guided through the thalamus to the visual cortex (VC). Dedicated photoreceptors in the retina, the ipRGCs, transport photic information to the internal master clock in the hypothalamic suprachiasmatic nucleus (SCN). The SCN adapts its oscillations according to the photic information. Through neuronal, hormonal, and temperature pathways, the rhythm is spread throughout the brain and body into every cell. This does not lead to a singular rhythm but rather to a multitude of rhythms depending on the tissue and the organ. The time-varying interconnections of these internal rhythms produce rhythms on the system level, e.g., as circadian changes in cognitive or physical performance, mood, or vigilance.

2.1.3 Relevance of the connection

Since the discovery of these melanopsin-containing cells early in the new millennium [11, 12], a wide range of effects has been linked to ipRGC stimulation. These nonvisual effects of light include the suppression of melatonin at night [14, 15], circadian phase shift [16], change of acute alertness and performance [17-20], mood [21, 22], sleep quality [23], and pupil constriction [24]. Under natural conditions, the effects occur at the right time, since the stimulus is generated by daylight. However, humans today often live in conditions that are partially decoupled from a day-and-night rhythm.

For most of human history, the circadian system had to almost exclusively deal with daylight, apart from the comparatively weak moon- and starlight, or red-enriched firelight [2, 7]. This changed drastically with the advent of widespread artificial lighting systems in living- and workplaces about four generations ago, i.e., very recently from an evolutionary viewpoint [25]. Today's society of "interior dwellers" has minimized the personal dynamic range of light, with an overwhelming portion of daytime spent in spaces commonly having less than 1% of daylight intensity [7, 26], and freely available artificial light at night. The consequences are a weakened circadian system with negative effects on performance, mood, resilience, and metabolic and immune function (for a review see Foster (27)). In extreme cases, internal clocks are severely disconnected from the *Zeitgeber*, called *Chronodisruption* [28]. This, in turn, is connected to neural pathologies, metabolic and cardiovascular diseases, and cancer [29, 30]. *Chronodisruption* is best studied in the context of light at night, especially for shift workers, where the long-term effects due to light have to be weighed against the short-term benefits of good visual performance and increased alertness [31].

2.2 Investigating melanopic effects on the ANS

An impressive amount of research in the past twenty years has focused on ipRGC sensitivity and their dose-response relationships (for a review see Brown (32)). Since melanopsin is the photopigment responsible for ipRGC photosensitivity, the term *melanopic* has been coined to describe all nonvisual effects connected to the ipRGCs [13]. However, ipRGCs also integrate external input from cones and rods [33]. This means that the necessary stimuli for nonvisual effects of light can, and do, deviate from the single-opsin sensitivity [34, 35]. The deviations depend on the effect under investigation and the circumstances, like stimulus duration for melatonin suppression [34], or twilight conditions for phase shift [36].

The extrinsic photoreceptor- and circadian influences are relevant, as lighting products and systems are developed to boost positive, and reduce unintended, nonvisual effects. A prime example is the supposedly non-melatonin-suppressing light spectrum of certain commercially available products, where blue wavelengths at and around the ipRGC sensitivity are substituted by very short wavelengths at around 400 nm. While this is plausible based on the single-opsin sensitivity alone, these products have not been shown to prevent melatonin suppression significantly [35]. Without sound knowledge about how

light influences these ANS-mediated effects there is always the risk of unintended side effects.

One circumstance that has a major mediating effect on the nonvisual system is the circadian timing, or internal time of day. Commonly, there is a difference between external and internal time; the difference is called the *phase of entrainment*. Individual differences in the phase of entrainment are expressed as chronotypes [5]. Chronotype also refers to the time of preference, i.e., whether a person has a preference for the morning, evening, or intermediary time of day [37]. The gold standard to determine the phase of entrainment is through the time of the dim light melatonin onset (DLMO) in the evening through series of melatonin measurements. Dedicated Questionnaires provide easier, faster, and cheaper measures for the phase of entrainment, but are less precise compared to the DLMO [38].

2.2.1 Applicability of previous findings

The argument above necessitates more research focused on reexamining previous findings in the context of common, real-life scenarios, to improve their applicability. This dissertation focuses on two specific autonomous functions influenced by light: the autonomic control of cardiac contraction force through sympathetic stimulation, and the autonomic control of the pupil through sympathetic dilation and parasympathetic contraction. In both cases we investigate how these effects are dependent on ipRGC sensitivity, i.e., on the melanopic stimulus. Time-of-day interactions are important in this context, as the spectral dependency might change over the course of the day. Both studies from the dissertation show that there are influencing factors to the spectral dependency of acute non-visual effects of light that cannot be explained by just the sensitivity of ipRGCs alone. Rather, multiple photoreceptor inputs and interactions with other parameters such as (circadian) time are required to explain the effects.

2.2.2 Cardiac contraction force

Figure 2-2. Impression of the experimental room lighting scenarios. The three pictures show a liberal re-enaction of the cardiac-contraction-force experiment in the study room with the low, middle, and high melanopic intensity setting (left, middle, and right, respectively). In all cases, the illuminance at desk-height, measured horizontally, is identical. Source: Johanna Weber, Munich University of Applied Sciences

The first study by Zauner et al. (39) is about the autonomic control of the cardiac contraction force. A study by Lasauskaite and Cajochen (40) in 2018 showed that the properties of light, more specifically its color temperature, influenced how the cardiac contraction force changed between a cognitive task and a baseline in a time range of a few minutes. The contraction force is modulated only by the sympathetic nervous system, if properly controlled for moderating factors. The authors linked this influence of light to ipRGC-photoreceptors, thereby categorizing it as a non-visual effect of light. However, they used a setup of light application which is uncharacteristic of real-world lighting, as was their stimulus intensity. Coming from this, the main resulting questions were whether (1) this effect was replicable under (2) more reasonable lighting conditions in terms of workplace lighting, whether it (3) depended on the melanopic stimulus size, and whether (4) there was a time-of-day interaction present.

Compared to the second study of the dissertation, this study was focused on the applicability aspect, since we chose the experimental lighting conditions to resemble the situation in a common workplace. To analyze the results from the first study, we relied on linear-mixed effect models [41]. This type of model works well for regression with *repeated measures* data. The method was comparatively novel, but it had been used in the field of lighting research before [42] and is quite common now [43-46].

One major prerequisite of the first study was the installed dynamic lighting in the study room which enabled the various light settings used in the experimental protocol. This dynamic lighting was not available prior to the project described in this dissertation and was designed, implemented, and commissioned for the experiment. While implementation was done by a third party (see above under *Contribution to Paper I*), the author of this dissertation handled the other parts. To this end, a simulation-based nonvisual lighting design process was developed that allows for the specification of lighting components during the design stage to reach a given melanopic stimulus. This process was tested as part of the evaluation of lighting systems in homes for the elderly by Plischke et al. (47). *Figure 2-2* shows the three room lighting scenarios in a liberal re-enaction of the experiment. *Figure 2-3* shows the simulation results for the three scenarios with photometric and melanopic stimulus parameters. The process was finally published in an application-centric paper by Zauner and Plischke (48) along with an in-depth example. Other researchers may profit from the ability to specify lighting components in the experimental design stage instead of having to gather empirical knowledge.

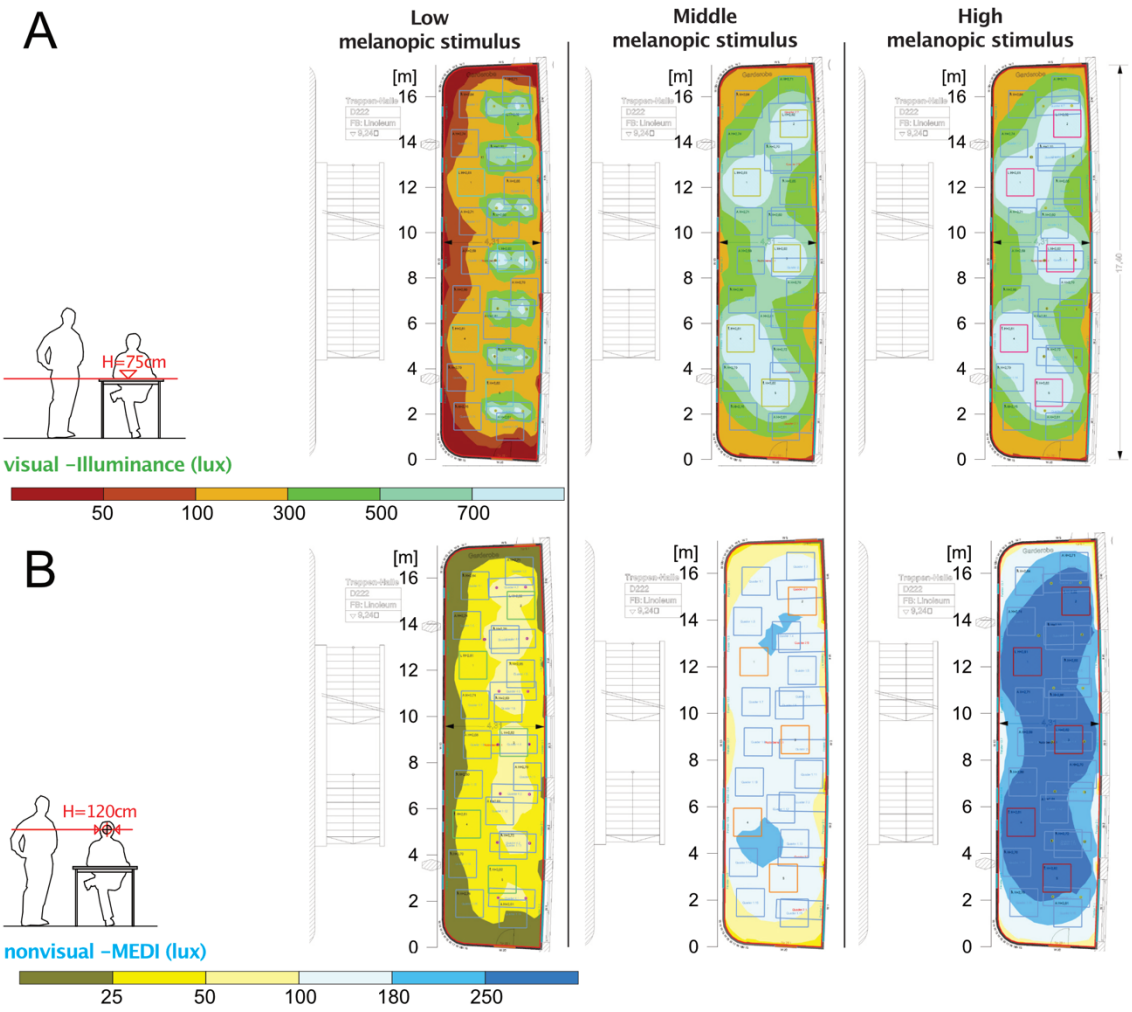

Figure 2-3. Simulation results for the visual and nonvisual parameter. The figure shows false-color floor plans of the study room containing simulation results. The false-color scales are shown on the left, together with a schematic of where, at a given point in the floor plan, the simulation result is taken from (regarding height and direction). The leftmost floor plans show results for the lowest melanopic stimulus intensity, the middle floor plans for the middle setting, and the rightmost floor plans for the highest melanopic stimulus. The nonvisual lighting design process was developed for the study room and published with an in-depth example for an industrial workplace by Zauner and Plischke (48). (A) Illuminance results at desk height (75 cm above floor level). On the desk, all melanopic stimulus levels show the same illuminance of about 500 lux. (B) Melanopic equivalent of daylight (D65) illuminance (MEDI) cylindrically at eye-level in a sitting position (120 cm above floor level). At eye level, the melanopic stimulus (indexed through MEDI) shows a considerable difference between the three experimental settings.

2.2.3 Pupillary dilation and contraction

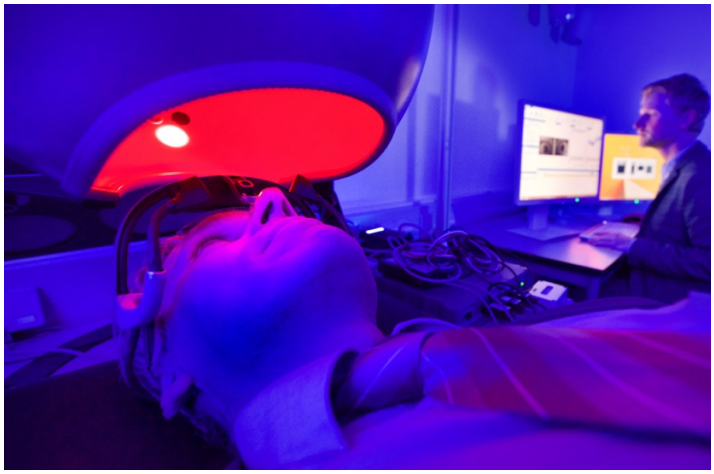

Figure 2-4. Impression of the pupillometry study setting. The picture shows a liberal re-enaction of the experiment in the laboratory for the pupillometry study. Source: Christian Rudnik, Fotodesign

The second study by Zauner et al. (49) is about the autonomic control of the human pupil. Several studies from the past fifteen years have shown ipRGC influence on various aspects of the pupillary light reflex. Specifically, wavelengths at and around peak ipRGC sensitivity inhibit the sympathetic modulation of the pupil in that re-dilation is slowed. Since ipRGCs act sluggishly, this effect is best seen during singularly applied, long-lasting narrowband light stimuli [50], or during the re-dilation phase after light offset [51]. Traditionally, pupil models use L+M-cone derived action spectra, i.e., photometric brightness. This contrasts with the recent findings on ipRGC input, but also with older publications about monochromatic light. The main questions arising from the previous findings where (1) whether spectral ipRGC dependency manifests in a long-lasting light stimulus of changing dominant wavelength, and (2) whether individual traits and circadian aspects such as chronotype and time of day interact with that dependency.

Compared to the first study, the second might seem far removed from any practical application. Indeed, however, these investigations are important in the context of the evaluation of real-life lighting. Chromatic pupillometry (CP) was specifically devised to test the functionality of individual photoreceptor-types, including the ipRGCs, rendering CP a fast, noninvasive diagnostic tool for the health of the nonvisual pathway [52]. There is further potential for application, since the nonvisual pathway not only depends on ipRGC health, but can also be affected by many ocular and neuronal pathologies such as glaucoma [53], age-related macular degeneration [54], diabetes with or without retinopathy [55], Parkinson´s disease [56], or seasonal affective disorder [57] (for a review see Rukmini et al. (58)). Beyond the diagnosis of pathologies, there is an interesting application for CP in real-life situations. Pupillometry has been shown potentially suitable as a marker for the nonvisual effect of ambient light exposure by de Zeeuw et al. (59). This is exciting, as it would provide the means to quickly evaluate the nonvisual effect that lighting has on an individual, instead of deducing the probable effect from the more generic

melanopic stimulus measurement. The applicability is limited, however, by the protocol requirements of having several seconds of darkness between one-second light stimuli. A continuous measurement with extraction of a nonvisual effect would be far more appealing. Basic research was necessary before that, however, to investigate whether continuous light applications would show the same ipRGC-influence on the pupil as singular (pulsed) stimuli do. The second publication of the dissertation provides the results of this investigation, which showed a clear advantage of singular light stimuli for the evaluation of ipRGC effects among a possible circadian effect for continuous stimuli. To analyze the results from the second study, we mostly relied on generalized additive mixed-effect models (GAMMs) [60]. This comparatively novel and very powerful class of models fits nonparametric curve functions (called *smooths*) to predictors, but can fit parametric coefficients as well. The mixed-effect approach models deviations from these smooths for the individual participant [61]. Up until now, GA(M)Ms have been sparingly used in ecology, finance, and linguistics [60-63]. However, GAMMs are ideal for use in the context of pupillometry, where many factors influence the pupillary reaction (with a large interindividual variance [64]). We thus introduced the method to the field as part of the second study. The second paper includes an explanatory section, *Statistical methods* about GAMMs, as part of *Methods and materials*.

One major prerequisite of the second study was the design and installation of a light dome which generated all light stimuli for the pupillometry experiments (*Figure 2-4* and *2-5*). The light dome was not available in its current form prior to the project described in this dissertation. A basic Ganzfeld dome – the same model that Brainard and colleagues used to describe the original action spectrum for melatonin suppression [14] – was enhanced into an automated and programmable apparatus. A total of five undergraduate and postgraduate thesis', supervised by the author of this dissertation, focused on various aspects of the light dome. The most important additions were (1) an integrated housing for the light source and a (hand-controlled) monochromator; (2) a motor-controlled shutter to allow for periods of darkness; (3) a stepper motor to drive the monochromator; (4) a connected *Arduino* computer to automate the shutter and the stepper motor; (5) *Arduino* source files enabling the automated experimental protocols. Importantly, (5) contain calibration functions to adjust for differing speeds when setting the peak wavelength with the monochromator. While the resulting apparatus still has technical limitations, the pupillometry study would not have been possible with the original equipment. Finally, the apparatus is still of use for the next generation of pupillometry projects that use virtual reality (VR) headsets to combine stimulus applicator and eye tracker. While the new gear allows for a greatly increased flexibility in terms of stimulus positioning, the stimulus spectrum is still limited by the RGB displays. The light dome will provide a useful reference for pupil behavior under single narrowband spectra, compared to the additive chromatic spectra of the VR headsets.

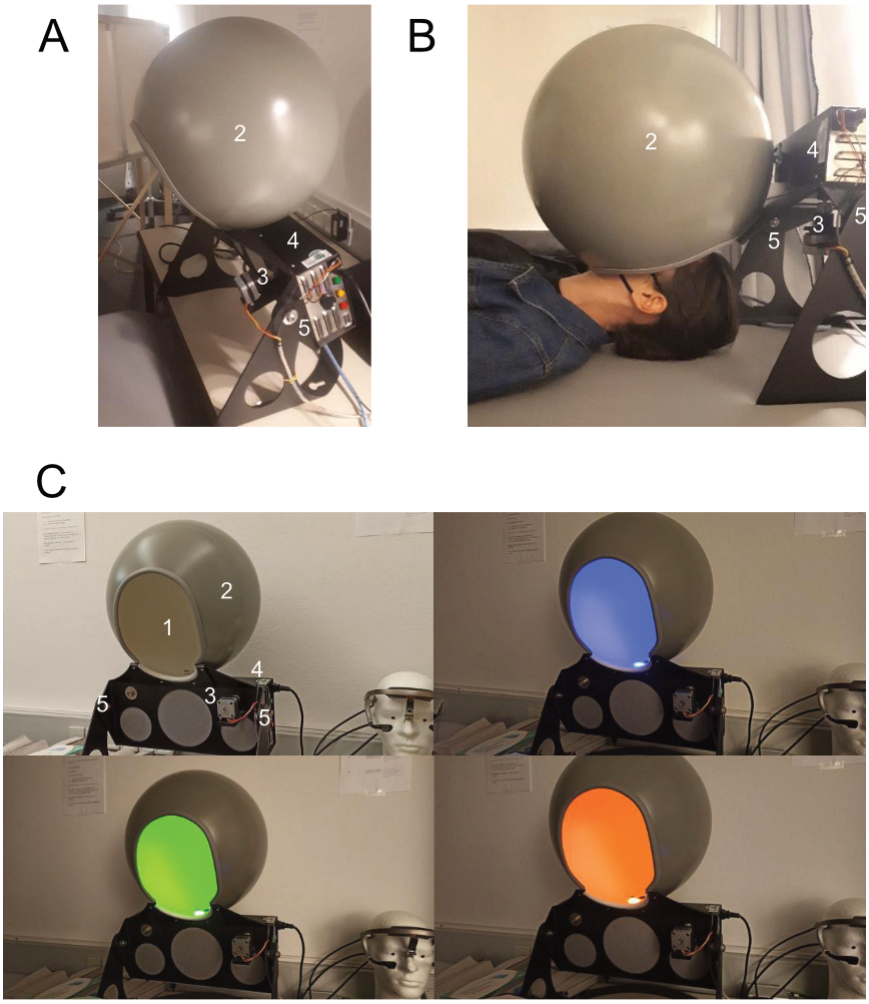

Figure 2-5. Light dome, used for the Ganzfeld stimulation in all pupillometry experiments. 1: *Spectralite* interior surface of the light dome (uniform white with high reflectance); 2: light dome; 3: stepper motor to adjust the peak wavelength of the monochromator; 4: housing for the Xenon light source, the monochromator, and the shutter; 5: pivot point. (A) Side view of the light dome in an upright position. (B) Side view of the light dome when lowered over a participants face. (C) front view of the light dome with different settings: Off (upper left); 450 nm (upper right); 550 nm (lower left); 600 nm (lower right). Sources: (A and B): Regina Heiß; (C): Daniel Setzensack

3. Abstract

Introduction Humans perceive light through the visual sense, but nonvisual effects of ocular light on vigilance, mood, well-being, and several autonomous functions are well known. Autonomic functions influenced by light include the nocturnal secretion of melatonin, setting the phase and amplitude of circadian rhythms, the cardiac contraction force, and the pupillary light reflex (PLR). Nonvisual effects are thought to be mainly governed by a group of short-wavelength-sensitive intrinsically photosensitive retinal ganglion cells (ipRGC). Yet other photoreceptors also contribute with their respective spectral sensitivity. This complicates the generalization of the results. The spectral dependency of the effects can vary depending on the experimental circumstances, especially regarding the time of day, as the roles of contributing receptors vary. The overall aim of this dissertation was to improve the real-life applicability of previous findings in the field of nonvisual light effects through two studies: 1) The PEP study investigated the change in cardiac contraction force through sympathetic activation under common lighting conditions at two different times of day, to explore whether this effect was relevant under normal working conditions. 2) The PLR study investigated the spectral and circadian dependency of the pupillary light reflex under continuous, changing light compared to singularly applied (pulsed) light, to thereby explore whether previous findings about the ipRGC influence would hold up under continuous light. If so, it would be one important steppingstone on the way to a continuously measurable marker of nonvisual effects in a real-life lighting scenario.

Methodology Both studies involved healthy, human participants who came to the experimental room (for the PEP study) or to the laboratory (for the PLR study). The studies were approved by the ethics committee of the Munich University of Applied Sciences, and all participants received written information about the study and gave their informed consent. In the PEP study, participants were exposed to three different lighting conditions, having differing melanopic stimuli but identical brightness at task level, at two times of the day. Lighting conditions in these settings resembled that of a workplace. At each setting, participants performed a challenging cognitive task after a baseline period. Measurements included impedance cardiography (ICG) and electrocardiography (ECG), mainly to calculate the effort-related change in the left ventricular pre-ejection period (ΔPEP) which is an index for the sympathetically induced change in cardiac contraction force. Task performance was measured through the computer program. Individual traits and conditions were derived by questionnaire, such as chronotype, sleepiness, and subjective task load. Data were analyzed with novel linear mixed-effect models.

In the PLR study, participants were exposed to narrowband light in the mesopic range under Ganzfeld conditions. Nine protocols across three experiments contained series of continuous or discontinuous light stimuli after a dark adaptation period. Pupil diameters were measured with an eye tracker, individual traits such as chronotype were derived by questionnaire. Pupil diameters were used to calculate the normalized pupillary constriction (nPC) relative to a dark-adapted protocol-baseline diameter. Most data were analyzed with novel generalized additive mixed-effect models (GAMMs). GAMMs are

nonlinear statistical methods where the relationship between predictors and dependent variable are disentangled into nonparametric, so-called smooth functions, and parametric coefficients. This powerful type of model was introduced to the field of pupillometry as part of this study as it proved a particularly good fit for handling the complex coaction of various predictors on the pupil, such as wavelength, time, sequence, irradiance, time of day, and chronotype.

Results The PEP study showed that there is an effect of light on ΔPEP under common lighting conditions. However, the effect did not depend on the melanopic stimulus alone. The middle lighting condition in terms of the melanopic stimulus led to the highest sympathetic activation and thus higher effort without improving performance measures. The result is an inverted U-shaped relationship between the effect on ΔPEP and the melanopic stimulus predictor. While the session in the late afternoon led to greater effort compared to the morning session, there was no interaction of the time of day with the lighting conditions.

The PLR study showed that short wavelength around the ipRGC maximum sensitivity had comparatively little influence on the nPC when the light stimuli were applied continuously. Instead, the wavelength dependency was conditional on the continuity of light. When the series of light stimuli was interrupted by short intervals of darkness, shorter wavelengths became more important, consistent with past research. The results for continuous light further indicate a circadian modulation of the wavelength dependency. This is consistent with a varying ipRGC influence across the day, dependent on a person's chronotype. Regarding the re-dilation after light offset, ipRGC influence was apparent. Re-dilation was slowest for very short wavelengths below the ipRGC sensitivity under some circumstances, however, indicating the influence of other receptors.

Limitations The PEP study has a chronotype bias, as most participants were neutral or morning types. The time-of-day effect might be different for evening chronotypes. The PLR study is limited mostly by the apparatus, as the light dome only provided mesopic narrowband lighting conditions and results might differ with brighter light. Further, not all wavelengths had the same spectral irradiance, necessitating a mathematical correction as part of the data analysis.

Conclusions In both studies, a spectral ipRGC dependency was not readily present in the main results. In the PEP study, a mediating influence of cone photoreceptors seems likely but cannot be proven with the study data. Importantly, the effect of light on the effort-related cardiac changes is present and relevant for common lighting conditions. As the light setting which resembles classical workplace conditions most closely also led to the highest effort, the other lighting conditions can be seen as an ergonomic improvement. In the PLR study, spectral ipRGC dependency is present in some of the protocols. The results indicate that the singularly applied (pulsed) stimuli are to be preferred when indexing a nonvisual effect. Continuously applied stimuli might still be relevant, however, as the circadian effect of wavelength dependency could be used as a marker for the phase of entrainment (i.e., chronotype) during continuous measurements – provided the effect can be replicated in this context in a future study.

4. Zusammenfassung:

Einführung Neben der visuellen Sinneswahrnehmung von Licht sind nichtvisuelle okulare Effekte von Licht auf Aufmerksamkeit, Stimmung, Wohlbefinden, und verschiedene autonome Funktionen des Menschen gut bekannt. Diese autonomen Funktionen umfassen bspw. die nächtliche Ausschüttung von Melatonin, die Steuerung der Phase und Amplitude des circadianen Rhythmus, die kardiale Kontraktionskraft, und den Pupillenlichtreflex (PLR). Gemeinhin wird angenommen, dass nichtvisuelle Effekte über eine, vor allem in den kurzen Wellenlängen um 480 nm sensitive, Population intrinsisch photosensitiver retinaler Ganglienziellen (ipRGC) vermittelt werden. Doch auch andere Photorezeptoren mit ihrer eigenen spektralen Sensitivität tragen zu diesen Effekten bei. Dieser extrinsische Einfluss auf die ipRGC erschwert die Verallgemeinerung von Ergebnissen. Denn die spektrale Abhängigkeit eines Effekts kann, abhängig von den experimentellen Umständen, von unterschiedlichen Photorezeptoren bestimmt sein, etwa abhängig von der Tageszeit. Das übergeordnete Ziel dieser Dissertation ist die verbesserte Anwendbarkeit vorangegangener Erkenntnisse anhand zweier Studien: 1) In der PEP-Studie wurde die Veränderung der kardialen Kontraktionskraft durch sympathische Aktivierung betrachtet. Unter üblichen Beleuchtungsbedingungen und zu zwei Tageszeiten wurde so untersucht, ob ein messbarer und relevanter Effekt auftritt. 2) In der PLR-Studie wurde die spektrale und circadiane Abhängigkeit des Pupillendurchmessers betrachtet. Im Vergleich von kontinuierlichem Licht mit wechselnder Wellenlänge zu einzeln dargebotenen Stimuli wurde so untersucht, ob bereits bekannte ipRGC-Einflüsse unter kontinuierlichem Licht auftreten. Dies wäre ein wichtiger Meilenstein im Hinblick auf einen kontinuierlich messbaren Marker des nichtvisuellen Effekts in einer realen Beleuchtungsumgebung.

Methodik An beiden Studien nahmen gesunde menschliche Probanden teil, entweder im experimentellen Studienraum (für die PEP-Studie) oder dem Labor (für die PLR Studie). Die Studien wurden von der Ethikkomission der Hochschule München genehmigt. Alle Versuchsteilnehmer wurden schriftlich zur Studie aufgeklärt und gaben anschließend ihre schriftliche Einwilligung zur Teilnahme.

Bei Probanden der PEP-Studie wurden drei unterschiedlichen Beleuchtungsbedingungen zu je zwei Tageszeiten untersucht. Die Beleuchtung unterschied sich im melanopischen (d.h. nichtvisuellen) Stimulus, war aber identisch in Bezug auf die resultierende Beleuchtungsstärke auf der Arbeitsoberfläche. Die Beleuchtungsbedingungen entsprachen jenen einer Büroarbeitsstätte. Probanden bearbeiteten unter jeder Beleuchtungsbedingung eine kognitiv anstrengende Aufgabe nach einer Ruhe-Referenzperiode. Messmethoden umfassten u.a. die Impedanzkardiographie (ICG) und Elektrokardiographie (EKG), primär um die anstrengungsbedingte Veränderung der linksventrikulären Präejektionsperiode (ΔPEP) zu berechnen. Die ΔPEP operationalisiert die sympathische Veränderung der kardialen Kontraktionskraft. Die kognitive Aufgaben wurde durch ein Computerprogramm gestellt, welches auch die Aufgabenleistung erfasste. Weitere Parameter zur Charakterisierung der Person wurden über Fragebögen erhoben, wie etwa

der Chronotyp, Müdigkeit, oder die subjektive Aufgabenschwierigkeit. Die Daten wurden mit neuartigen linearen gemischten Modellen analysiert.

In der PLR-Studie wurden engbandige (chromatische) Lichtreize auf mesopischem Helligkeitsniveau in einer Ganzfeld-Kugel appliziert. Diese Lichtreize folgten auf eine Dunkeladaptionsperiode und waren in Dauer und Abfolge abhängig vom Studienprotokoll. Insgesamt wurden neun Protokolle entwickelt, verteilt auf drei Experimente. Die Pupillendurchmesser der Probanden wurden mit einem Eye-Tracker gemessen. Weitere Merkmale, wie etwa der Chronotyp, wurden mittels Fragebogen erhoben. Aus dem zeitabhängigen Pupillendurchmesser wurde die normalisierte Pupillenkonstriktion (nPC) berechnet, basierend auf einem dunkeladaptierten Referenzdurchmesser. Der Großteil der Daten wurde mit generalisierten additiven gemischten Modellen (GAMM) analysiert. GAMMs zählen zu den nichtlinearen statistischen Modellen. Mittels GAMMs werden die Zusammenhänge zwischen abhängiger und unabhängigen Variablen in nichtparametrische Funktionen und parametrische Koeffizienten aufgelöst. Im Rahmen der PLR-Studie wurde dieser neuartige Modelltyp in die Pupillen-Forschung eingeführt, da er sich hervorragend für die komplexe Verschränkung unterschiedlicher Einflussfaktoren auf die Pupille eignet, wie etwa Wellenlänge, Zeit, Reihenfolge, Bestrahlungsstärke, Tageszeit, und Chronotyp.

Ergebnisse Die PEP-Studie zeigt einen Lichteffekt auf ΔPEP unter üblichen Beleuchtungsbedingungen. Der Effekt kann jedoch nicht auf den melanopischen Stimulus (allein) zurückgeführt werden. Die mittlere Beleuchtungsbedingung im Hinblick auf den melanopischen Stimulus resultiert in der stärksten sympathischen Aktivierung – und damit auch Anstrengung – ohne eine Verbesserung der Aufgabenleistung gegenüber den anderen Lichtbedingungen. Es resultiert ein umgekehrt-U-förmiger Zusammenhang zwischen dem Effekt auf die ΔPEP und der Intensität des melanopischen Stimulus. In Bezug auf die Tageszeit ist der Spätnachmittag gegenüber dem Morgen mit erhöhter Anstrengung verbunden, jedoch ohne eine Interaktion mit den Beleuchtungsbedingungen.

Die PLR-Studie zeigt geringen Einfluss von Wellenlängen im Bereich des ipRGC Sensitivitätsmaximum auf die nPC, wenn die Lichtreize kontinuierlich appliziert werden. Werden die Lichtreize hingegen von kurzen Dunkelintervallen unterbrochen, besitzen Wellenlängen im ipRGC Sensitivitätsbereich höhere Wirkung und entsprechen eher den bisher veröffentlichten Ergebnissen. Weiterhin zeigt sich ein circadianer Mediatoreffekt auf die spektrale Abhängigkeit, insbesondere bei kontinuierlich applizierten Lichtreizen. Dies ist konsistent mit einer Modulation des ipRGC Einflusses auf die Pupille, abhängig von der Tageszeit und dem Chronotyp. Bezüglich der Redilation der Pupille nach einem Lichtreiz zeigt sich ein ipRGC Einfluss. Unter einigen experimentellen Randbedingungen ist die Redilation jedoch von sehr kurzen Wellenlängen unterhalb des ipRGC Maximums bestimmt, was auf einen Einfluss anderer Photorezeptoren hindeutet.

Einschränkungen. Die PEP-Studie weist einen Bias bzgl. der Anzahl der teilnehmenden Probanden eines Chronotyps auf. Die meisten Probanden waren Neutral- oder Morgentypen. Der tageszeitabhängige Effekt könnte sich daher bei Abendtypen anders verhalten als in der Studie gezeigt. Die PLR-Studie ist hauptsächlich durch die Ganzfeld-

Kugel limitiert, deren chromatisches Licht lediglich ein mesopisches Helligkeitsniveau erreicht. Die Ergebnisse könnten für hellere Beleuchtungsbedingungen abweichen. Zudem ist die spektrale Bestrahlungsstärke nicht über alle Wellenlängen hinweg konstant, was jedoch durch eine mathematische Korrektur im Rahmen der Datenanalyse berücksichtigt werden konnte.

Schlussfolgerung. In beiden Studien zeigt sich eine Abhängigkeit von der spektralen ipRGC-Sensitivität nicht direkt aus den Hauptergebnissen. In der PEP-Studie scheint eine Mediation durch Zapfen-Rezeptoren wahrscheinlich, kann aber nicht mit den vorliegenden Daten erwiesen werden. Wichtig ist jedoch, dass es einen Effekt der Beleuchtungssituation auf die anstrengungsbedingte kardiale Kontraktionskraftänderung gibt, die auch unter üblichen Arbeitslichtbedingungen relevant ist. Da die Beleuchtungsbedingung, die einer typischen Arbeitsbeleuchtung am nächsten kommt, auch zur größten Anstrengung bei gleicher Leistung führt, können die anderen Beleuchtungsbedingungen als ergonomische Verbesserung angesehen werden. In der PLR-Studie ist eine ipRGC-Abhängigkeit in manchen Protokollen ersichtlich. Die Ergebnisse deuten darauf hin, dass singulär applizierte Lichtreize in dieser Hinsicht zu bevorzugen sind. Kontinuierlich applizierte Lichtreize bieten aufgrund der circadianen Mediation der Pupille hingegen möglicherweise einen Ansatz zur Durchführung von kontinuierlichen Pupillenmessungen, als Marker für die Chronotypenbestimmung (d.h. *Phase of Entrainment*). Die Voraussetzung dafür ist eine Replikation des Effekts in diesem Kontext in einer zukünftigen Studie.

5. Paper I: light-induced change in the cardiac contraction force

Title:

Influence of common lighting conditions and time-of-day on the effort-related cardiac response

Authors:

Johannes Zauner[1]*, Herbert Plischke[1¶], Hanna Stijnen[2], Ulrich T. Schwarz[2], and Hans Strasburger[3¶]

[1]Munich University of Applied Sciences, Munich, Germany

[2]Institute of Physics, Chemnitz University of Technology, Chemnitz, Germany

[3]Institute of Medical Psychology, Ludwig-Maximilians-Universität, Munich, Germany

¶ HP and HS are Joint Senior Supervisors

The publication in this section was accepted by PLoS ONE on September 9th, 2020, and is also available at https://doi.org/10.1371/journal.pone.0239553

5.1 Abstract

Melanopic stimuli trigger diverse non-image-forming effects. However, evidence of a melanopic contribution to acute effects on alertness and performance is inconclusive, especially under common lighting situations. Effects on cognitive performance are likely mediated by effort-related physiological changes. We assessed the acute effects of lighting in three scenarios, at two times of day, on effort-related changes to cardiac contraction as indexed by the cardiac pre-ejection period (PEP).

In a within-subject design, twenty-seven participants performed a cognitive task thrice during a morning and a late-afternoon session. We set the lighting at 500 lux in all three lighting scenarios, measured horizontally at the desk level, but with 54 lux, 128 lux, or 241 lux melanopic equivalent daylight illuminance at the eye level. Impedance cardiography and electrocardiography measurements were used to calculate PEP, for the baseline and task period. A shorter PEP during the task represents a sympathetic heart activation and therefore increased effort. Data were analysed with linear mixed-effect models.

PEP changes depended on both the light scene and time of day ($p=0.01$ and $p=0.002$, respectively). The highest change (sympathetic activation) occurred for the medium one of the three stimuli (128 lux) during the late-afternoon session. However, effect sizes for the singular effects were small, and only for the combined effect of light and time of day middle-sized. Performance scores or self-reported scores on alertness and task demand did not change with the light scene.

In conclusion, participants reached the same performance most efficiently at both the highest and lowest melanopic setting, and during the morning session. The resulting U-shaped relation between melanopic stimulus intensity and PEP is likely not dependent solely on intrinsic ipRGC stimuli, and might be moderated by extrinsic cone input.

Since lighting situations were modelled according to current integrative lighting strategies and real-life indoor light intensities, the result has implications for artificial lighting in a work environment.

Keywords: CIE integrative lighting, human-centric lighting, effort-related cardiac response, pre-ejection period, PEP, melanopic, non-visual, non-image-forming, ipRGC, cognitive performance.

5.2 Introduction

Understanding the physiological impact that common lighting conditions have on human readiness to perform is paramount when designing artificial lighting. Light falling onto the retina serves multiple functions beyond those of visual perception, adaptation, and accommodation. First and foremost, light is the most potent *Zeitgeber* for the circadian clock. Light can phase-shift, stabilize, or destabilize circadian rhythms, leading to a wide array of health-related effects [65-67]. Light also affects sleep onset and quality of sleep, melatonin synthesis, mood, and alertness [19, 68-70]. Instrumental to these effects are

intrinsically photosensitive retinal ganglion cells (ipRGCs) in the retinal ganglion cell layer [12]. IpRGCs contain the photopigment melanopsin, which is most sensitive to a wavelength at around 480 nm [71]. These ganglion cells project through neural pathways different from those of the visual system and exert so-called *non-image-forming effects* (NIF, also called melanopic effects). The effects can be acute or can take a slower course, over a more extended period of time [33, 72]. When describing the NIF stimulus, the main focus is on ipRGC sensitivity, and, to a lesser degree, on the spatial distribution of light in the visual field [13, 73]. Recent studies help better understand known effects and discover new dependencies of physiological parameters on light. However, to transfer these findings to more common lighting situations, the eye-level stimulus used in the respective studies needs to be realistic with respect to its spatial distribution as well as its intensity. Additionally, the influence of intrinsic and extrinsic stimuli in ipRGC signalling have made it difficult to quantify light characteristics with respect to their melanopic effects. Recent SI-compliant metrics [73] seem to best describe physiological responses under common intensities [32], but are not yet universally adopted. When possible, SI-compliant melanopic illuminance values were calculated for literature references in this paper.

One NIF-effect example worth exploring are acute melanopic effects on the heart, and their connection to alertness and cognitive performance. There are conflicting findings regarding this topic in the current literature. For a critical review of how daytime alertness and mood depend on a melanopic stimulus, see Pachito et al. (74).

Changes in colour-temperature conditions lead to a change of effort-related cardiac response intensity (see below). In a between-subject design, Lasauskaite and Cajochen (40) tested 74 young participants under differing lighting conditions during daytime. The hypothesis of the researchers stated that higher correlated colour temperature would increase alertness (mediated mainly by ipRGCs), and therefore readiness to perform. This, in turn, should lead to a lower experienced task demand and, therefore, effort. The experimental, white LED light was set at four combinations of colour temperature and melanopic intensity, 2800 K / 301 lux, 4000 K / 415 lux, 5000K / 454 lux, or 6500K / 563 lux (correlated colour-temperature / melanopic equivalent daylight [D65] illuminance, abbreviated as MEDI). A vertical, uniformly illuminated front panel provided the light stimulus, emitting about 500 lux at the eye level, regardless of the spectrum. At the beginning of the test procedure, the test subjects were asked to read a simple text for 15 minutes, after which a demanding cognitive task was carried out. Task performance and self-reported task demand did not vary between the four lighting conditions. Cardiac pre-ejection-period (PEP) reaction as a marker for sympathetic nervous system activation and the experienced task demand were shown to vary. Under 4000K lighting, sympathetic activation was highest. At 6500K, sympathetic activation was lowest, with no change to the PEP baseline on average. The authors conclude that working under cooler light might lead to a lower effort, while leading to the same performance. This would be important for real life performance contexts, like office and school work. The construct of *effort* in the context of cardiovascular response reflects the integration of the *active-coping theory*

of Obrist (75) with the *motivational intensity theory* of Brehm and Self (76). This combination can be summarized as stating that the magnitude of the effort that a person invests in instrumental behaviour depends on the experienced demand, provided that success is regarded by that person as both worthwhile and possible. The mobilized effort is proportional to the task demand, with psychophysiological moderators that influence the perception of *necessary* and *justified* action. The mobilized effort manifests itself, e.g., in an activation of the sympathetic nervous system [77]. Sympathetic activation, in turn, can be indexed by non-invasive electrophysiological measures of cardiac reaction [78]. The advantage of this concept is that *effort* can be indexed through an objective psychometric marker.

While the above-mentioned study is the first (and to date only) one to show this dependency of pre-ejection period changes on light, there are two recent notable exploratory studies. Prayag et al. (79) looked at twenty-eight male participants in a within-subject design. They compared two white-LED-light setups with 254 lux and 100 lux MEDI, respectively, testing each twice for 50 minutes, in the evening between 7:00 pm and 11:00 pm. They conducted several physiological measurements and performance tests, and obtained self-reports. Various NIF responses were found, with influences of light on cardiac parameters (heart rate and heart-rate variability) after two minutes of light onset. Heart rate and electroencephalogram markers for alertness increased equally in both lighting scenarios. Heart-rate variability depended on the lighting situation, with an increase in low-to-high-frequency ratio for the first episode of the lower melanopic stimulus, but not the second. According to the authors, this indicates a more pronounced sympathetic influence on the sympathovagal balance. No changes in cognitive performance were found when comparing the experimental episodes. The second study, by Scholkmann et al. (80), used a monochromatic light screen with intermittent 20-sec light pulses during a 10-minute phase. The LED light was kept at 20 lux at eye level, for 682 nm (red), 515 nm (green), and 465 nm (blue) light, which translates to about 0.01 lux, 28 lux, and 230 lux MEDI, respectively. Fourteen volunteers participated in this within-subject experiment; cerebral hemodynamics and cardiorespiratory activity during midday were assessed. Blue light was shown to stimulate the pre-frontal cortex significantly more than red and green light, implying the presence of a pathway for higher autonomic functions through blue light, according to the authors. For heart rate variability, red light elicited an increase at high frequencies (indicating a stronger vagal modulation), while green light decreased the low-to-high-frequency ratio (indicating a stronger parasympathetic influence on the sympathovagal balance, according to the authors). While the studies by Prayag et al. (79) and Scholkmann et al. (80) showed a varying impact on heart rate variability, the autonomous activity coupled with that is not evident, since it is in dispute whether the low-to-high-frequency ratio accurately measures the cardiac sympathovagal balance [81]. The studies described above show a definitive impact of light on the heart, in particular when compared to dim light (not described here). However, how pronounced any downstream effects of melanopic stimuli on sympathetic heart activation are, and whether these effects are activating or inhibitory, is still inconclusive.

The purpose of the present study was to test whether the reported results by Lasauskaite and Cajochen (40) can be replicated under more common lighting conditions, and under the current knowledge of factors determining the melanopic stimulus. The experimental setup in that study used a participant-to-light-source geometry and level of brightness at the eye that are unlikely to be found in a real-world lighting scenario. Our study was carried out in a university study room with an LED lighting installation that enabled different light intensities, light-incident angles, and light spectra. Since other NIF effects are best predicted by the intrinsic ipRGC stimulus [32], we hypothesized that, with variations to the melanopic stimulus at eye level but constant illuminance on the task area (desk), the effort-related cardiac response would show a decrease when stimulus intensity for the ipRGCs rises. Furthermore, interaction effects of a light stimulus with time of day are almost ubiquitous for NIF effects, such as circadian phase changes, Melatonin suppression, and the post-illumination pupil reflex (PIPR). In those cases, the same light/melanopic stimulus at different times of day/night changes the intensity of the effect [82, 83] or even leads to the opposite effect [16]. Additionally, it is reported that people are more alert and that cognitive tasks are more easily carried out early after sleep, compared to later in the day when sleep load accumulates, with the variations depending on chronotype [84]. Following the reasoning of Lasauskaite and Cajochen (40) on the effect of alertness on perceived task demand, mobilized effort, and cardiac reaction, we thus further hypothesized that the effort-related cardiac response is higher later in the day, compared to early after sleep, and that time of day will interact with the light stimulus.

5.3 Materials and methods

5.3.1 Participants and study design

Twenty-seven young and healthy volunteers participated in the study (14 females and 13 males; average age: 26.2 ± 4.3 years; Morningness-Eveningness Score: 53.1 ± 10.5 [37]; body mass index, BMI: 23.2 ± 2.8). Based on effect sizes from Lasauskaite and Cajochen (40), we aimed at a sample size of thirty (G*Power 3 [85], with repeated-measures and within-factors setting: effect size: middle, power: 0.8), but were only able to recruit twenty-seven participants during the time window of the study. Participants were paid EUR 30 each (equivalent to USD 33) for taking part. Participants were recruited through messages on bulletin boards and announcements at classes at the Munich University of Applied Sciences. Exclusion criteria for participants were cardiovascular diseases, epilepsy, or antidepressant medication. Participants were instructed to refrain from sport and caffeine intake before experimental sessions. We used a 2×3 within-subject experimental design with two time-of-day scenarios, each comprising three lighting scenarios (see below). Each participant took part in every scenario. To account for learning effects for the cognitive task (especially when done three times in a row), and for potential carry-over effects of light from one scene to the next, the order in which time-of-day and lighting scenarios were tested was randomized for each participant. Cardio-

vascular data of two participants at evening sessions were lost due to technical problems, resulting in a final sample of 160 measurements (27×2×3 -2) of pre-ejection period (PEP), heart rate (HR), and left ventricular ejection time (LVET), in 27 participants.

5.3.2 Experimental conditions – lighting and time-of-day

The study was carried out in a learning/study room at the Munich University of Applied Sciences with a dynamic lighting installation that allows varying light intensities, light angle, and light spectrum. Experimental sessions took place from the end of November to February, at two times-of-day: morning and late afternoon. Morning sessions started at 07:00 am, before dawn, late-afternoon sessions at 5:00 pm, after dusk. To eliminate the possibility of residual/dawning daylight or streetlight having an impact on the measurements, window blinds were drawn shut before each session ($\tau_{vis,\ blinds}$: 0). Measurements during the morning session thus took place mainly between 7:30 am and 8:30 am, which corresponds to the beginning of a workday; measurements during the late-afternoon session took place mainly between 5:30 pm and 6:30 pm, corresponding to the end of a workday.

Three different lighting scenarios were tested. Lighting settings were chosen to maximize or minimize the effective melanopic stimulus at the eye level (i.e., 120 cm height above the floor, vertical alignment) relative to a medium intensity setting, while keeping the illuminance at the task level at 500 lux (75 cm height above the floor, horizontal alignment). Task-level illuminance was chosen as required by the standards for office workspaces in Europe [86]. Fisheye photographs, together with irradiance distributions from the participants' perspective, are shown in *Figure 5-1*. Measurements at the eye level and desk surface are presented in *Table 5-1*. The CIE S 026 standard was used for metrology [73]. While to be expected [87], it is notable that, through the influence of room surface reflections, the spectral distributions at eye-level differ from those of the light radiating from the lighting fixtures. In Scene 1, the melanopic stimulus is maximized, with light mainly coming from areal light sources at the ceiling. The spectral composition of light is dominated by short wavelengths (blue) compared to medium wavelengths (red/green). Correlated colour temperature, CCT, of the lights is at 7000 Kelvin (K). Scene 2 represents the most common workplace lighting scenario in terms of its spectrum (CCT of the lights being at 4000 K) and its horizontal-to-vertical illuminance ratio. In Scene 3, the melanopic stimulus is minimized, with light mainly coming from spotlight sources at the ceiling. The light spectrum contains very little short-wavelength energy compared to medium wavelengths (CCT of the lights at 2700 K). During the study, the lighting scenarios were manipulated by the experimenter via a smartphone application. Glare was not an issue in all three lighting scenarios; i.e., there was no reflection glare on the desk surface or the monitor. Average luminance ratios of the task area to the surrounding area were 2:1, 3:1, and 6:1 (Scene 1, 2, and 3), respectively, indicating no source of discomfort from task-surround luminance differences. The standardized computerized task used a positive contrast on the monitor (luminance ratio 15:1), which led to high luminance ratios to the

surrounding task area of up to 100:1. However, this was equal for all experimental conditions, and none of the participants reported having problems reading text on the screen. In conclusion, the melanopic intensity decreased from Scene 1 over Scene 2 to Scene 3, while illuminance at (and luminance coming from) the desk surface remained constant. The raw measurement data for each lighting scenario are provided in *S5-5*.

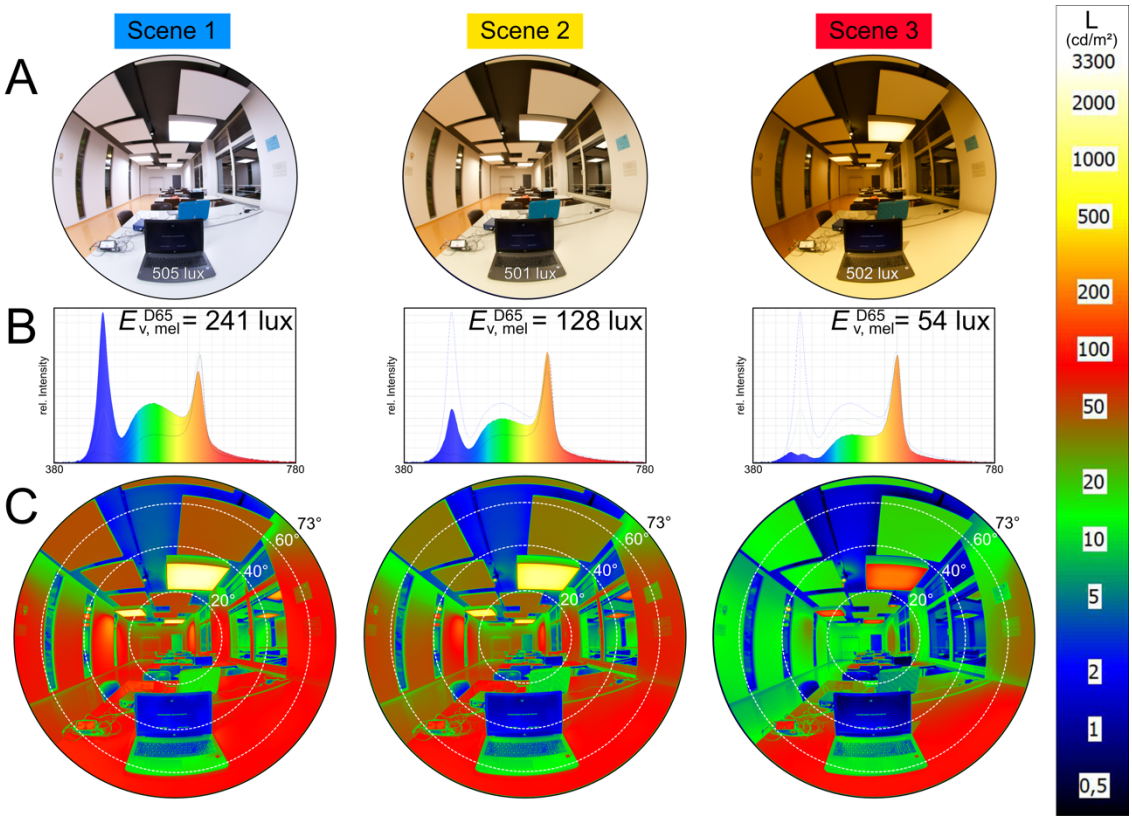

Figure 5-1. Overview of light scenes. From left to right: Scene 1, 2, and 3. Pictures and measurements are taken from the participant's viewpoint. Height 120 cm above the floor, with vertical alignment. (A) 150° fisheye photograph, with illuminance measurement value at the desk surface. (B) Spectral relative intensity from a wavelength (λ) of 380 to 780 nm; $E^{D65}_{v,mel}$: melanopic equivalent daylight (D65) illuminance according to CIE S 026. (C) False-colour luminance distribution in a 150° fisheye photograph; scale on the right-hand side in cd/m^2. Dotted lines indicate 20°-viewing-angle increments from the vertical centre point.

Table 5-1. Lighting scenarios – Settings and measurement values

	Scene 1		Scene 2		Scene 3	
General settings and measurement values[1]						
CCT of the light source (K)	7000		4000		2700	
Horizontal Illuminance at the desk surface (lux)	505		501		502	
Measurements at eye level[2]						
CCT at eye level (K)	5912		3539		2489	
Colour-Rendering Index	91		94		91	
Illuminance (lux)	261		209		146	
α-opic equivalent daylight (D65) illuminance[3]						
	Full	FOV	Full	FOV	Full	FOV
Melanopsin (MEDI; lux)	241	215	128	100	54	31
S-cone (lux)	246	219	101	78	32	17
M-cone (lux)	251	224	179	140	111	65
L-cone (lux)	261	232	211	165	150	89
Rods (lux)	241	215	141	111	69	40

[1] CCT of the light source is according to the programmed setting, not a measurement value.
[2] Measurements were taken at a height of 120 cm above floor level, vertically aligned.
[3] Calculations are according to CIE S 026 (2018). Measurements are either taken over the full vertical hemisphere ("Full") or with restrictions of the field of view ("FOV") according to CIE S 026 Annex 4, Table A (Indoor). Melanopic equivalent daylight (D65) illuminance values are shown in bold.

Table 5-1 (α-opic equivalent daylight (D65) illuminance) and *Figure 5-1* (B) show that the light-setting changes influence multiple receptor stimuli, not just the melanopsin stimulus. With spectral changes, this is most often the case and can only be avoided by comparing reactions to receptor-specific metameric stimuli, such as Spitschan and Woelders (88) reported. However, the required lighting spectra for melanopsin metamerism are artificially truncated. This would impact the study setup, which uses common lighting conditions, including conditions for good colour rendering. Our use of non-metameric differences in the lighting scenarios, therefore, will not allow inferring the Melanopsin contribution to the effect in question. However, if the change in PEP is mainly mediated by ipRGC sensitivity, as is hypothesized, the experimental change in the light setting should affect the change in PEP according to the ipRGC stimulus.

5.3.3 Measurements

A Biopac MP36 data acquisition system with a non-invasive cardiac output sensor SS31I and BioPac BSL 4.1 software on a personal computer (PC) were used to record an impedance cardiogram (ICG) and, simultaneously, an electrocardiogram (ECG). Measurement parameters were *impedance* (Z, measured in Ohm), *impedance change over time* (dZ/dt, measured in Ohm/sec), and *ECG Lead II* (measured in mV) with a sampling rate of 2000 Hz. Output was stored in a text file for analysis on the PC. For this device, four disposable strip electrodes (ICG) and two disposable spot electrodes (ECG) were used. The impedance was measured in a four-wire configuration to exclude the effects of skin, electrode, and lead-wire resistance. For this, strip electrodes were attached at the left

body side. Two were attached at the base of the neck, with a parallel gap of 3 cm to one another; the other two strip electrodes were placed horizontally and 3 cm below the thoracic xiphisternal joint, with a 3-cm gap to one another. An alternating current was injected via the outer electrodes and the resultant voltage measured from the inner electrodes. For the ECG, one spot electrode was placed above the left ankle, the other one above the right wrist. Jewellery, mobile phones, keys, and other electronics were removed from the body before the measurement. See Sherwood et al. (89) for methodological guidelines. For spectral measurements, we used a *Jeti Specbos 1208* spectrometer; see *Table 5-1* for results. For luminance measurements, we used a *TechnoTeam calibrated Canon EOS D7* camera with fisheye-lens; see *Figure 5-1* for results. We further measured ambient room temperature, humidity, and carbon-dioxide level (at a nearby desk) with an *Ahlborn ALMEMO Datalogger* and *Ahlborn D7 sensory equipment,* to control for other criteria that might influence the cardiac reaction. Due to a technical malfunction, these data were partly lost, however, and are only available for 86 of the measurement episodes.

5.3.4 Procedure

The experimental procedure was adapted from Lasauskaite and Cajochen (40). It was approved by the Ethics Committee of the Munich University of Applied Sciences. Participants arrived at the learning room at the appointed time (either 7:00 am or 5:00 pm) and were welcomed and seated in a wooden chair. Wood was chosen in order to minimize possible electrostatic charge, e.g. from clothing with synthetic fibres. Participant then read and signed the prepared informed consent form and filled out a questionnaire, containing four parts: (1) The German translation of the Morningness-Eveningness Questionnaire for testing chronotype (D-MEQ [37]); (2) the Karolinska-Sleepiness Scale for sleepiness (KSS [90, 91]); (3) general demographic questions; (4) questions regarding participants' current state of health, and activities on the day, and the night before, the appointed time and day of testing (e.g. bedtime, wake-up time). Absence of sleepiness is commonly used as measure of alertness [92] and will be used as such in the present study. The experimenter then applied the electrodes, started the ICG/ECG measurements, and visually controlled for acceptable signal patterns. Participants then tried one block of the cognitive task described below. Up to this point, lighting was set to Scene 3 to minimize potential blue-light-induced carry-over effects to the first experimental episode. Before the first light scene change and before every subsequent change, room windows were opened briefly for cross ventilation. Participants were informed that lighting would be changed (i.e., both when the scene was changed or left unchanged) and that a "relaxation phase" of ten minutes would follow. Lighting remained the same until the end of the experimental episode (see *Figure 5-2*). During the baseline phase, participants were provided with current popular magazines for light reading. After the ten-minute baseline, they performed a computerized cognitive task (Sternberg task, PEBL 2.0 [93, 94]), which took about five minutes to complete. The Sternberg task is a letter-memorization task; default software settings were used. The task was divided into six blocks, each containing fifty trials. The blocks varied in the number of letters to be memorized,

counterbalanced for two, four, and six letters. Each trial consisted of a single letter, presented on-screen. By pressing one of two buttons, the participant chose whether the presented letter was among the series of letters memorized at the beginning of each block. The participants had feedback on whether their response was correct. When they chose incorrectly, the memorized letter series would be presented briefly (750 ms). After finishing this task, ICG/ECG measurements were ended, and participants filled out questionnaires. These were: (1) the Karolinska Sleepiness Scale (KSS, see above), where participants rated their sleepiness on a scale of 1 (*extremely awake*) to 9 (*extremely sleepy – fighting sleep*). Then followed (2) the NASA Task Load Index Questionnaire (TLX [95]), where participants rated the task difficulty level in categories of *mental demand*, *physical demand*, *temporal demand*, *performance*, *effort*, and *frustration,* on a scale of 0 (low) to 20 (high). (3) Finally, participants also ranked the appeal of the lighting situation on a 5-level ordinal scale (*very good*, *somewhat good*, *neither good nor bad*, *somewhat bad*, *very bad*). After the second or third lighting condition of the experimental session, participants ranked the appeal of the lighting situation in comparison to the previous one *(better*, *similar*, *worse*). After the questionnaires were filled out, the lighting scenario was switched to the second experimental condition and the same tasks performed, and finally the third light scene tested in the same way. Participants then left, coming back at the second appointed day and time. Then, all steps described above were repeated, save for filling out the consent form (the first one already covered the whole experiment) and questionnaires on chronotype and demographic data. At the end of the second experimental session, participants were thanked, debriefed, and received their payment. The total time participants spent for the experiment was about 180 minutes, with about 90 minutes per experimental session.

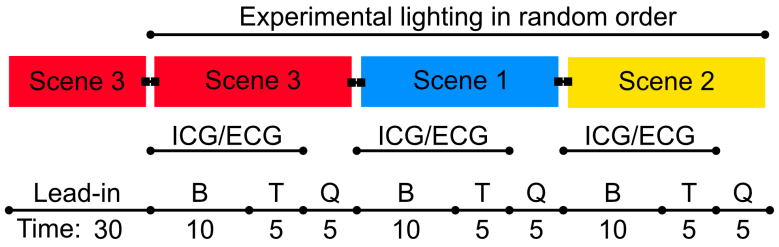

Figure 5-2. Experimental procedure. Schematic depiction of periods for one experimental session (identical for both morning and afternoon sessions) with exemplary order of lighting scenarios. Light is switched instantly between scenarios. The unit for *Time* is minutes. B: Baseline period; T: Task period; Q: Questionnaires; ICG/ECG: Cardiac measurement.

5.3.5 Data analysis

The pre-ejection-period (PEP) is the time span between the depolarization of the left ventricle (Q onset) and opening of the aortic valve (B point) [96, 97]. For practical reasons, the R onset (Q peak) is taken as a fiducial indicator of the beginning of the depolarization and can be picked up from the ECG signal [97]. As signature for the beginning

of the depolarization, we took the minimum of the ECG's second derivative. Its peak indicates the maximum curvature at the start of the R onset which, concurrently, represents the peak of the Q wave. Since the electrical dipole during the Q wave is approximately orthogonal to the Lead-II axis, and the electrical axis of the heart varies between the individual subject and its posture, using this electrode configuration may result in an absence, or large between-subject variability, of the Q-wave in the ECG signal [97]. The minimum of the ECG's second derivative neither depends on the visibility of the Q wave nor the amplitude of its peak, which makes it a reliable indicator for the R-onset. Furthermore, we restricted the possible occurrences of R onset to a time window preceding the, easily identifiable, R peak. Within that window, the R onset is typically seen as a clear negative peak of the ECG signal's second derivative, which can be located reliably and with high precision, and thus allows a reliable identification of the PEP onset. Heart rate (HR) was then calculated from the time difference of subsequent R peaks.

The time point for the opening of the aortic valve (B point) was derived from the impedance cardiogram (ICG). The impedance Z, and thus the ICG, are sensitive to a variation of blood volume in the thorax [89]. The first derivative, dZ/dt, corresponds to blood flow. The second derivative d^2Z/dt^2, in turn, corresponds to a change of the blood flow and is thus indicative for the opening of the heart valves. The B point is the onset of the aortic valve's opening, indicated by a negative peak in the third derivative, d^3Z/dt^3. While, compared to ECG, the ICG signal is smooth and devoid of characteristic spikes, its first, second, and third derivative show distinct features. As selection criterion for picking the correct peak of the third derivative, we used the, easily identifiable, peak of the first derivative, dZ/dt. The B point is obtained as the minimum of d^3Z/dt^3 that occurs just before the maximum in dZ/dt. This strategy allows for an automated evaluation of the PEP interval for the large data sets, with few outliers and the required precision.

Numerically, the ICG and ECG signals were processed offline using a *Wolfram Mathematica Notebook* script, written for this project. To calculate the derivatives of the measured signals, we used the *Savitzky-Golay* filter [98], as described in *Numerical Recipes* [99]. This method allows data smoothing, while keeping intact signatures like peaks, and the simultaneous determination of derivatives. Similar to a moving average, a moving section of the data is selected. However, instead of a simple averaging, the algorithm fits a polynomial of given degree to the selected sequence. Then, one point of the fitted polynomial (usually the central point) is taken as value for the smoothed curve. Higher derivatives are taken from the corresponding derivatives of the fitted polynomial at the respective point. The *Savitzky-Golay* filter is implemented numerically by a list convolution with a kernel. That kernel is calculated in advance for the number of points for the moving fitting, the order of the polynomial, and the order of the derivative. The routines for the kernel's calculation and for list convolution are provided by *Mathematica*, but are available in most numerical environments. We used a kernel length of 100 points, corresponding to a time interval of 50 ms, and a 3rd-order polynomial for all kernels and for the ICG and ECG signals. The third derivative of the ICG signal was calculated from the first derivative of the ICG signal, which, together with Z, was provided by the *Biopac*

MP36 system. We ensured that no time lag was introduced between the ICG and ECG signals and their derivatives by the *Savitzky-Golay* filter. While the *Savitzky-Golay* filter is conceptually straightforward, other higher-order finite, or infinite, impulse response filters (FIR or IIR filters) would produce similar results with appropriate filter settings. Other examples for a calculation of the B point from Z and its derivatives can be found in the literature [89, 96, 100].

Thus, PEP and LVET data were extracted from the ICG and ECG measurements in a semi-automated way and with a by-heartbeat resolution. The *Mathematica Notebook* output was stored in a text file, with separate files for the baseline and the task period. Each text file contained a timestamp containing the corresponding length of cardiac PEP, LVET, and HR for each heartbeat. The described *Mathematica Notebook* script is part of the *Supporting Information* as *S5-3 Script PEP*. We encourage its use by other researchers.

In the next step, we eliminated artefacts and implausible values (using a one-minute moving average and visual control in Microsoft Excel). We also controlled for possible preload or afterload effects (ventricular filling or arterial pressure, respectively), by comparing changes in PEP to changes in LVET [101, 102]. This was done by calculating the period of the electromechanical systole (EMS) as the sum of PEP and LVET. According to Sherwood and colleagues [89], decreases in PEP should be accompanied by decreases in EMS, i.e. positively correlated, in order to tentatively infer increased beta-adrenergic activation without loading factors. Correlation was visually inspected for each episode. Finally, for every measurement period (baseline or task), the average PEP, LVET, and HR were calculated, together with their standard deviations, and the correlation of each parameter with time was further determined. Cardiac reaction scores were calculated by subtracting the task average from the corresponding baseline average; they are marked with the Greek letter '∆' preceding the variable (e.g., "∆PEP"). Negative ∆PEP values indicate shorter periods and thus more forceful cardiac contraction during the task period compared to the baseline. ∆PEP and ∆EMS were positively correlated between periods of rest and task (r=+0.39, $p<0.001$). This, in combination with the visual inspection of the unaggregated data, leads us to believe that no systematic loading effects were introduced to the ∆PEP data, leaving changes in positive inotropic, i.e. adrenergic, agents as the main cause for changes in PEP. A more forceful cardiac contraction, excluding preload and afterload effects, is the result of higher sympathetic activation of the heart [103] and is indicative of a higher experienced task demand and effort [78].

5.3.6 Statistical methods

We used the *R* software [104] with the *lme4* package [41] to perform a *linear mixed-effects analysis* of the relationship between ∆PEP, and the light scene plus time-of-day. As random effects, we had intercepts for participants. Following Barr et al. (105), we tested random slopes for participants, but models in that case would not converge. We also tried other ways to include random slopes in partial models which, however, led to the same outcome. Random slopes were therefore left out of the final model [105]. Visual

inspection of residual plots and random-intercept plots of the used model did not reveal any apparent deviations from homoscedasticity or normality. If not stated otherwise, p-values were obtained by likelihood-ratio tests of the full model with the effect in question, against the model without the effect. P-values less than or equal to 0.05 were considered significant. Beta coefficients (β) from the final mixed-effect model are given where appropriate. They represent the change in value of the dependent variable, when increasing the continuous predictor variable by one unit, or when changing the state of a nominal predictor variable. The continuous predictor variable or, respectively, the nominal state, is indicated by the beta coefficient's subscript. For *light scene*, Scene 2 is always used as the baseline; with respect to *time of day*, late afternoon is the baseline. Group averages (M) and standard deviations (SD) are given for all dependent variables; those for the cardiac reactivity parameters are displayed in a dedicated table. The proportion of variance accounted for (R^2), as well as effect size (f^2), was calculated according to Selya et al. (106). Values of $f^2 \geq 0.02$ are considered small effect sizes, $f^2 \geq 0.15$ medium, and $f^2 \geq 0.35$ large effects [106]. 95% confidence intervals for beta coefficients are denoted with *CI,* and units are left out for clarity. Confidence intervals were calculated as *profile confidence intervals* using the *lme4* package. The described methods and principles were also used for exploring other dependencies of light, time of day, and several other variables on cardiovascular baselines, cardiovascular reactivity of HR and LVET, task ratings, and task performance, even though we did not formulate *a-priori* hypotheses for these cases.

We used *Lilliefors test for normality* [107] on cardiac parameter values, to test the normality assumption prior to the *linear mixed-effect analysis*. All values are normally distributed at a 0.05 level of significance.

The appeal of the current lighting situation, in general as well as compared to the prior light scene, was analysed using *cumulative link mixed models* with the ordinal package in *R* [108].

Plots in the *Results* section were made with the R software. Raincloud plots were made according to Allen et al. (109). The R code to create the plots from the data in this study is provided as part of the *Supporting Information,* in the file *S5-2 R Code*.

5.4 Results

5.4.1 Preliminary analysis

In a preliminary analysis, we looked at time effects within the different experimental periods, sleepiness scores at the beginning of each session, and room-level measurements. We tested for time effects during baseline and task periods, i.e., tested whether the values for PEP, HR, or LVET changed with the duration of the respective period, using the correlation with time (r_t) as the dependent variable in a linear regression model. During the baseline period, PEP was not dependent on time (p=0.40), and neither was HR (p=0.21), but LVET declined slightly with duration (r_t=-0.05, p=0.01). During the task

period, PEP was not dependent on time (p=0.27), but HR increased (r_t=0.16, p<0.001) and LVET declined (r_t=-0.11, p<0.001). Neither the light scene nor the time of day were predictive of r_t values of PEP, HR, or LVET (all p≥0.12).

Further, sleepiness (KSS score) was tested for the beginning of each time-of-day session (KSS_D). KSS_D scores (M_{KSS_D}=4.39, SD_{KSS_D}=1.83) showed no dependency on time-of-day, sex, or chronotype (all p>0.35), but were dependent on sleep duration in the night before the experiment (p=0.02), with decreasing sleepiness for increasing sleep duration (β_{sleep}=-0.20, CI: -0.37 to -0.03).

Finally, we tested whether room levels of carbon dioxide (CO_2), temperature (T), or relative humidity (H) differed between experimental scenarios and whether they were predictors of ΔPEP. None of those variables showed dependency on the light scenario (all p>0.30). CO_2 levels (M_{CO2}=900 ppm, SD_{CO2}=14 ppm) were dependent on time-of-day (p=0.02), with slightly lower values in the morning session, compared to late afternoon ($\beta_{Morning}$=-6 ppm, CI: -11 to -1). Temperature levels (M_T=22.35 °C, SD_T=1.54 °C) were dependent on time-of-day (p<0.001) as well, with slightly lower values during the morning session, compared to late afternoon ($\beta_{Morning}$=-0.96 °C, CI: -1.42 to -0.50). Humidity levels (M_H=25.3%, SD_H=6.4%) did not vary between time of day (p=0.59).

5.4.2 Cardiac reactivity

Cardiac reaction scores, calculated as differences from baseline to task values, are presented in *Table 5-2*.

Table 5-2. Cardiac reactivity scores.

	Scene 1	Scene 2	Scene 3
	Morning session		
ΔPEP	-0.05 (±0.77)	-2.02 (±1.08)	-0.63 (±0.75)
ΔHR	0.27 (±0.71)	1.00 (±0.65)	0.39 (±0.60)
ΔLVET	3.20 (±2.01)	-1.93 (±2.23)	1.70 (±1.80)
	Late-afternoon session		
ΔPEP	-1.72 (±0.78)	-3.88 (±0.99)	-2.27 (±0.98)
ΔHR	1.53 (±0.50)	2.01 (±0.81)	1.96 (±0.73)
ΔLVET	1.57 (±2.15)	2.84 (±1.42)	-0.22 (±1.93)

Means and standard errors (in parentheses) for changes in (1) the pre-ejection period (ΔPEP), (2) heart rate (ΔHR), and (3) left ventricular ejection time (ΔLVET), from baseline to task periods. Measurement units are milliseconds (ms) for ΔPEP and ΔLVET, and beats per minute (bpm) for ΔHR. N=26 for late-afternoon sessions of Scene 1 and Scene 2, n=27 for all other sessions.

5.4.2.1 Cardiac PEP reactivity: contraction

With respect to PEP reactivity, results for ΔPEP are shown in *Figure 5-3*. Increased cardiac contraction, i.e., a decreased systolic time interval for the pre-ejection period (ΔPEP), was dependent on the light scene (p=0.01). A ΔPEP value of zero indicates no change in PEP from baseline to the task. Relative to Scene 2, Scenes 1 and 3 both led

to a reduced cardiac contraction (β_{Scene1}=+1.97 ms, CI: 0.60 to 3.33; β_{Scene3}=+1.50 ms, CI: 0.14 to 2.85). Overall effect size for *light scene* ($f^2_{light\text{-}scene}$) was 0.07.

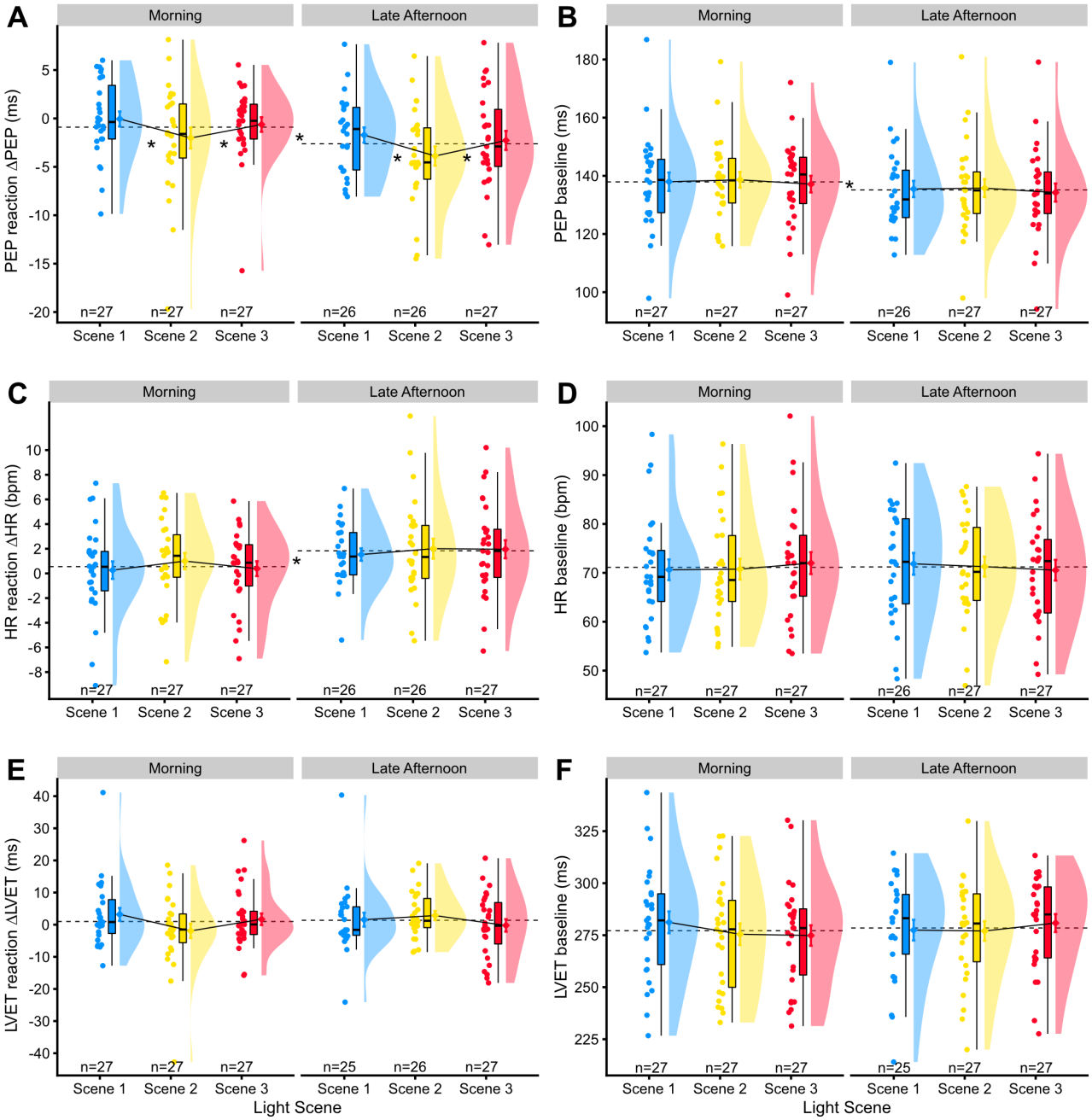

Figure 5-3. Raincloud plots for cardiac reaction scores and baseline scores. (A), (C), and (E) show cardiac reaction scores, and (B), (D), and (F) cardiac baseline scores, each differentiating between the factors of light scene and time of day. There are three Raincloud plots at each time of day (blue, yellow, and red); each of these consists, from left to right, of (a) the raw data, horizontally jittered to improve readability, (b) a Boxplot, and (c) a density plot of the data, with a dot with whiskers on its left, indicating its mean and standard error of the mean. Continuous sloped black lines between the means track the differences between light scenes. Horizontal dashed lines indicate the mean over all three light scenes during the respective morning or late-afternoon session. Asterisks indicate a significant change between the respective conditions, marked by the continuous or dashed lines. The number n at the bottom of each plot indicates the sample size for the respective Raincloud plot. Abbreviations: PEP: cardiac pre-ejection period; ΔPEP: change in PEP; HR: heart rate; ΔHR: change in HR; LVET: cardiac left ventricular ejection time; ΔLVET: change in LVET; bpm: beats per minute; ms: milliseconds

Besides being dependent on the lighting scenario, ΔPEP also depended on the time of day (p=0.002). During morning sessions, the change in cardiac contraction was reduced compared to late afternoon ($\beta_{Morning}$=+1.78 ms, CI: 0.67 to 2.89). Effect size ($f^2_{time\text{-}of\text{-}day}$) was 0.08. The interaction of light scene and time of day on ΔPEP was tested but had no relevant predictive power (p=0.99). Sex, age, BMI, sleep duration, chronotype, and KSS_D were no relevant predictors (all p≥0.65).

The mixed-effect model with light-scene and time-of-day predictors had an effect size f^2_{total} of 1.05 and R^2_{total} of 0.51, but this includes the random effect for participants and therefore mostly accounts for the inter-individual variance ($SD_{Participants}$=2.89 ms), not the experimental conditions. When using a random-effect-only model as a reference, the combined effect size for the light scene and time of day was f^2 =0.15, and the explained variance R^2=0.13 ($SD_{Residual}$=3.55 ms).

Finally, we also tested for influential data points on a by-participant level, i.e., we dropped individuals from the analysis to test whether the reported effects depended on those participants. For the predictors *light scene* and *time of day*, there was no influential participant. However, the CI for β_{Scene3} crossed the zero mark four times (i.e. was not part of the 95% CI) out of twenty-seven participants. This means that there is some sensitivity to the sample for Scene 3 being significantly different from Scene 2 in the effect on ΔPEP values (see Figure 5-4 (A) for the individual trends between light scenes). The empirical trend, i.e. the difference of ΔPEP between Scene 2 and Scene 3, stayed broadly the same, regardless of the excluded participant.

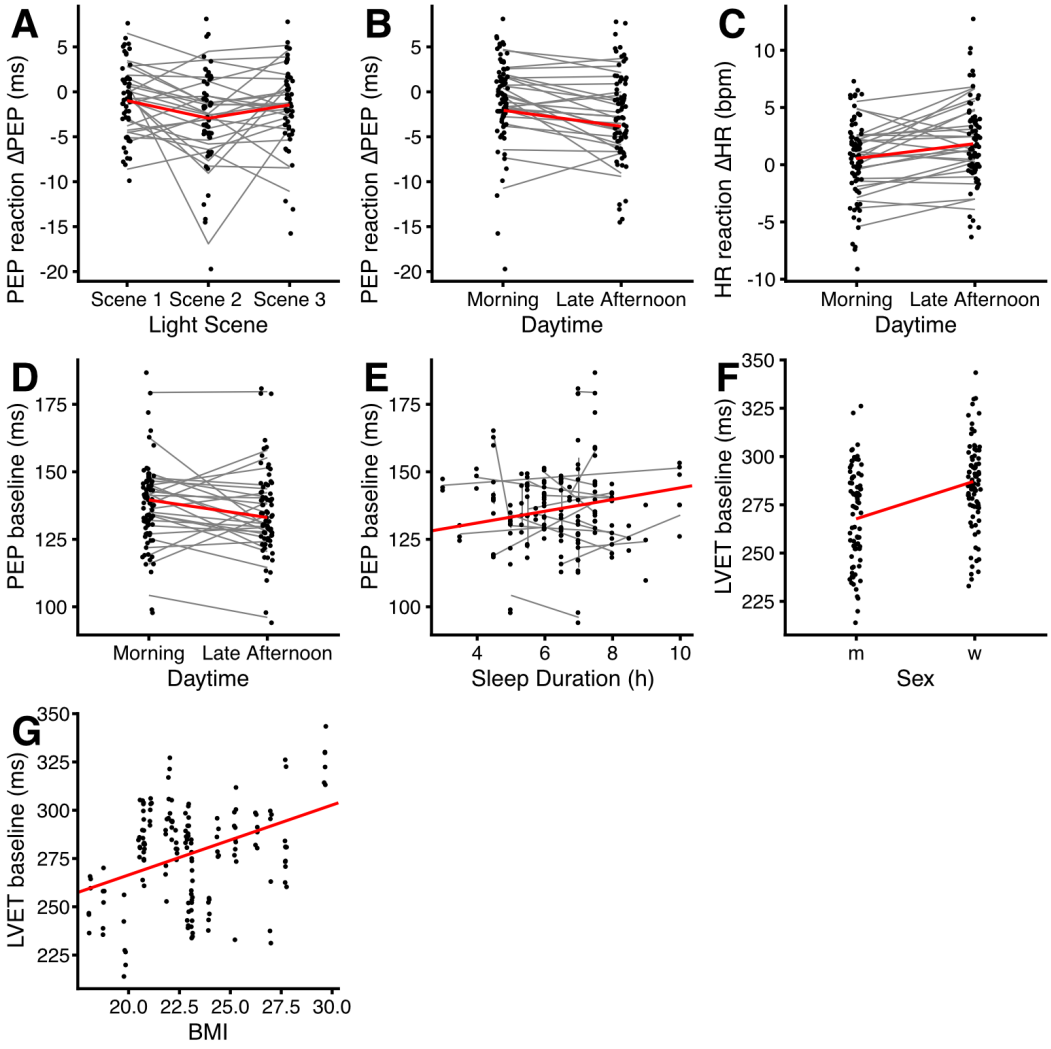

Figure 5-4. Scatterplots of cardiovascular dependencies on a number of predictors. Points show individual values; grey lines indicate the intraindividual change between predictor levels. Each of these lines connects the predicted means of up to three individual values. Regression lines when all other predictors are held constant on an average level are shown in red. For the categorical predictors (A – D, and F), points are jittered horizontally to improve readability. (A) ΔPEP values are lowest for Scene 2. (B) ΔPEP values are higher in the morning, compared to late afternoon. (C) ΔHR is lower in the morning, compared to late afternoon. (D) PEP baseline values are higher in the morning, compared to late afternoon. (E) PEP baseline values increase slightly with sleep duration. Sleep duration refers to the sleep the night before the respective experimental session. (F) LVET baseline values are higher for females (w) than for males (m). (G) LVET baseline values increase with BMI values. Abbreviations: PEP: cardiac pre-ejection period; ΔPEP: change in PEP; HR: heart rate; LVET: cardiac left ventricular ejection time; BMI: body mass index; bpm: beats per minute; ms: milliseconds

5.4.2.2 HR and LVT reactivity

With respect to the other cardiac reactivity variables, we tested ΔHR and ΔLVET for dependencies on the light scene, time of day, the interaction between light and daytime, sex, age, BMI, sleep duration, chronotype, and KSS_D. Time of day was predictive of ΔHR (p=0.001), with a smaller increase in heart rate during the morning session compared to

late afternoon ($\beta_{Morning}$=-1.29 bpm, CI: -2.07 to -0.52; see Figure 5-3 and 5-4). Other parameters had no significant effect on ΔHR (all p≥0.08). None of the independent variables was predictive of ΔLVET (all p≥0.06).

5.4.3 Cardiovascular baselines

Cardiovascular baseline parameters in the study were PEP, HR, and LVET. We tested these values during the baseline period for dependencies on the light scene, time of day, interaction between light and daytime, sex, age, BMI, sleep duration, chronotype, and KSS_D. Figure 5-4 shows scatterplots of all cardiovascular dependencies.

PEP values (M_{PEP}=136.54 ms, SD_{PEP}=15.10 ms) were dependent on time of day (p<0.001) and on sleep duration (p=0.001), with higher values obtained during the morning session compared to late afternoon, and increasing values with longer sleep duration ($\beta_{Morning}$=+6.51 ms, CI: 3.43 to 9.58; β_{Sleep}=+2.17 ms, CI: 0.85 to 3.49). Other predictive parameters on PEP were not significant (all p≥0.09).

Surprisingly, HR baseline values (M_{HR}=71.17 bpm, SD_{HR}=10.89 bpm) were not dependent on the time of day, nor on any of the other parameters (all p≥0.08).

LVET values (M_{LVET}=277.80 ms, SD_{LVET}=24.96 ms) were dependent on sex (p=0.003) and BMI (p=0.002). Values for LVET were greater for females, compared to males. LVET values further increased with higher BMI–(β_{Female}=+19.53 ms, CI: 6.28 to 32.78; β_{BMI}=+3.62 ms, CI: 1.24 to 6.01). Other predictive parameters on LVET were not significant (all p≥0.22).

5.4.4 Task performance and retrospective self-report

5.4.4.1 Task performance

Task performance parameters were reaction time and accuracy. Both were tested for dependencies on the light scene, time of day, the interaction between light and daytime, sex, age, BMI, sleep duration, ΔPEP, chronotype, and KSS_D. Accuracy was logit transformed for linearization [107]. Besides calculating average performance values, the PEPL 2.0 software output includes performance for two, four, and six character blocks of the cognitive task. The block sizes can be likened to task difficulties.

Reaction time (grand M_{RT}=851 ms, SD_{RT}=178 ms) showed a dependency on sleep duration, but only for the four-character block (p=0.02), with increased reaction time with sleep duration (β_{Sleep}=+11.70 ms, CI: 1.90 to 21.50). Other predictive parameters on reaction time were not significant, regardless of character count (all p≥0.10).

Accuracy (grand M_{Acc}=97.7%, SD_{Acc}= 0.02%) was dependent on KSS_D, when testing for the six-character block or the average over all the blocks (p=0.002 and p=0.003, respectively). Accuracy decreased with increasing sleepiness score (six characters: β_{KSSD}=-0.25, CI: -0.41 to -0.08; average: β_{KSSD}=-0.19, CI: -0.31 to -0.07; β values and CI

relate to logit transformed accuracy values). Other predictive parameters on accuracy were not significant, regardless of character count (all p≥0.06).

5.4.4.2 Task ratings

Questionnaire-derived ratings for task demand consisted of all six items from the NASA Task-load-index. Scores for the items *mental demand*, *temporal demand*, *performance*, *effort* and *frustration* were summed up to calculate a Raw-TLX score (RTLX [110]). RTLX scores were tested for dependencies on the light scene, time of day, sex, KSS_D, sleep duration, and chronotype. Raw-TLX scores (M_{RTLX}=50.6, SD_{RTLX}=11.7) were dependent on time of day, sex, and sleep duration (p=0.017, 0.006, and 0.005, respectively). RTLX scores were higher for females, compared to males, and lower during morning sessions, compared to late afternoon. RTLX scores were further lower for increased sleep duration (β_{Female}=+10, CI: 2.6 to 17.4; $\beta_{Morning}$=-1.4, CI: -2.3 to -0.4; β_{Sleep}=-1.4, CI: -2.3 to -0.4). Other predictive parameters for RTLX were not significant (all p≥0.30).

Single-item-TLX scores showed those dependencies in parts. *Mental demand*, *physical demand*, *effort*, and *frustration* had different scores depending on sex (all p≤0.04). *Temporal demand* and *frustration* had different scores depending on the time of day (all p≤0.02). *Frustration* depended on sleep duration (p=0.008). Finally, *physical demand* and *performance* depended on KSS_D (all p≤0.04).

5.4.4.3 Other ratings

Other questionnaire-derived ratings contained sleepiness after each task period and the appeal of the lighting situation. KSS scores after each task period (KSS_S) were tested for dependencies on the light scene, time of day, sex, sleep duration, KSS_D (scores the sleepiness at the beginning of the session), chronotype, and ΔPEP. KSS_S scores (M_{KSS_S}=4.66, SD_{KSS_S}= 1.92) were dependent on KSS_D (p<0.001). Unsurprisingly, KSS_S scores increased with higher KSS_D scores (β_{KSSD}=+0.76, CI: 0.63 to 0.89). Other predictive parameters for KSS_S were not significant (all p≥0.06).

The appeal of the current lighting situation in general, as well as the appeal compared to the prior light scene, were tested for dependencies on the light scene, time of day, the interaction of light scene with the time of day, chronotype, sex, KSS_D, and prior light scene. The appeal of the current lighting situation, scored on a Likert scale from one to five, was dependent on the light scene (p<0.001), but not on other parameters (all p≥0.29). No participant rated the current lighting situation as *very bad* (lowest of five scores). It was more likely that participants rated Scene 1 lower than Scene 2. Scene 3 was rated about as appealing as Scene 2 (β_{Scene1}=-1.94, CI: -2.93 to -0.94; β_{Scene3}=-0.19, CI: -1.14 to +0.77; β values and CI relate to the *cumulative-link mixed-model* output).

The appeal of the current lighting situation compared to the prior situation, scored on a three-step ordinal scale, was dependent on the light scene (p=0.001), but not on other parameters (all p≥0.06). It was more likely that participants rated Scene 1 lower than

Scene 3 (β_{Scene1}=-1.05, CI: -2.11 to +0.01; β_{Scene3}=+1.03, CI: -0.21 to +2.26; β values and CI relate to the *cumulative-link mixed-model* output).

5.5 Discussion

In light of the results of Lasauskaite and Cajochen (40) and the assumed underlying mechanisms, we anticipated that an increase in melanopic stimulus intensity (increasing from Scene 3 over 2 to 1) would result in a decrease of cardiac contraction change, as measured by ΔPEP. However, while ΔPEP did indeed depend on the lighting conditions, the results show that the melanopic stimulus is not the singular, linear predictor that we expected. Rather, ΔPEP had a minimum at the medium-intense melanopic stimulus during Scene 2, and higher values for Scene 1 (~2.0 ms) and Scene 3 (~1.5 ms). A second-order predictor for the melanopic stimulus intensity would fit the experimental data, but there is no support for such a stimulus-effect connection in literature. Rather, a linear dependency would be expected when looking at other melanopic effects in a similar range of melanopic stimulus intensities [32, 68]. Since all photoreceptor types are influenced by the light-setting changes, they could be possible mediators for the effect on ΔPEP. However, no single receptor stimulus can be used to satisfactorily explain the results. We thus find it likely that a combination of receptor inputs mediate the effect. Therefore, another possibility for an interpretation is using both the melanopic stimulus intensity ($E_{V,mel}^{D65}$) and the level of vertical illuminance at the eye as predictors (p=0.003 and p=0.005, respectively; $\beta_{Ev,mel,D65}$=+0.06 ms, CI: 0.02 to 0.10; β_{Ev}=-0.10 ms, CI: -0.16 to -0.03). From a theoretical viewpoint, we favour that latter possibility even though our data do not provide direct evidence for this moderator effect of illuminance. In the literature, however, brightness has been shown to have alerting effects, independent of melanopic efficacy [31, 111], while downstream effects of a melanopic stimulus can counter sympathetic effects, such as pupil re-dilation [51]. From a physiological perspective, the intrinsic melanopic reaction could be moderated by an extrinsic cone input, as is the case with other NIF effects, such as pupil reaction [24, 112]. Extrinsic rod input is unlikely to occur, since even the lowest light setting is well above the saturation level of rods. Therefore, greater sympathetic activation (i.e. cardiac contraction) with increasing brightness and decreasing melanopic stimulus intensity could result in the present experimental outcome for a light-scene dependent ΔPEP. Further research would be needed, however, to support such an interpretation, especially considering the changes in multiple photoreceptor stimuli, as was discussed above and in *Materials and Methods*.

The second hypothesis - that there is a dependence of ΔPEP on time of day and interaction with the light scene - was only partly supported by the experimental outcome. During morning sessions, changes in cardiac contraction were lower by about 1.8 ms when compared to late-afternoon sessions, which is about the same amount as for a change in light scene from Scene 1, or 3, to 2. To the best of our knowledge, this time-of-day dependent, task-triggered change in cardiac contraction has not been reported before. It is unlike the exploratory findings from van Eekelen et al. (113), even though circadian effects on PEP itself are well known [114, 115] and nearly all physiological

processes appear to depend on circadian phase [116]. Our data did not support the hypothesized interaction of the light scene with time of day, but that might still occur for other scenarios, such as at late-night times. One limitation of the present study is a chronotype bias, where most of the participants were neutral types, some morning types, and only two were pronounced evening types. This skew in the chronotype distribution is possibly due to the early start for the morning session, which might have put off some prospective evening-type participants. Therefore, we do not know whether the changes due to time of day would be different for evening chronotype subjects, as is suggested in a study by Goldstein et al. (117).

Effect sizes for the light scene and time of day are small ($f^2_{time\text{-}of\text{-}day}$=0.08 and $f^2_{light\text{-}scene}$=0.07) to medium ($f^2_{combined}$=0.15), and this is to be expected. Firstly, using a repeated-measures design for the cognitive task usually, through learning effects, dampens the impact on the autonomous nervous system – even when this effect is excluded through randomization, as was done in the present study. Through repetition and learning, the task demand for the participant is expected to decrease, thereby reducing mobilized effort and sympathetic activation. However, this learning effect might more accurately reflect real-life physiological behaviour, where cognitive tasks are usually executed more than once. Secondly, from a theoretical perspective, cardiac contraction reactivity allows to adjust for widely different requirements and shows vast inter-individual differences [101]. Within reasonable limits, changes in lighting conditions and time of day have to be considered circumstantial to the task itself – we would not expect them to change the perception of a given task difficulty entirely. Instead, the effects of lighting and time of day seem to work rather subtly by adjusting the ergonomics and, therefore, perceived demand of a task, and their respective effect sizes do neither overstate their importance nor render them irrelevant. The proportion of possible change in resting PEP for our data is about ten percent, relative to an artificially induced maximum of about 40 ms [103].

Since we did not have an *a-priori* hypothesis for other parameters, the results for those will not be discussed in detail but only for providing context for the primary experimental outcome. The analysis of secondary parameters should also be viewed as exploratory, due to the accumulation of type I errors through the multitude of comparisons. As already stated above, physiological (and ultimately behavioural) parameters are expected to change with the time of day. It is therefore not surprising to see such dependencies for a range of cardiovascular parameters and task ratings. Peculiarly, heart rate itself was not dependent on time of day, but this might be because the morning and late-afternoon sessions show similar heart-rate levels in their respective points on the circadian curve [118].

Room-level data were limited, but they still show that there were systematic differences between morning and late-afternoon sessions. Room-temperature and carbon-dioxide levels have the potential to influence performance [119, 120], and therefore, likely, also the experienced task demand and the cardiac reaction. However, changes in carbon dioxide in the room were negligible in size, and a difference of about one degree Celsius between morning and late afternoon is not considered influential at about 22°C [120].

Temperature differences resulted mainly through the building's heating cycles during winter.

The lighting situation affected the physiological level, but we found no difference in task performance, neither with respect to reaction time nor accuracy. One possible interpretation is that, even though the experimental settings did not change performance, that was because participants were just more or less "efficient" in terms of energy usage and conservation, thereby achieving the same results. Alternatively, experimental settings did change performance, but on a level not detectable with the posed task, i.e., because statistical power was too low to detect the change. On average, performance accuracy was rather high, even for the six-character block (~96%). The lack of change might thus reflect a ceiling effect and future studies would need a higher difficulty level. Retrospective self-reports of psychophysical effects for task demand and alertness did not depend on the lighting scenario either, which might be interpreted in a similar way.

In comparison to Lasauskaite and Cajochen (40), we find that the minimum ∆PEP in both studies occurs at a medium setting (Scene 2 here, and the 4000K scene in that study), and is close to zero for the highest setting (Scene 1 and 6500K scene, respectively). While we find a significant difference from medium setting toward the lowest setting (Scene 3), results from Lasauskaite and Cajochen (40) in that respect are not significant, but tend in the same direction (2800K scene). It is important to note, that in terms of melanopic stimulus alone, the range of our study is between 54 and 241 lux MEDI, whereas in the other study the range is between 301 and 563 lux MEDI. This means that the lowest melanopic intensity from Lasauskaite and Cajochen is higher than the highest melanopic intensity in our study. Only in terms of light spectrum / spectral composition are the settings comparable between lowest, medium, and highest setting. This difference in the parameter settings adds weight to the discussion above, that the melanopic stimulus alone cannot predict the cardiac reaction, and that a different or at least additional mechanism is needed to explain the effect. Overall, the difference in ∆PEP from the light scene is smaller in our study (~2 ms between Scene 2 and 1, compared to ~3.5 ms between the 4000K and 6500K scene there). The lower effect might be explained by the overall lower, more moderate stimulus levels used here (e.g., ~241 lux MEDI for Scene 1, compared to ~563 lux MEDI in Lasauskaite & Cajochen's 6500K scene), or on the repeated-measures setup as explained above. The same applies when comparing effect sizes between the present study (small, $f^2_{light\text{-}scene}$ =0.07) to the other study (medium, d=0.51, p=0.034). The latter found a significant effect of light scenes on ∆PEP for baseline periods of exposure, compared to a habituation phase with 2800K. This was possible, because they used a three-step experimental procedure, as explained above. As we did not have a habituation phase prior to every baseline period, we could only test for differences in baseline PEP itself, but find no statistical dependency on the lighting scenario. As a further comparison, we calculated the Bayes Factor (BF) in that study from the p-value of the main effect of light (p=0.034; BF=0.31), and compared it with the Bayes Factor for only the *light-scene* variable in the present study (based on likelihood ratios; BF=0.014) [121]. BF values represent the odds of the null hypothesis

relative to the alternative hypothesis; lower values represent better evidence against the null hypothesis. The Bayes Factor for the present study is, by a factor of about 22, lower than in Lasauskaite & Cajochen's study (i.e., 0.31/0.014). Therefore, the present study adds firm evidence in favour of a real effect of lighting on ΔPEP, even though not stemming from the melanopic stimulus alone, as was initially hypothesized.

Looking at other publications on effort-related cardiac reactivity, we find similar differences in magnitude and direction of ΔPEP as found in the present study between Scene 2 and Scene 1 (~-2 ms). For example, the difference is similar when lowering the task difficulty (to *Low* instead of *Moderate* [122]), or when paying a lower reward (1 Swiss Franc instead of 15 [123]), or also when putting subjects in a bad mood (*negative mood* instead of *positive mood* [124]). As stated by Wright and Kirby (78), cardiac reaction will decrease when lowering task difficulty or reducing personal involvement. Nevertheless, only in connection with the task outcome, i.e. the performance result, can it be determined whether this is desirable or not. In the case of our present study, Scene 1 and 3 are preferable for the posed task compared to Scene 2: even though effort, and therefore energy consumption (sympathetic activity), was lower, task performance and self-reported task demand were the same.

Sikka et al. (125) showed that blood vessels express melanopsin and display vasorelaxation under blue light, and in a recent study, Stern et al. (126) measured a decrease of systolic blood pressure minutes after a full-body blue-light shower, with no changes in a control group. While the evidence for this effect is still limited, it is worth discussing it in the context of the present study. We cannot rule out the occurrence, or interaction, of blood-vessel mediated melanopic effects with retina-mediated melanopic effects, since the participants' skin was partly exposed to the room lighting, but we find it rather unlikely. Firstly, when compared to Stern et al. (126), the exposed skin areas of our participants were small, with only face and hands exposed by all participants, plus neck and arms by some. Secondly, irradiance levels were only one thousandth of those in that study. Thirdly, such an effect should have shown up in baseline PEP values, in which we had no relevant differences between lighting conditions nor a dependency on time. Lastly, since we were mainly interested in changes of PEP between two phases with the same lighting conditions, any general effect on blood pressure would influence both phases. We believe, therefore, that any blood-vessel mediated melanopic effect had no appreciable impact on our results for ΔPEP.

A number of studies found alerting effects of blue-wavelength-dominated light that we cannot confirm [17, 19, 20, 127, 128]. The different outcome in those studies compared to the present study might be explained by longer light-exposure periods, different light stimulus intensity or incident angle, night-time testing, or by using monochromatic light. Studies with a more common context in terms of stimulus and time of day share similar findings to the present study. Laszewska et al. (129), for example, experimented during regular work hours (noon) with results showing little to no acute impact of the light spectrum on alertness. Finally, as mentioned above, Prayag et al. (79) showed acute physi-

ological activation depending on the melanopic stimulus to some degree but without differences in actual performance. Lasauskaite and Cajochen predicted, that the change in cardiac reaction would be due to a higher alertness at higher colour temperature settings (their model, in brief: higher CCT [Light Scene] → higher alertness [KSS] → higher readiness to perform → less perceived task demand [TLX] → less mobilized effort → less sympathetic activation → less cardiac contraction change [∆PEP]). The authors could not test this in full, however, since alertness scores (measured as KSS) from the beginning of each session were lost due to technical failure. As stated above, we found no impact on alertness of the light scenes or of the time of day. Perceived task demand, operationalized through the NASA TLX score, neither depended on the light setting in the present nor in the other study. The lack of changes in either alertness or perceived task demand do not necessarily speak against the model from the other study. Since the singular effects of the light scene and time of day on ∆PEP are small, the KSS and TLX scores might not be reliable enough to detect an equally small, underlying change in alertness and perceived task demand, respectively, especially since both were queried in retrospect after the task.

5.6 Conclusion

We studied the question of whether changes in the melanopic stimulus, and the time of day would both influence the change in cardiac pre-ejection period (∆PEP) when performing a cognitive task. ∆PEP is considered a marker for sympathetic activation and, in turn, for mobilized effort and experienced task demand. Light scenes in our study were all constructed as “common indoor office lighting situations” in terms of their light spectrum, their intensity, and the geometric formation of the light sources. Changes in the melanopic stimulus are necessarily accompanied by changes in the activation of other photoreceptor types, when common white light conditions with good colour rendering are maintained. Therefore, a direct test of a pure melanopsin contribution cannot be achieved. However, differences in the light settings were designed to maximize or minimize the melanopic stimulus, starting from a baseline for all affected dimensions, while keeping other variations small. Under these conditions, the medium melanopic-stimulus setting resulted in a greater sympathetic activation compared to the lower- and higher-intensity setting. This result broadly confirms the connection between the spectral composition of light and cardiac contraction as found by Lasauskaite and Cajochen (40), yet with much stronger evidence as shown by the respective Bayes Factors for the overall effect of light in the two studies. Furthermore, it shows, for the first time, that the lighting setup is relevant in terms of ∆PEP under common lighting conditions. However, the result also shows that melanopic stimulus alone cannot account for the changes in sympathetic activation, as we had assumed. Another predictor is required to explain the peak in sympathetic activation at a medium-intense melanopic stimulus. We propose this predictor to be brightness, on theoretical grounds.

We demonstrated, for the first time, a connection between the effort-related change in ∆PEP and time of day, with smaller sympathetic activation during the morning-session

compared to that at late afternoon. Yet, importantly, the physiological changes were not accompanied by changes in performance, nor self-reported task demand or alertness. In the context of this study, Scenes 1 and 3 can be likened to an ergonomic optimization. Compared to Scene 2, the changed lighting condition will thus not change the way tasks are completed. The optimal lighting will rather minimize the required amount of sympathetic activation, i.e. the energy, to perform those cognitive tasks. According to literature, the effect is possibly mediated through heightened alertness and readiness to perform, resulting in a reduction in perceived task demand and mobilized effort.

Our findings have practical implications since they show that the way lighting systems are set-up to satisfy regulatory standards does matter on a physiological, effort-related level, even when acute effects do not manifest themselves in immediate performance increases or reduced task demand. We designed the lighting scenes following recommendations for dynamic, circadian lighting systems, with Scene 1 representing a morning setting, Scene 3 an evening setting [130, 131] and Scene 2 resembling a common approach to meet regulatory standards. It is likely that the acute effects found in the present study add to the positive, mid-to-long-term circadian effects of dynamic lighting.

5.7 Acknowledgements

We thank Timo Müller for his input on the lighting and control system, and for installing the components. We further thank an anonymous reviewer for suggesting Raincloud plots to visualize the raw data and their basic parameters.

5.8 Supporting information

All supporting information can be found at
https://doi.org/10.1371/journal.pone.0239553

S5-1 Dataset. Comma-separated-value (CSV) data table used for all linear regression, linear mixed-effect, and cumulative link mixed-model analysis.

S5-2 R Code. A ZIP file containing the R code used for every variable (*.R file extensions). The code can be executed with the free R software (GNU General Public License). The plots, included in the *Results* section, can be created directly from the study data with the file *PEP_Plots.R*. For the *Raincloud plots,* additional source files are needed from Allen et al. (109). Further, the ZIP file contains text files with the R software console output, showing the executed code and the results (*.txt file extensions). Lastly, S5-2 contains PDF files for all dependent variables with significant predictor variables. The PDF files contain two plots each, showing the QQ-Plots for *Random Intercepts* and *Residuals* from the linear mixed-effect model.

S5-3 Script PEP. A ZIP file containing The *Wolfram Mathematica Notebook* script for processing electrocardiogram (ECG) and impedance cardiogram (ICG) data into heart rate (HR), cardiac pre-ejection period (PEP) and cardiac left ventricular ejection time

(LVET), as discussed in the section on *Data analysis*. The ZIP file also contains a PDF file with a printout of the executed script for reference. The script was written for the present study, but we encourage its use by other researchers. Test data is provided as *S5-4 Example Data PEP*. The script is annotated on a-step-by-step basis, and can be executed with *Wolfram Mathematica*. In addition to the PDF file provided as part of S5-3, the script can be viewed with the free *Wolfram Player*.

S5-4 Example Data PEP. A ZIP file containing two text files with sample ECG and ICG data. One file contains a large dataset, the other a smaller subset. The files are intended as example data for the *Wolfram Mathematica Notebook* script in *S5-3 Script PEP*.

S5-5 Measurements Light Spectrum. A CSV file containing the spectral measurements for all three lighting scenarios, with, and without the field-of-view (FOV) occlusion.

6. Paper II: Spectral dependency of the human pupillary light reflex

Title:

Spectral dependency of the human pupillary light reflex. Influences of pre-adaptation and chronotype.

Authors:

Johannes Zauner[1]*, Herbert Plischke[1¶], and Hans Strasburger[2¶]

[1]Munich University of Applied Sciences, Munich, Germany

[2]Institute of Medical Psychology, Ludwig-Maximilians-Universität, Munich, Germany

¶ HP and HS are Joint Senior Supervisors

The publication in this section was accepted by PLoS ONE on November 2nd, 2021, and is also available at https://doi.org/10.1371/journal.pone.0253030

6.1 Abstract

Non-visual photoreceptors (ipRGCs) and rods both exert a strong influence on the human pupil, yet pupil models regularly use cone-derived sensitivity as their basis. This inconsistency is further exacerbated by the fact that circadian effects can modulate the wavelength sensitivity. We assessed the pupillary reaction to narrowband light stimuli in the mesopic range. Pupil size for eighty-three healthy participants with normal color vision was measured in nine experimental protocols with varying series of continuous or discontinuous light stimuli under Ganzfeld conditions, presented after 90 seconds of dark adaptation. One hundred and fifty series of stimulation were conducted across three experiments, and were analyzed for wavelength-dependency on the normalized pupillary constriction (nPC), conditional on experimental settings and individual traits. Traits were surveyed by questionnaire; color vision was tested by *Ishihara plates* or the *Lanthony D15* test. Data were analyzed with generalized additive mixed models (GAMM). The normalized pupillary constriction response is consistent with L+M-cone derived sensitivity when the series of light stimuli is continuous, i.e., is not interrupted by periods of darkness, but not otherwise. The results also show that a mesopic illuminance weighing led to an overall best prediction of pupillary constriction compared to other types of illuminance measures. IpRGC influence on nPC is not readily apparent from the results. When we explored the interaction of chronotype and time of day on the wavelength dependency, differences consistent with ipRGC influence became apparent. The models indicate that subjects of differing chronotype show a heightened or lowered sensitivity to short wavelengths, depending on their time of preference. IpRGC influence is also seen in the post-illumination pupil reflex if the prior light-stimulus duration is one second. However, shorter wavelengths than expected become more important if the light-stimulus duration is fifteen or thirty seconds. The influence of sex on nPC was present, but showed no interaction with wavelength. Our results help to define the conditions, under which the different wavelength sensitivities in the literature hold up for narrowband light settings. The chronotype effect might signify a mechanism for strengthening the individual´s chronotype. It could also be the result of the participant's prior exposure to light (*light history*). Our explorative findings for this effect demand replication in a controlled study.

Keywords: transient, sustained, pupillary constriction amplitude, pupillary light reflex, pupillary light response, spectral sensitivity, melanopic, nonvisual, non-image-forming, ipRGC, PIPR, post-illumination pupil response, chronotype, circadian.

6.2 Introduction

The human pupil is of interest to various research fields, such as vision research, neurobiology, ophthalmology, and psychology. Pupil constriction and size are controlled by parasympathetic pathways, and pupil dilation through sympathetic pathways [132, 133]. Pupillary reaction thus acts as a window into the autonomous nervous system. Diagnostic methods were developed around various aspects of the pupil's behavior and a vast

body of research is dedicated to the pupillary reaction to light. One of the most fundamental aspects in that context is the dependency of the pupillary light reflex (PLR) on the spectral composition of light.

Up until now, the literature is somewhat divided on what the appropriate spectral weighing function should be for capturing the effects of light on pupil size and constriction. Pupil models derived from research using white light stimuli, i.e., polychromatic light spectra, generally employ stimulus luminance or retinal illuminance as predictors. Watson and Yellott (134) in 2012 reviewed eight pupil models published between 1926 and 1999. They created a ninth model by incorporating elements of the previous ones. What is important in our case is that all these models, including the newly created one, work with standard photometric dimensions, and spectral calculations are thus based on the V(λ) weighing function, regardless of stimulus characteristics. However, the V(λ) function may not be the best-suited for predicting pupil size in all cases.

The V(λ) function peaks at around 555 nm wavelength. Yet studies using narrowband light stimuli generally report a maximum sensitivity for PLR at around 480 – 510 nm. Early publications to this effect are notably by Wagman and Gullberg (135) in 1942, by Alpern and Campbell (136) in 1962, and the often-cited paper by Bouma (137) in 1962. These authors attributed the PLR's spectral dependency mainly to the characteristics of rod photoreceptors, but possibly also to those of short-wavelength cone receptors. Adrian (138) in 2003 tried to explain the apparent blue shift in sensitivity, reporting that, with appropriate adjustments, stimulus luminance was sufficient for explaining the PLR. According to the paper, a $V_{10}(\lambda)$ spectral weighing function which is based on the larger 10-degree field should be used instead of the usual 2-degree field (on which V(λ) is based) which, according to the author, is valid for the often-used Ganzfeld conditions. Furthermore, Adrian argues, mesopic conditions should be adequately addressed by using $V_{eq}(\lambda)$ weighting functions as intermediaries between the photopic $V_{10}(\lambda)$ and the scotopic V'(λ) functions. With these adjustments, pupil size depended linearly on (adjusted) luminance. While Adrian (138) performed his analysis on data from a single subject and, very likely, did not know about the spectral-temporal changes of the PLR as found in later studies, his argument about the appropriate luminance function remains valid, even when it was not widely adopted.

With the discovery of intrinsically photosensitive retinal ganglion cells (ipRGCs) at the beginning of the 21st century [12], and their potential to drive pupillary constriction [139], researchers began looking for their influence in PLR experiments. In 2007, Gamlin et al. (24) made the ipRGC influence on pupilloconstriction evident in the macaque with pharmacological blockade of rod and cone photoreceptors. They also showed ipRGC dependency for the post-illumination pupil reflex (PIPR) of humans. Zaidi et al. (140), also in 2007, confirmed the human pupilloconstriction's dependency on ipRGC sensitivity in a blind person who lacked an outer retina. In 2009, Mure et al. [50] found ipRGC-dependent pupilloconstriction in the PIPR of sighted humans and, more importantly, during more prolonged light stimulation than used in previous studies (five minutes, compared to a few seconds in earlier studies). In 2010, McDougal and Gamlin (112) investigated

the contributions of individual receptors to the PLR, for stimulus durations between 1 and 100 seconds. They did this through parameter fitting in a custom-derived function based on theoretical assumptions. They found that rods play an essential role for most stimulus durations, while cones contribute only minimally after just 10 seconds of stimulus onset. At about 18 seconds after stimulus onset, the ipRGC sensitivity curve already provided the most prominent contribution. It has not been confirmed whether the stated time intervals for the receptor types are valid in humans. In 2012, Gooley et al. (141) used stimulus durations from 2 to 90 minutes, showing for the PLR, among others, the dominance of shorter wavelengths at around 490 nm, compared to the brighter settings around 555 nm, especially for longer stimulus durations.

Spitschan (142) showed the inadequacy of using V(λ)-derived luminance instead of a melanopic weighing function by reanalyzing the data from Bouma (137). He estimated the possible error for the stimulus calculation to predict pupil size at about one order of magnitude for typical white-light sources, with the actual error and relevance depending on the application's circumstances. A recent paper by Zandi et al. (143) looked at the prediction accuracy of the models of Watson and Yellott (134). They found that the prediction error was greatest for chromatic spectra, especially for longer exposure times. In the four cases of short chromatic light stimuli of equal luminance (1 second, 100 cd/m²), Zandi et al. (143) found that the significant differences between wavelengths were relatively small. For more extended stimulation periods of 60 and 300 seconds, a luminance-based approach led to considerable error. Together with findings from polychromatic spectra, the authors therefore advocated for the inclusion of time and spectrum in pupil models. Rao et al. (144) suggested a pupil model based on a combined measure of photopic luminance and an action spectrum based on melatonin suppression (*C(λ), cirtopic sensitivity*) that takes spectral differences of the stimulus into account. While Spitschan (142) calls it a good start, both he and Zandi et al. (143) find shortcomings, ranging from the narrow luminance range under which the model parameters were estimated [142], the use of the non-standardized cirtopic sensitivity function, the relatively small expected improvement in prediction accuracy, to the lack of (stimulus) time as part of the model [143]. _ENREF_15

In summary, by addressing the effects of time since light onset, the ipRGC's influence on PLR has become evident for narrowband stimuli [13]. It is also accepted that the many metrics of the PLR, like latency to constriction, peak constriction, rhodopsin- and melanopsin-mediated PIPR amplitude, or melanopsin-mediated PIPR amplitude, differ in their retinal circuitry and thus their spectral sensitivity [64, 142]. These findings sparked the development of diagnostic methods [58] for assessing the health of the nonvisual pathway [52] and circadian system [145], and spotting specific pathologies early on, such as glaucoma [146] and diabetic retinopathy [147]. However, what is still lacking is knowledge about why the PLR in terms of pupil size and constriction during light stimulation seems to differ in spectral sensitivity between narrowband light and polychromatic (white) light. The applicability of prior findings based on narrowband stimuli may be lim-

ited for polychromatic or even narrowband settings. Furthermore, there is still little research into differences of spectral dependency beyond comparing particular wavelengths, mostly those of the blue and red peaks. Most of the studies that use a broad range of wavelengths are based on a comparatively small sample size. The largest of the studies reviewed above had twenty-four participants [141], while the median is only four participants [24, 50, 112, 135-138, 140, 141]. While this is enough for investigating the fundamentals of the PLR's wavelength sensitivity, exploring distributional relationships will require more participants.

We initially set out to take a comparatively large sample of participants for looking at the conditional spectral dependency of pupilloconstriction. Since the ipRGC influence on PLR is mainly present for long-lasting narrowband light stimuli, we believed that, basically, pupilloconstriction would approximately follow the ipRGC sensitivity curve for a series of continuously applied narrowband light stimuli that change in wavelength over several minutes. Preliminary measurements supported this view and further indicated a dependence on sex that we included as an exploratory variable in the main experiment since there is also some support for sex differences in the literature [148]. We were further interested in the influence of chronotype and time of day (cf. [83, 145]); findings from Zele et al. (149) suggested that there is a circadian variation in the wavelength-dependency, as demonstrated by pupil reactions to red and blue stimuli. In our main experiment with a balanced design, wavelengths around the V(λ) function's peak led to the highest constriction. Based on these findings, we designed an exploratory, second experiment, to test whether our findings held up with a changed stimulus series. The findings were indeed replicated, but only in the case when light remained on continuously. When light was discontinuous, i.e., when short intervals of darkness were introduced between the light steps, shorter wavelengths became more influential, in line with published literature. The newly introduced periods of darkness in the second experiment additionally allowed spectral analysis of the post-illumination pupil reflex (PIPR). In a third experiment, we therefore investigated (1) the spectral dependency of the PLR for longer-lasting light steps with short, intermediate periods of darkness, as well as (2) the PIPR for short light steps with more prolonged intermediate periods of darkness.

We believe our findings will help bridge the gap between the canonical divide of luminance-based versus short-wavelength-based pupil models by showing that the PLR's response to narrowband light stimuli can go both ways, depending on pre-adaptation to light. We also show the influence of chronotype on pupilloconstriction, depending on the time of day. Statistical analyses employ generalized additive models (GAMs), which to our knowledge have not been used in pupillometry before. They appear particularly well suited for disentangling the complex coaction of influences.

6.3 Materials and methods

6.3.1 Participants

We recruited a total of 83 young, healthy participants across three experiments through bulletin boards and announcements at the Munich University of Applied Sciences (45 females and 38 males; age: median 26 yr., range 18 – 36; chronotype score: 50 ± 10.6 on the Morningness-Eveningness Questionnaire, where a score between 40 to 60 signifies an intermediary chronotype, below 40 an evening type, and above 60 a morning type [37]). All procedures were approved by the Ethics Committee of the Munich University of Applied Sciences. Exclusion criteria were age (above 39), issues of psychiatric or neuronal health, addiction diseases, regular intake of stimulants or sedatives, acute jetlag or shiftwork (during the past three months), ocular diseases, or epilepsy. Participants were instructed to refrain from caffeine intake prior to the experimental sessions. We further checked participants for normal color vision (Lanthony D15 test [150] or Ishihara plates [151]). Additional participants were tested but their results not included in the analysis [152]; these participants either only took part in the preliminary measurements (see below), did not fit the inclusion criteria, or were tested after the experiment's cut-off date.

6.3.2 Apparatus

The light stimuli were presented in a Ganzfeld dome setup (Light Dome Model *XE 509, Monocrom,* Stockholm). The light source was a 100-Watt Xenon lamp. Full-spectrum light (6000 Kelvin correlated color temperature) was filtered through a stepper-controlled monochromator and led into the dome's interior by a diffusor which was positioned above and behind participants' eyes and thus not visible during the experiment. Light onset and offset were controlled by a shutter mechanism, located between the monochromator and the diffusor. Shutter response time, i.e., the time between open and closed states, was about 100 ms. Changes in peak wavelength occurred at a speed of about 35 nm/s. An *Arduino MEGA-2560* embedded computer with custom-written software controlled the monochromator and shutter.

The setup allows generating narrowband light, with spectral peaks at between 400 nm and 700 nm, and a width (full width at half maximum) of 12 nm ± 1 nm (*Figure 6-1*). We used 61 or 31 peaks, depending on the experiment. The radiant output from the light source is dependent on wavelength (a limitation of the apparatus) and irradiance increases by about one order of magnitude from 404 nm to 450 nm; above that and up to 690 nm, irradiance is comparatively constant at a level of -1,62 ± 0.04 $\log_{10}(W/m^2)$. To accommodate for that dependency, in particular the lower irradiance levels for the wavelengths at and below 450 nm, we included the $\log_{10}$ of the irradiance as a covariate in all statistical analyses when it was not already included implicitly, i.e., as following from illuminance. Measurements of spectral irradiance were taken at the eye level under the light dome. Measurements further included a human field-of-view restriction suggested by CIE Standard *S 026/E:2018* [73]. Therefore, the irradiance measurements represent

the corneal level, as do the various illuminance calculations based on those measurements (*Figure 6-1*). Unobstructed measurements, i.e., *regul*ar irradiance measurements, were about 24% higher. Plots of all spectral peaks are available in the supplemental *Figure S6-17*. We measured the spectral irradiance of each wavelength step multiple times before each experiment to ensure stability in irradiance and wavelength peak. Differences in irradiance were relatively consistent across the spectrum and were smaller than 5%, which equals about 1% on the log irradiance scale from the values shown in *Figure 6-1A* (see supplemental *Figure S6-18* for a regular scale). Differences in wavelength peak were between 0 to 1 nm, which is within the measurement accuracy of the spectrometer. The light source was not monitored during the experiments other than to ensure that it performed on a constant operating temperature.

Park et al. (52) summarized stimuli sizes from three studies [24, 112, 153], stating that melanopsin responses were "observed in a range between ~11 to >14 log quanta/cm²/s for a 470-nm light". Our stimulus for 471 nm lies at 12.75 quanta/cm²/s at the corneal level. However, this is not directly comparable to the summary from Park et al. (52) since those studies used focused light projections. Park et al. (52) converted these measures to luminance values (-0.7 to 2.3 log cd/m²). In our setup, the lower limit of that study translates to -2.3 log W/m², compared to our corneal irradiance of -1.6 log W/m² at 471 nm.

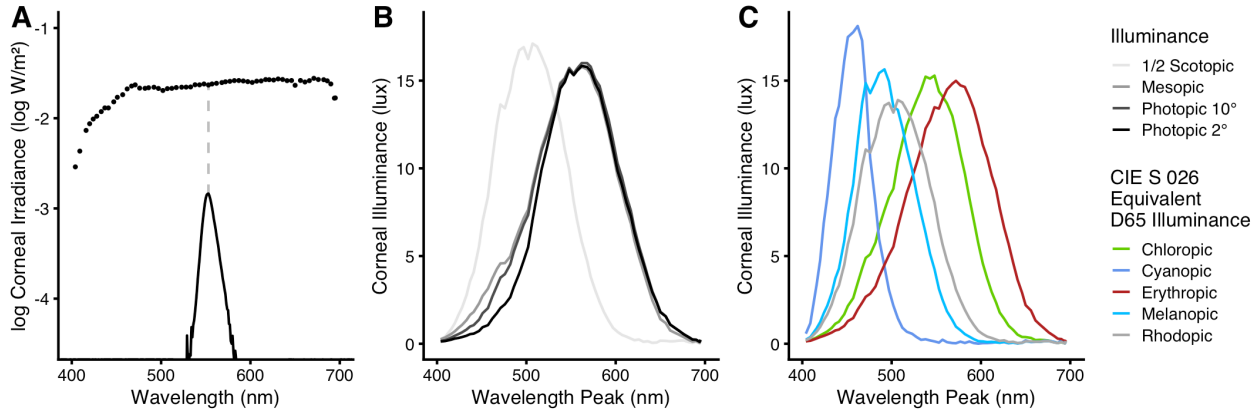

Figure 6-1 Spectral irradiance measurements and calculated illuminance values at the eye level. All displayed values are based on spectral irradiance measurements with a field-of-view restriction according to the CIE *S 026* standard [73]. In our case, these measurements are 24% lower than those of the unobstructed sensor diffusor. Differences in irradiance measurements from the mean were smaller than 5%, or about 1% on the log irradiance scale. Differences in wavelength peak were between 0 to 1 nm. (A) Dots show the log of the corneal irradiance (in log W/m²) of exemplary steps at their respective peak wavelength. Each dot represents a narrowband peak, similar to the spectral example distribution with a peak at 553 nm (the peak is indicated by the gray dashed line). (B) Corneal illuminance values for the narrowband light steps at each peak wavelength. Besides the *standard* photopic CIE-1931 V(λ) weighing for the 2° observer (black line), illuminance values were calculated based on the weightings of $V_{10}(\lambda)$ (10° observer, photopic vision, dark grey), of V'(λ) (scotopic vision, light grey), and of $V_{eq}(\lambda)$ (mesopic vision, medium grey). To show the scotopic illuminance values along with the other curves, they are drawn at half their original value (light-gray curve). (C) Corneal alpha-opic equivalent-daylight illuminance for all receptor types according to the CIE *S 026* standard [73].

6.3.3 Measurement equipment

An eye tracker (*Dikablis Professional Glasses*, *Ergoneers GmbH*, Munich) recorded the pupils by a dual infrared camera setup for simultaneous measurement of the two eyes, at a sampling rate of 60 Hz. Cameras in that setup are located at the end of flexible arms and are adjustable for an optimal view of the pupil and distance from eye level. Each camera has a resolution of 384 by 288 pixel. Camera pictures were analyzed in real time while recording through the *D-Lab 3.5* software (*Ergoneers GmbH*) on a connected personal computer. The software extracted several pupil parameters for each eye in pixel units, including pupil area, height, and width. These time-stamped variables were then exported to a comma-separated-value (CSV) file for later analysis. Spectral irradiance measurements with a 1-nm resolution were performed using a *JETI Specbos 1201* spectroradiometer (*JETI Technische Instrumente GmbH*, Jena; see *Figure 6-1*), with the *JETI LiVal V6.14.2* software running on a connected personal computer. The spectroradiometer's relative measurement accuracy is 2%.

6.3.4 Experimental Design

6.3.4.1 Preliminary measurements

In the relevant literature, the employed periods of dark adaptation (DAP) before light onset vary widely, if reported at all. They range from no-DAP [24] to 40 minutes [50]; the use of an in-between value of 20 minutes for full dark adaptation is recommended by Kelbsch et al. (64). This value is commonly used when there is a main stimulus following the DAP. Since we planned on using comparatively long experimental light durations of around 15 minutes containing a chain of wavelength peaks, all equally important, we did not want dark adaptation to overly influence the spectral dependency during the first light steps of the experiment, compared to the last steps, where light adaption would have happened for several minutes, regardless of the dark adaptation period before the first presented stimulus. We tried periods of 90 seconds, 180 seconds, and 900 seconds on two participants with the *Up* protocol in three experimental runs, which is described under *Experiment I* below. The longer the DAP, the greater was pupilloconstriction during the first third of the steps (see supplemental *Figure S6-1*). We compared the results to a second run of the *Up* protocol directly after the first one. In this second run, wavelengths from the first half of the protocol had no prior dark adaptation phase as they are presented right after the first run. The 90-second DAP pupilloconstriction curve was closest to this second run. Therefore, we chose this period for the main experiments.

We also performed preliminary measurements with the *Up* protocol on ten subjects before the main experiments, to explore the behavior of pupilloconstriction in our setup. In those subjects, we found differences dependent on sex, particularly at the longer wavelengths (not shown). This observation was our rationale to explore this relationship in the actual experiment.

6.3.4.2 Experiment I

Experiment I was divided into two protocols, in each of which the stimuli consisted of a stepwise sweep across the available spectrum (*Figure 6-2*). One such sweep (*Up*) went from the lowest to the highest wavelength, the other (*Down*) from the highest to the lowest. Light onset happened after a dark adaptation period of 90 seconds duration at the beginning of each protocol (see above), and light remained on during the entire protocol. Light steps lasted 15 seconds each, followed by the next light step at a spectral distance of about 5 nm. We hypothesized that with continuous light that shifted slightly in peak wavelength with each step we would see the ipRGC influence in the pupil constriction amplitude by wavelength. Due to the sluggish nature of ipRGC responses [50, 112, 141], ipRGC-driven constriction might trail behind, which was an additional reason to balance the spectral protocol series by an up-down alternation. McDougal and Gamlin (112) report that ipRGC-influence at 10 to 18 seconds after light onset takes over as the strongest relative influence on pupil constriction, with rods being a close second; cones were found to have, after 10 seconds, about 1.5 to 2 orders of magnitude lower sensitivity. Since each step in *Experiment I* lasts 15 seconds, we expect a one-step delay to ipRGC pupil constriction, which would equal a 5-nm wavelength shift when looking at just one protocol. Since the changes between each wavelength step were small, the pupils quickly adjusted, usually within one or two seconds after each shift, followed by typical pupil oscillations and pupillary escape. Each protocol consisted of 61 light steps, totaling 915 seconds of light (15.25 minutes), or 1005 seconds including dark adaptation (16.75 minutes). Seventy-five participants were enrolled in *Experiment I*. Due to technical difficulties, the *Down* protocol was not available when *Experiment I* started, and was therefore measured consecutively to the *Up* protocol. Due to this sequence, the number of partaking subjects differs between the protocols, with 57 participants in the *Up* and 23 in the *Down* protocol. Of those taking part in the *Down* protocol, we measured five randomly selected participants in both protocols to check whether there were any systematic differences between the protocol groups, which was not the case. Mixed models were used in the statistical analysis to take these factors into account.

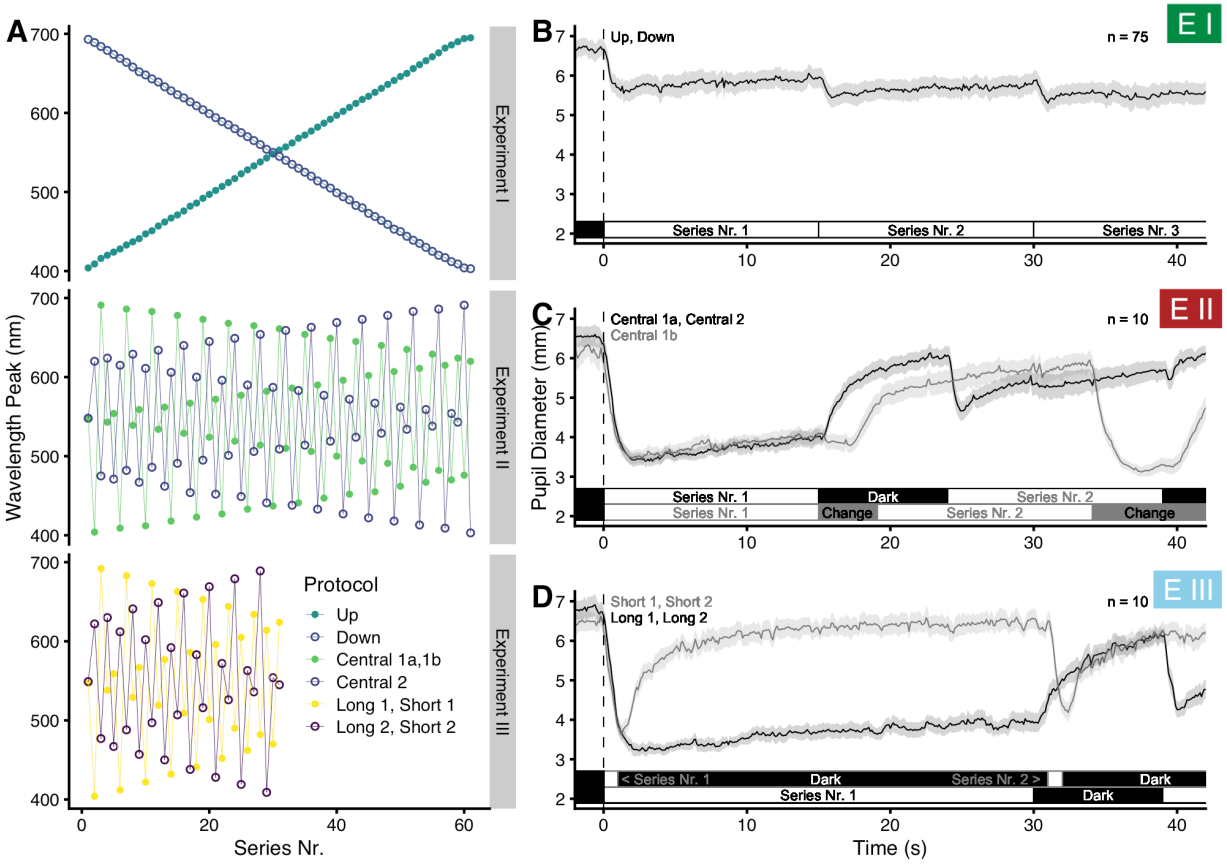

Figure 6-2 Experimental Protocols. (A) Series of peak wavelengths for each experiment and protocol. A list for the respective order of wavelength peaks is available as part of the *Supporting Information S6-4 file*. (B, C, D) Schematics of the first 40 seconds of each experimental protocol. Light onset after dark adaptation occurs at zero seconds (dotted black line). Traces show the average pupil diameter, with a ribbon representing the SEM. For visual reasons, only one of the two protocols sharing the same procedure is shown. These are *Up* (B), *Central 1a* (C), and *Short 1* and *Long 1* (D).

6.3.4.3 Experiment II

The surprise outcome in *Experiment I* was the comparatively high wavelength of 540 nm at which pupil constriction amplitude was at its maximum (see below under *Results* for all outcomes and the corresponding figures). In *Experiment II*, we thus tested whether this was due to our experimental design of small step changes along the spectrum in *Experiment I*. We wanted the series of wavelengths to be continuous, i.e., that wavelength changes would happen near instantaneous, which would be the same as in *Experiment I*. However, the monochromator required considerably more time for the changes of wavelength between steps than in *Experiment I*. We therefore designed three new protocols (*Figure 6-2 A* and 6-2 *C*). All three protocols started, after a dark adaptation phase of 90 seconds, at 548 nm, which is halfway on the available range of wavelengths. Both comprise 61 light steps in total. The series are not random, which would have led to an imprecise estimate of wavelength peaks, as we found in early tests. However, the series are designed to be as diverse as possible in terms of wavelength

changes, and regarding when in the series specific wavelengths are presented. Except for the first step, the protocols are symmetrical to the midpoint of the series axis. The protocols *Central 1a* and *Central 2* continued with differing spectral-wavelength shifts between steps. In these two protocols, the shutter was closed during the wavelength adjustment. In the longest case, the wavelength change lasted just under 9 seconds, and we set the shutter closure time to that value for all steps. The result, for both protocols, was 15 seconds of light followed by 9 seconds of darkness at each step, totaling 24 seconds per wavelength; the total series had 1464 seconds after light onset and 1554 seconds including dark adaptation, i.e. just under 26 minutes). Since the presence of dark periods between light steps in the two protocols above introduced a new factor to the experimental design, we designed the further protocol *Central 1b*. This third protocol was identical to *Central 1a*, except that the shutter stayed open at all times, i.e., there were no dark phases in between light steps, and the 15 seconds per light step started right after the wavelength adjustment (*Figure 6-2 C*).As an undesired side effect, participants perceived the adjustment of wavelengths in that series. We reasoned, however, that these brief periods (about 28 ms per 1 nm wavelength) would not influence pupil constriction amplitude 10 to 15 seconds later in a relevant manner. With all three protocols taken together we could test whether the wavelength dependency in the first experiment was due to the sequence of stimuli and whether the interruption of light in the first two protocols in *Experiment II* influenced the wavelength dependency in this experiment. Since changes in wavelength between light steps were larger in *Experiment II* than in *Experiment I*, the pupillary reactions were also stronger. In protocols with discontinuous light, the phasic part of the pupillary light reaction took about five seconds or less before changing to a tonic movement with typical oscillations and pupillary escape.

Ten participants took part in *Experiment II*. The sample size was chosen based on the first experiment. There, we saw that a random sample of ten out of the available sample for every protocol resulted in the same primary outcome for the spectral dependency. Each participant took part in every protocol.

6.3.4.4 Experiment III

Two main results in *Experiment II* led us to the design of a further experiment. *Experiment II* had shown that the spectral dependency of the nPC depended on whether or not there were periods of darkness between light steps, i.e., whether the light stimulus was discontinuous or continuous. Of particular interest was an apparent shift in wavelength sensitivity over time when light steps were discontinuous, but not otherwise. The experiment had further allowed looking at the wavelength dependency of the PIPR during the intervals of darkness. We designed *Experiment III* to build on these results. It comprised four protocols (see *Figure 6-2 D*), each of which consisted of 31 light steps following the 90-second dark adaptation phase. Light steps followed the series structure of *Central 1a* and *Central 2* from *Experiment II*; however, since each light step was longer in *Experiment III*, we halved the number of steps to not overly tire participants. The spectrum was therefore divided into steps of about 10 nm wavelength difference. The series *Long 1* and *Long 2* were designed to analyze wavelength-dependency changes over a more

extended period of time. Accordingly, each step's period was extended from 15 to 30 seconds duration, followed by 9 seconds of darkness between the steps (1209 seconds after light onset; 1299 seconds including dark adaptation, or about 21.5 minutes). The protocols *Short 1* and *Short 2* were designed to analyze the PIPR over a more extended period. Accordingly, each step's light stimulus lasted 1 second, with 30 seconds of darkness between steps (in total 961 seconds after light onset; 1051 seconds including dark adaptation, or about 17.5 minutes). In the *Long* protocols of *Experiment III*, pupil behavior was like in *Experiment II*, with an extension to the tonic part due to the prolonged stimulus. Ten participants took part in *Experiment III*. Each participant took part in every protocol.

6.3.5 Procedure

Participants arrived at the appointed time in the laboratory and were welcomed and seated. Measurements were restricted to daytime hours and were scheduled from 08:00 am to 08:00 pm (taking place, on average, at 01:30 pm ± 2:45 h:m). The laboratory was a windowless room with constant temperature, mechanical ventilation, and lit with warm-white artificial light (about 50 to 100 Lux, depending on position). Participants read and signed the prepared informed-consent form. Color vision was tested first. Illumination on the tests was cool white, with a high color-rendering index. Participants then filled out a three-part questionnaire, (1) the German translation of the Morningness-Eveningness Questionnaire for testing chronotype (D-MEQ; scores the time of preference; according to the MEQ manual [37], chronotype scores from 60 and above are considered *morning types* or *Larks*, below 40 *evening types* or *Owls*, and in between *Neutral types*); (2) general demographic questions, and (3) general questions regarding participants' current health. The experimenter then fitted the pupillometry apparatus to the participants' head and the participant lied down on a flat treatment couch with a small pillow under the head. The experimenter ensured that the infrared cameras were positioned correctly so that pupil diameter could later be calculated from camera pictures, either by adjusting the distance to the eye (in *Experiment I)* or by presenting a reference scale at eye level (in *Experiment II* and *III*). The Ganzfeld dome was then pivoted over the participants head until the eyes were at a predetermined position and only the dome's inside was visible. Room lighting was then switched off, and a black, opaque curtain between the participant and the experimenter was drawn shut. Thereby the eye-tracker camera output could be monitored on a personal computer without stray light influencing the experimental setup. Participants were instructed to relax and look straight ahead, with minimal blinking. The experimenter repeated the instructions in following procedures if compliance faded. The appropriate protocol was then started, each beginning with its 90-second dark adaptation phase, followed by the respective series (see above). Participants' eyes were not medically dilated, and both eyes received the light stimulus (closed-loop paradigm [64]). If participants took part in more than one protocol (primarily in *Experiment II* and *III*, see above), protocol order was randomized. Participants further got up from the treatment couch for about five minutes in-between protocols during which room lighting was switched on, as in the initial setting. At the end of the experimental

session, participants were thanked and debriefed. The total time participants spent on site was between thirty minutes in *Experiment I* and about two hours in *Experiment II* and *III*.

6.3.6 Data analysis

Bio-signal data analysis covered converting raw pupil data to a time series of constriction amplitudes for each participant and protocol. It further covered spectral calculations to derive photopic, mesopic, and scotopic illuminance values for each narrowband wavelength peak.

6.3.6.1 Normalized pupillary constriction

We used the *R* software (Version 4.0.2) [104] with several packages for data analysis (*anytime*, *cowplot*, *ggplot2*, *ggmisc*, *knitr*, *readxl*, *signal, tidyverse)*. Raw pupil data were stored in pixel-based units by the measurement software, and exported to CSV files. These values were converted to mm and mm² by a factor derived from the *ImageJ* software [154], using screenshots from the eye tracker videos with included reference scales (see above). Blinks and other artefacts were then removed by calculating a *circularity index* (ratio of pupil height to width, and width to height). Pupil values with a *circularity index* smaller than 0.7 were removed [50, 155]. We also removed pupil diameter values outside reasonable thresholds, usually when above 8.5 mm or below 1.5 mm pupil diameter. However, in some cases, a different cut-off was decided upon after visual inspection. A Savitzky-Golay filter [98] with a third-degree polynomial [83, 156] was used for smoothing of the pupil data; filter length was set to 31 data points or about 0.5 seconds. The same filter was also used to calculate the second derivative of the smoothed curve – valleys in the second derivative coincide with the early stages of pupil constriction. The timestamps of these valleys were used to shift the measurement time according to light onset. The shift was monitored visually and, when necessary, manually adjusted. After this correction, time values are negative during dark adaptation, light onset happens at zero seconds, and the experimental lighting conditions occur at positive time values according to the protocol.

In the next step, the normalized pupillary constriction (nPC) was calculated at each time step *i, as*

$$nPC_i = \frac{diameter_{baseline} - diameter_i}{diameter_{baseline}} \times 100\% \quad (1).$$

We use the term nPC instead of *pupillary constriction amplitude* suggested by Kelbsch et al. (64). Both are calculated the same way. However, nPC (since it does not refer to an amplitude) might be the more natural term for the prolonged stimulation in our experiments. The normalized pupillary constriction is defined as the decrease of pupil diameter, normalized to a baseline level (generally the baseline before stimulation [64]), thereby controlling for the considerable variation of inter-individual pupil size, as well as for its (smaller) intra-individual variation [64, 143]. The baseline diameter corresponds to 0% constriction, and the (impossible) pupil diameter of 0 mm would correspond to 100%

constriction. As an example, a light-adapted diameter of 2 mm from a baseline pupil diameter of 8 mm equals 75% constriction amplitude. As we used a comparatively short dark adaptation period, followed by a long series of light steps, we believe that the pupil diameter at the end of the dark adaption phase somewhat loses its prominence, as it is mostly unrelated to any particular wavelength peak across the protocols. Therefore, we used the largest one-second-mean pupil diameter (see below) as the pupil baseline, taken from the period between the last seconds of dark adaptation until the end of each protocol. This baseline still takes interindividual differences into account, while intraindividual differences are already taken care of through the continuous measurement over all wavelengths per person and protocol. By definition, nPC can only take positive values here. To check whether our normalization method affected the results in an undesirable way, we performed an additional primary analysis without normalization in *Experiment I*, and further tried an alternative normalization in *Experiment II* and *III* to the average diameter during the last second of darkness before each light step. Since we had measurements for both eyes, one eye was discarded at the next step; the eye with the highest count of remaining data points was kept unless visual inspection showed abnormalities. The CSV export from the collected steps above contained the pupil diameter (mm), nPC_i (%), Series number, time since dark adaptation/light onset (s), time since the start of the light step (s), wavelength (nm), baseline diameter (mm), participant code, eye, date, time, and protocol name. Data in the CSV export file were further aggregated in two ways, so besides unaggregated pupil data (i.e., with 60 Hz sampling frequency) the file contained one-second means, and means over specific periods. The specific periods were the last five seconds of each light step, for every protocol except *Short 1 or Short 2,* in which the sixth second after light offset was used instead [52]. In a final step before the statistical analysis, the pupil data were combined with participant data (sex, age, chronotype), and spectral data (see *Figure 6-1* and below). The scripts to derive the input data for the statistical analysis are available as *R-Markdown* files as part of the *Supporting Information*, in the S5-*2 file*. All data used in the statistical analyses are available as CSV files from the *Open Science Framework* [157]. Before the experiments we tested and calibrated the eye tracker on a reference head and pupil. Camera resolution, combined with the mean camera-to-eye distance of 27.5 mm, led to a resolution of 10 pixel per mm at pupil level. Pupil height or width changes can thus be tracked to about 0.1 mm accuracy or 1.5% nPC, assuming a baseline pupil of just under 7 mm.

6.3.6.2 Spectral calculations

From the spectral irradiance measurements, total irradiance was calculated automatically by the measurement software (see above). Similarly, illuminance values were automatically calculated according to the CIE-1931 standard 2° photopic observer which uses the V(λ) function [158], as well as according to the CIE-1964 standard 10° photopic observer, which uses the $V_{10}(\lambda)$ function [159]. The five types of alpha-opic equivalent (D65) daylight illuminance were calculated according to the CIE S 026 standard *(CIE-S-026-EDI-Toolbox-vE1.051*) [73]. We also used the *Melanopic-light-sources_Toolkit*

(*V13.12*), which was developed and provided to us by Dieter Lang [160]. The toolkit provided illuminance values for the CIE-1951 scotopic observer with V'(λ) [161] spectral weighing in addition to the alpha-opic values. Illuminance for the mesopic observer was calculated according to the German standards DIN 5031-2 [162] and DIN 5031-3 [163] through $V_{eq}(\lambda)$ weighing functions. The standards were recommended by Adrian (138). The CIE has since released the standard CIE 191:2010 for mesopic photometry, which is based on the same basic principles but uses a different calculation procedure and notation ($V_{mes;m}(\lambda)$) [164]. In the German standards, illuminance calculations for the mesopic observer use spectral weighing functions $V_{eq}(\lambda)$ that are intermediary between the photopic $V_{10}(\lambda)$ and the scotopic V'(λ) function, in addition to intermediary luminous efficacies of radiation. These intermediaries are chosen based on the adapting equivalent luminance L_{eq} for a 10° observer on a $\log_{10}$-based scale between the photopic (100 cd/m²) and scotopic (10^{-5} cd/m²) endpoints defined by the standards. Our calculations were performed using *Microsoft Excel* software. We used the corneal stimulus intensity (log irradiance, without prereceptoral filtering) in our analysis. Estimates for prereceptoral filtering on irradiance and photon density are available as part of the *S6-3 file.* We used the method from Lund et al. (165) to calculate the age-dependent filtering as suggested in the CIE *S 026* standard [73]. A visual comparison of spectral irradiance with vs. without prereceptoral filtering for the median age of 26 years is displayed in the supplemental *Fig S6-17*. Peak wavelength-shifts due to prereceptoral filtering were small and did not occur above 428 nm. Spectral irradiance with filtering had a higher peak wavelength of 1 nm for 428, 424, and 420 nm; it was 3 nm higher for 416 nm and 409 nm, and 5 nm higher for 404 nm. These changes in peak wavelength are identical through our age range between 18 and 36 years. The spectral measurements for the range of peak wavelengths, including total irradiance and all types of illuminance values are provided as part of the *Supporting Information*, in the *S6-3 file*.

6.3.7 Statistical methods

We used the *R* software (Version 4.0.2) [104] with the *mgcv* (Version 1.8-31) [60] package to perform a *generalized additive mixed-effect analysis* on the connection between normalized pupillary constriction and the empirically and theoretically derived predictors. *Generalized Additive Models* (GAMs) [60, 166] allow for a data-driven decomposition of the relationship between a dependent variable and user-defined predictor variables in both a parametric and nonparametric fashion. A variant of GAMs are *Generalized Additive Mixed-Models* (GAMMs or HGAMs), used in the context of hierarchical data as is the case in any repeated-measures setup such as ours [62]. GAMs are widely used in *Biology*, *Ecology*, and *Linguistics* [60]. GAM(M)s are not yet used often in *Human Life Sciences* [167], but we find them an excellent match for the analysis at hand, and mixed-effect models gain support in biophysiological research such as visual perception [168] and nonvisual effects of light [39]. Guidelines on the theory behind GAMs and their practical use can be found in Wood (60), Simpson (63), Pedersen et al. (61), and the guide by Sóskuthy (62).

The nonparametric parts of GAMs take the form of *smooth* functions (*smooths*, in short), describing the connection between the outcome variable and a predictor. A *smooth* function $f(x_i)$ is the weighted sum of a number k of basis functions b_j at the i-th value of a predictor variable x:

$$f(x_i) = \sum_{j=1}^{k} b_j(x_i)\beta_j \quad (2)$$

The β_j in *eq 2* denote the weights (the *smooth* coefficients) of the basis functions $b_j(x_i)$. Since GAMs are not yet widely familiar in this field of research, their concept is visualized in *Figure 6-3 A*. The type of basis function is chosen as part of the model construction, with *cubic regression splines* being probably the most well-known type (*Figure 6-3 A1*). Unless otherwise stated, we used the *mgcv*-default type of basis functions, which are *thin plate regression splines* (TPS). Wood (60) gives a comprehensive overview of basis functions and their suitability depending on the context. Unlike coefficients in a normal parametric regression, the basis-function weights β_j in generalized additive models are not by themselves interpretable towards the modelled relationship (*Figure 6-3 A2*). Only by knowledge of the set of basis functions and their eponymous weighted addition ("*additive" models*) can the resulting *smooth* function be interpreted (*Figure 6-3 A3*). One of the underlying assumptions to the *smooths* is a constancy of complexity across the value range of x. That means that *smooths* do not do well without additional adjustments, if constructed from relationships that vary heavily in their dynamics across the range, or that exhibit discontinuous changes (step-changes). These adjustments include the use of *adaptive splines* for varying dynamics, or the use of factors for step-changes [60]. *Smooth* functions can be multi-dimensional, thereby describing interdependent relationships or interaction effects between predictors and the outcome variable. The number k of basis functions is chosen based on the complexity of the modelled relationship present in the data. Overfitting is avoided through the penalization of complexity as part of the likelihood optimization. Therefore, added complexity (or *wiggliness* [60]) in the *smooth* needs to improve the model fit enough – compared to, e.g., a straight line – to outweigh the penalization. More broadly, GAMs ascertain to model the simplest possible relationship between variables, or no relationship at all, without leaving out relevant structural components depending on any given predictor.

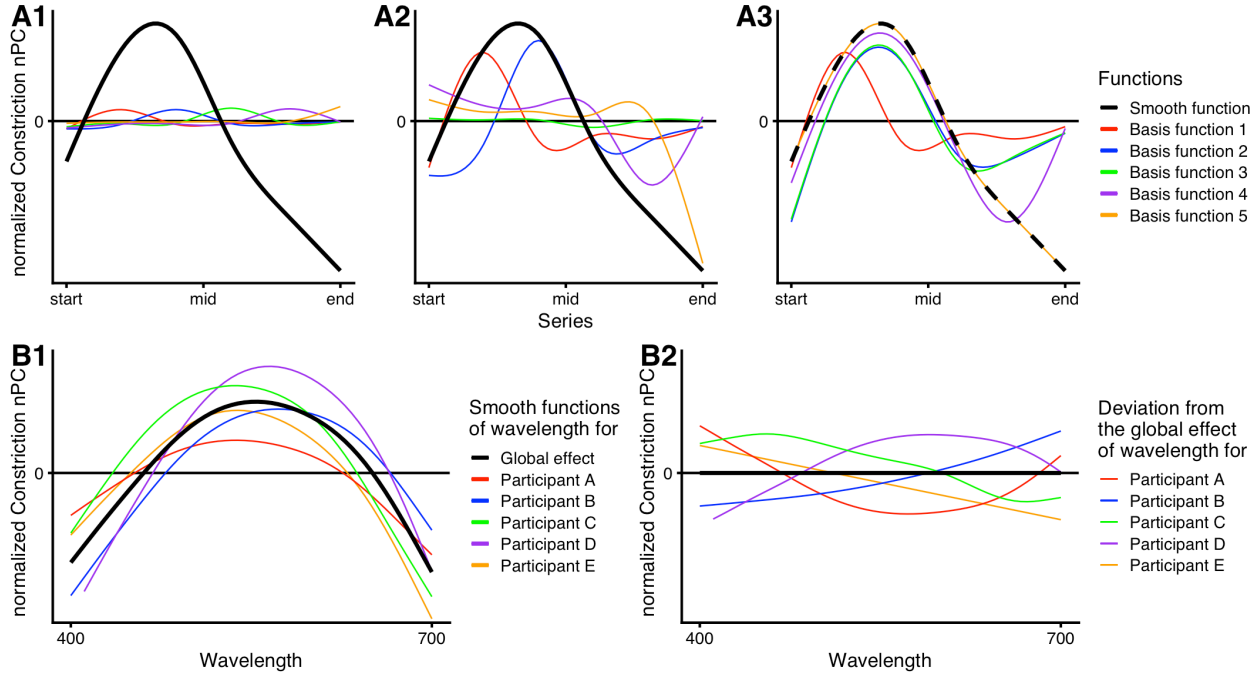

Figure 6-3 Concepts of additive (mixed-effect) models. (A) Construction of a *smooth* through *basis expansion*. Every *smooth* is constructed from a number of basis functions, usually spread evenly across the value range of a predictor. In the shown case, five cubic regression splines were used as basis functions to demonstrate the concept. The thick black line represents the final *smooth* function, describing the relationship between the predictor and the outcome variable. Colored traces show the basis functions. (A1) Unscaled basis functions – their type and maximum number are part of the input for model generation. (A2) Scaled basis functions – for each basis function, a respective weight is estimated by which the function is scaled. (A3) Summation of basis functions, starting with the first and then, successively, adding the others; the generated *smooth* can then be used for prediction. The *smooth* is shown as dashed curve to show that, with the addition of the last basis function (orange line), the resulting curve is equal to the *smooth* function. (B) Concept of global effects with random *smooths*. (B1) The thick black line represents the global effect, describing the average relationship between the predictor and outcome variable. Colored traces show the individual's effect of the same predictor, demonstrating interindividual differences. The model takes these differences into account through the so-called random *smooths* (i.e. "random" in that their contribution depends on the subject). (B2) Random *smooths* are *smooths* describing the deviations from the global effect. The colored traces show the deviations present in panel B1. Because the global *smooth* and the random *smooths* are estimated together, the deviations disappear on average, i.e., not all deviations will tend in the same direction, but are spread around the global effect.

If not stated otherwise, we used *Akaike's Information Criterion* (AIC) for model selection, as suggested by several sources on GAM(M)s [60-63, 169]. The AIC incorporates model fit (likelihood) and model size (number of parameters) [60]. It can further be compared between similar models, with the lower value indicating the better-suited model. Following the example of Pedersen et al. (61), models that differ by two units or less from the lower AIC have substantial support, with the more parsimonious model to be preferred. We report ΔAIC values when there is support for the inclusion of a predictor.

T-tests obtain p-values for parametric terms. The p-values for nonparametric terms are *approximate p-values*, so called owing to the complexity of the *degrees-of-freedom* (*df*) concept used for statistical testing, and other underlying assumptions [60, 62]. For non-parametric terms, the hypothesis tested-against states that the relationship between predictor and dependent variable is a horizontal, flat line. P-values less than or equal to 0.05 were considered significant. Confidence intervals in prediction plots account for the model's overall uncertainty, not for the respective plotted predictor alone.

We explored the nPC's relationship with *wavelength*, *irradiance*, *series, time*, *time of day*, *sex*, *chronotype*, and *age* by the methods described above. We further looked for the nPC's best fit to *photopic, scotopic, and mesopic illuminance*, and *alpha-opic equivalent-daylight illuminance* values. The variable *wavelength* refers to the dominant or peak wavelength of the narrowband stimuli as described above. After light offset, *wavelength* refers to the prior light stimulus. *Series* refers to the numbers of light steps after the dark adaptation phase. *Time* refers to the time since the start of the current light stimulus, i.e., light onset or change in wavelength. Several additional R packages were used for the statistical analysis and plot generation (*tidyverse*, *ggplot2*, *readxl*, *dplyr*, *cowplot*, *lubridate*, *itsadug*, *printr*, *patchwork*, *here, reshape2, plotly*, *gganimate*, *gridGraphics*, *transformr*, *glue, magick,* and *DT)*. All scripts for analysis and plot generation are available as *R Markdown* files in the *Supporting Information*, S6-*4 file*.

6.3.7.1 Base model structure

While the relevant code is included as part of the *S6-4* file, we believe it helps explaining the basic model structure and settings used to analyze the experimental outcome. The model structure is one of five basic GAMM variants (according to Pedersen et al. (61)), which differ in how fixed and random effects are included. The chosen variant, by way of AIC comparison and model diagnostics, is shown in the following equation:

$$E(nPC_i) = \alpha + f_1(wavelength_i) + f_2(series_i) + \beta_1 \times log_{10}(irradiance_i) + b_p + f_p(wavelength_i),\ where\ nPC_i \sim \frac{N(\mu_i, \sigma^2)}{\sqrt{\frac{\chi^2_n}{n}}},\ and\ b_p \sim N(0, \sigma_b^2) \qquad (3)$$

Eq 3 shows the statistical base model, where the expected value of nPC $E(nPC_i)$ is modelled by *smooths* as a function of *wavelength* (f_1) and *series*(f_2), and a parametric effect of *log*$_{10}$*(irradiance)*; α is the average nPC, when all other terms are zero, also called the intercept; β_1 is the parametric coefficient, or slope, for *log*$_{10}$*(irradiance)*; b_p are random intercepts by participant; and $f_p(wavelength_i)$ are random *smooths* by participant.

Wavelength is the main predictor, *series* was included for empirical reasons, i.e., in the cases when visualization of the nPC data in *Experiment I* showed the influence of the protocol (*series)*. As stated above under *Apparatus*, *irradiance* is theoretically motivated to compensate for lower irradiance levels under 450 nm wavelength. However, *smooth* behavior from 400 to 450 nm still has to be interpreted tentatively, since the estimate for *irradiance* might under- or overcompensate the effect, thereby distorting the influence of

the lowest wavelengths on nPC. We account for this by leaving *irradiance* out of the model in a secondary analysis and discuss differences between the variants.

As random effects in *Experiment I* we had random intercepts b_p and random *smooths* $f_p(wavelength_i)$ for each participant *p*. In *Experiment II* and *III*, all participants took part in all protocols; we, therefore, had random effects for participants-by-protocol in those cases [62]. Random intercepts describe the deviation from the average nPC (α) depending on the participant (or participant-and-protocol), with independent and gaussian distributed values. Random *smooths* can be thought of as the nonparametric version of random slopes in *linear mixed-effect models*. Random *smooths* allow for the individual's deviation from the global effect $f_1(wavelength_i)$, but zero-out on the global effect when viewed on average across participants (*Figure 6-3 B*).

For the distribution of our response variable, PCA_i, which takes positive values between 0 and 1, the *gamma* or *beta* distribution seemed sensible assumptions initially. However, model diagnostics with those were poor compared to even the standard *gaussian* error distribution. Instead, we thus went with the *scaled-t* (*scat in mgcv*) distribution family, which is less susceptible to outliers and indeed greatly improved residual distribution. Eq 3 states that PCA_i varies around its mean μ_i with a t-distribution based on the standard deviation σ and n degrees of freedom. We also tested a model with the *gaussian location-scale* (*gaulss in mgcv*) family. This distribution allows the variance to change depending on a predictor, just like the mean. However, we did not find relevant differences in variance, and the model with the *scat* family performed similarly well with respect to the AIC. The *gaulss* family did further not allow for the computationally faster *bam* command, so we used the *scat* family for the analysis.

We used the *gam.check* function of *mgcv*, which includes several residual plots for model diagnosis. Visual inspection of these plots did not reveal any apparent deviation from homoscedasticity or normality. Models were further controlled for autocorrelation in the residuals. In all models that used only one timestep per wavelength peak (5-second average nPC), the inclusion of random effects diminished all relevant autocorrelation. In models that used 1-second averages for nPC, random *smooths* by *wavelength* left serious residual autocorrelation present. Random *smooths* by both *wavelength* and *time* proved too computationally intensive in those cases and we instead included the remaining autocorrelation with an autoregressive error model [62, 63], in addition to random *smooths* by *wavelength*. Finally, the number of knots for each *smooth* (i.e., how many basis functions comprise the *smooth*) was also checked (*k.check*) and was increased, when theoretically sensible, until autocorrelation along the *smooth* vanished [61]. For computational speed reasons, we used the *bam* function with *fREML* in R instead of the standard function of *gam* with *REML*. *Bam* is optimized for big data sets and model structures.

If not otherwise stated, GAMs in the *Results* section were used to model normalized pupillary constriction (nPC) according to *eq 3,* the latter also called the base model. Ad-

ditional parametric and nonparametric predictors were explored – their addition to or removal from *eq 3* are stated in the respective sections. The default nPC is the average value of each light step's last five seconds, as described above.

6.3.7.2 Linear mixed-effect model structure

We used the *lme4* package [41] to perform a *linear mixed-effects analysis* of the relationship between nPC and the various illuminance variables described above:

$$E(nPC_i) = \alpha + (\beta_1 + \beta_p) \times log_{10}(illuminance_i) + b_p,$$
$$where\ nPC_i \sim (\mu_i, \sigma^2), b_p \sim N\left(0, \sigma_b^2\right), and\ \beta_p \sim N\left(0, \sigma_\beta^2\right) \quad (4)$$

Intercept α and slope β_1 are the fixed effects of the model described in *eq 4.* The intercept α indicates the value of nPC, when all other terms in the equation are zero. The slopes, or beta coefficients, β_1 and β_p, represent the change in the expected value of nPC_i when increasing illuminance by one log unit. As random effects we included random intercepts by participant, b_p, and random slopes by participant, β_p, both of which have independent values with a *gaussian* distribution. Random intercepts b_p show how much individuals deviate from the average nPC α with a variance of σ_b^2. Random slopes, similarly, show how much the relationship between the predictor and outcome variable deviate from the fixed effect β_1 with the variance σ_β^2. nPC_i has a *gaussian* distribution, with variance σ^2 around its mean μ_i. The proportion of variance-accounted-for (R^2) was calculated according to Xu (170).

6.4 Results

An overview of the experimental data and circumstantial conditions is shown in *Figure 6-4*. *Figure 6-4 A* shows plots for nPC vs. wavelength for each protocol, where the underlying data are not controlled for any dependencies. Non-normalized pupil diameters vs. wavelength are shown in supplemental *Figure S6-16. Figure 6-4 B* shows *chronotype* vs. *time of day*. Noteworthy is the lack of *Owl* chronotypes before midday, as well as pronounced *Larks* in the morning. *Figure 6-4 C* shows at what time in the year the experiments took place, as suggested by Veitch and Knoop (171). Experiments took place in 2019 (preliminary measurements, *Experiment I*) and in 2020 (all experiments).

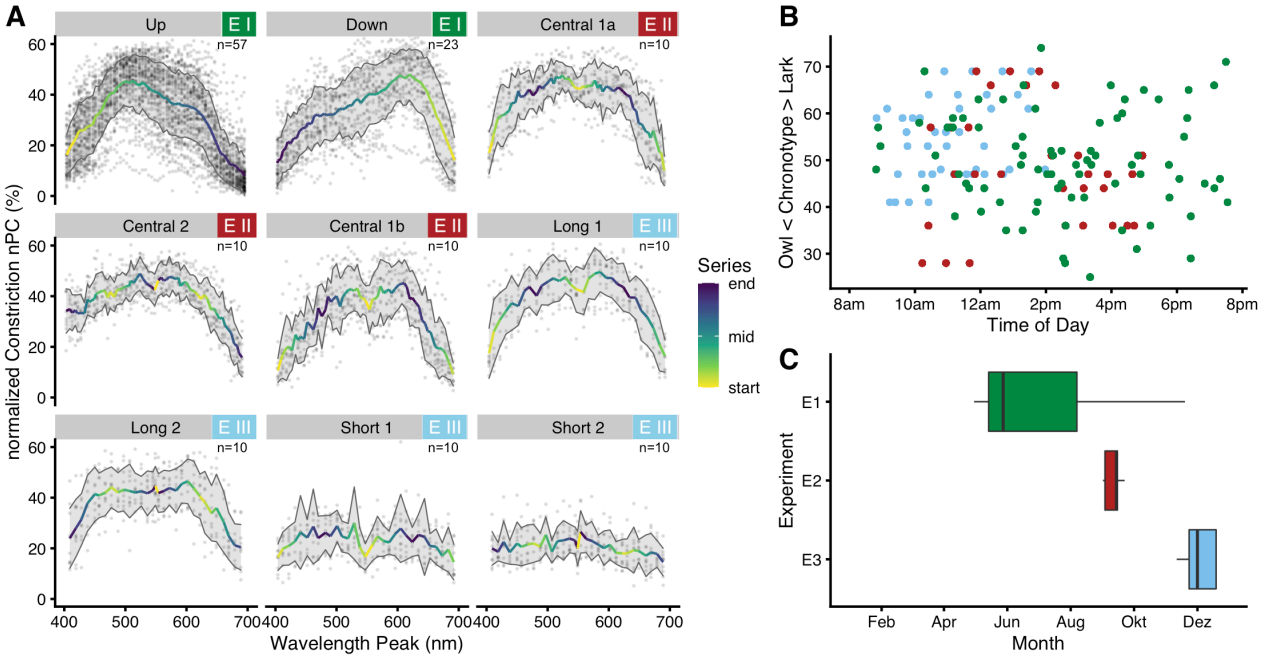

Figure 6-4 Experimental data and circumstances. (A) Normalized pupillary constriction (nPC) plotted against wavelength, for each of the nine protocols. The color scale shows at which point in the series a specific wavelength was presented; light yellow represents early in the series. For all but the *Short* protocols, points represent the average nPC during the respective last five seconds of a light step. In the two *Short* protocols, points represent the average nPC during the sixth second after lights-off (or sevenths second after lights-on). Traces show the mean nPC, ribbons its standard deviation. The number in the upper right corner of each plot shows the corresponding sample size. (B) Scatterplot of when subjects of a certain chronotype started their respective protocols. The color scheme is according to (C), i.e. green, red, and blue correspond to Exp. I – III, respectively. Note the lack of *Lark* and *Owl* chronotypes in *Experiment I* before midday. (C) Boxplot of the time of the year when the experiments took place. Preliminary measurements and parts of *Experiment I* took place in 2019, the other measurements in 2020.

6.4.1 Experiment I

6.4.1.1 Base model results

The results for the base model of all three experiments are shown together in *Figure 6-5,* for better comparison. The results for *Experiment I* are shown in *Figure 6-5 A* and are reported in this section; the results for *Experiment II* and *III*, as well as secondary results for *Experiment I* are shown here in *Figure 6-5 B*, *C*, and *D*, respectively, but are reported below in the respective sections. The statistical base model contains *wavelength* and *series* as nonparametric predictors, and log_{10}*(irradiance)* for the average nPC during the last five seconds of each light step as a parametric predictor. There is strong support for a dependence on *wavelength* in its implemented form versus other random effect structures (minimal ΔAIC = 33), or no wavelength dependence (ΔAIC = 4963), as there is for including *series* as predictor (ΔAIC = 390). *Irradiance* did improve the model further (ΔAIC = 17). All p-values in the final model were below 0.001. The dependence on *wavelength* shows an inverted-U shaped curve with a peak at 540 nm, and an average nPC

of about 38% when controlling for all other factors (*Figure 6-5 A1*). Compared to the maximum, nPC is predicted by the model as up to 11% lower for short wavelengths and up to 17% lower for long wavelengths. The dependence on *wavelength* shows a peak at 550 nm when not controlling for *irradiance* (supplemental *Figure S6-15A*). With respect to series effects, nPC increases slightly with *series* up to step 18 (by about 3%), which occurs at about 360 seconds after the protocol start, or, respectively, 270 seconds after lights-on (*Figure 6-5 A2*). After this point, nPC declines by about 13% until the end of the protocol. nPC further increases with *irradiance* ($\beta_{log10(irradiance)}$ = +6.5% ±1.4% SE), as seen in *Figure 6-5 A3*. The standard deviation of the random intercept by participant, σ_b^2, was 8% in *Experiment I*. While a balanced sample between the *Up* and *Down* protocols would have been preferable, GAM(M)s allow for imbalanced data. Larger sample groups are not weighted more heavily, and global effects are adjusted for across groups. We also performed the base-model analysis with a random sample of ten participants from the *Up* and *Down* protocols, obtaining the same outcome for wavelength dependency (see the *Supporting Information, S6-4*). We thus decided on a sample size of ten subjects for *Experiment II* and *III*.

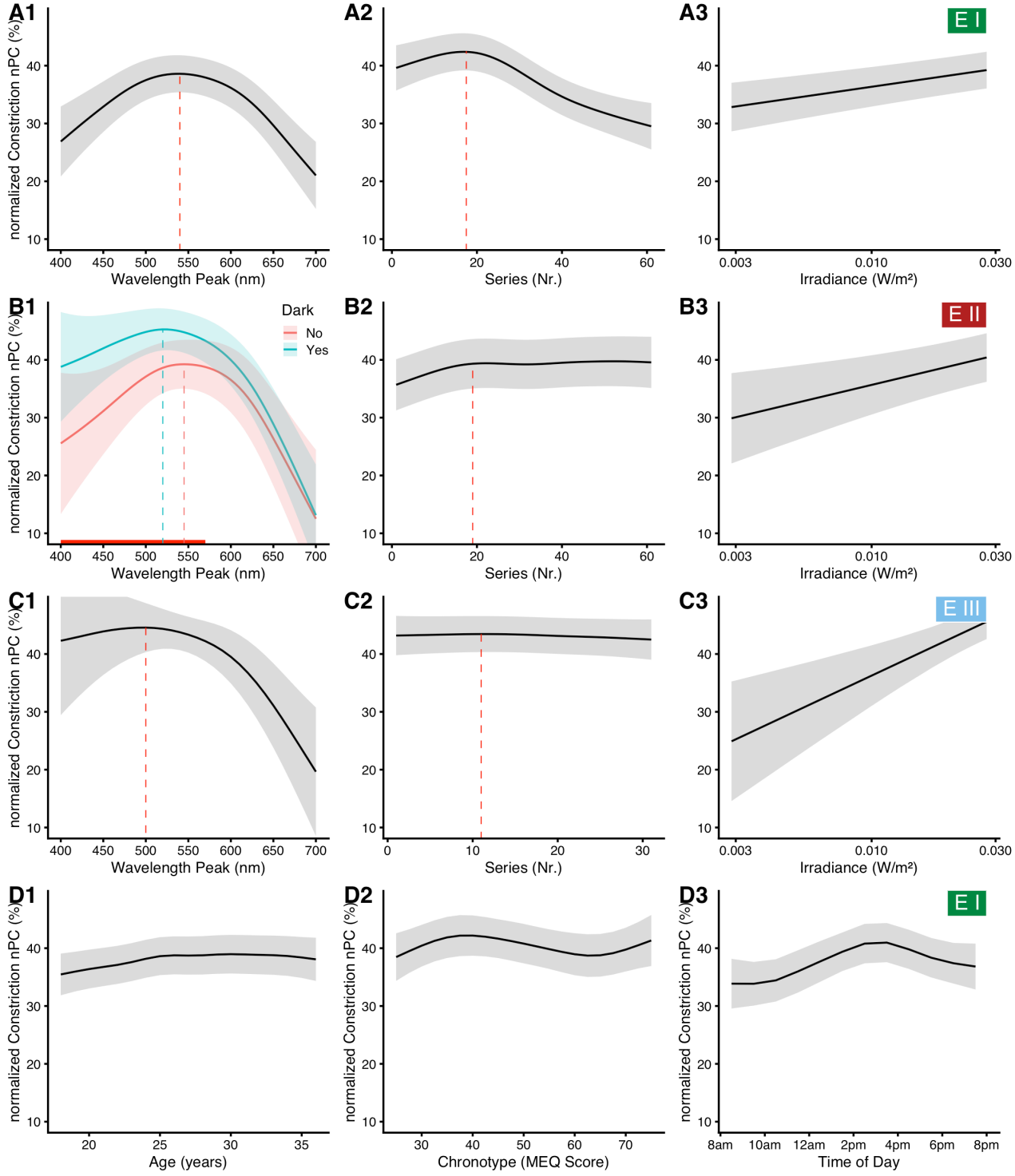

Figure 6-5 Model predictions. Model predictions for normalized pupillary constriction (nPC) as depending on several main predictors, when all other predictors are held at an average, constant level. Traces show the model prediction for the mean, ribbons its 95% confidence interval. Dotted lines show a peak that is discussed in the main text. In (A3, B3, and C3), the x-axis is logarithmically scaled to reflect the logarithmic transformation of *irradiance* in the model. (A) and (D) show dependencies in *Experiment I*, discussed here, (B) and (C) dependencies in *Experiment II* and III, respectively, discussed later. (B) The red line at the bottom of (B1) indicates where the two curves differ significantly at the 0.05 level of significance.

6.4.1.2 Interaction of series and wavelength

There is some support for an interaction of *wavelength* with *series*, i.e., that changes of nPC with *wavelength* depend on when, in the series, specific wavelengths are presented (ΔAIC = 5). Results for that are shown in a supplemental figure (S5-5). The model prediction with the interaction effect shows little or no deviation from the basic model results at the instances with data. Compared to the model without interaction, nPC is predicted to be lower for very short and long wavelengths occurring right after light onset. Wavelengths around 600 nm further lead to a more pronounced nPC during the early steps of the series, while for wavelengths around 500 nm nPC is slightly lower during the later steps. In terms of ipRGC sensitivity, it seems as though, compared to the model without the interaction, nPC is heightened at, and a few steps after, reaching the sensitive wavelengths around 490 nm, but the effect is small. With the interaction effect as part of the model, *irradiance* is no longer significant ($p = 0.31$).

6.4.1.3 Sex and age

There is further support for an influence of *sex* on the nPC (ΔAIC = 85). On average, women had a smaller nPC than men (β_{Women} = –4.4% ±0.4% SE, $p < 0.001$). The mean difference in pupil constriction (not normalized) between the groups was 0.21 mm ±0.024 mm SE. Our preliminary measurements indicated that the *wavelength* dependency of nPC is conditional on *sex* (not shown). There was, however, no interaction of *sex* with either *wavelength* ($p = 0.98$) or *series* ($p = 0.27$) based on the larger sample from *Experiment I.* With *age* as a predictor (*Figure 6-5 D1*), nPC increased by about 3% from age 18 up to about age 25 (ΔAIC = 245, $p < 0.001$). At higher age, nPC reached a plateau. We did not see changes in *wavelength* with *age* ($p = 0.67$).

6.4.1.4 Chronotype and time of day

There is strong support to include *chronotype* and *time of day* as predictors, together with a three-way interaction of these with *wavelength* (ΔAIC = 47 and ΔAIC = 130, respectively). Main effects of *chronotype* and *time of day* are shown above in *Figure 6-5 D2* and *D3.* In general, *Owls* have a slightly higher nPC compared to *Larks* (*Figure 6-5 D2*), and nPC was highest during the early afternoon around 3 pm (*Figure 6-5 D3*). According to the interaction model, subjects with neutral chronotype (chronotype score of 50) showed no substantial change in wavelength dependency across the day (*Figure 6-6 A2,* blue curves). In contrast, subjects with pronounced chronotype did (*Figure 6-6 A2,* green and red curves; for a complete overview from 8:30 am to 7:30 pm see supplemental *Figure S6-7*). *Larks* (green traces) were shifted in sensitivity towards short wavelengths before midday, were about equal to *Neutral* types at around noon and early afternoon, and were more sensitive to longer wavelengths in the late afternoon. *Owls* (red traces), on the other hand, were shifted opposite; before midday they were more sensitive to longer wavelengths, were close to *Neutral* types at midday and early afternoon, and were more sensitive towards shorter wavelengths during the evening hours. Not every point of this three-dimensional interaction structure has enough data points to support all predictor

variable combinations. Missing combinations occur in particular for extreme chronotypes and measurement hours, as was shown in *Figure 6-4 B* above. However, enough structural points are present to support the dependency thus described (see supplemental *Figure S6-8* for more details). To test whether the chronotype effect that we saw was confounded by *age* or by a covariance between *chronotype* and *time of day*, we calculated the Pearson correlation between the variables. Neither of the combinations of *age*, *chronotype*, or *time of day* had a strong correlation (all $r \leq 0.13$) or was even significant (all $p \geq 0.26$). To increase the number of combinations, we pooled the data from all experiments. The results from the pooled data model are shown in *Figure 6-6 B*, but reported further below.

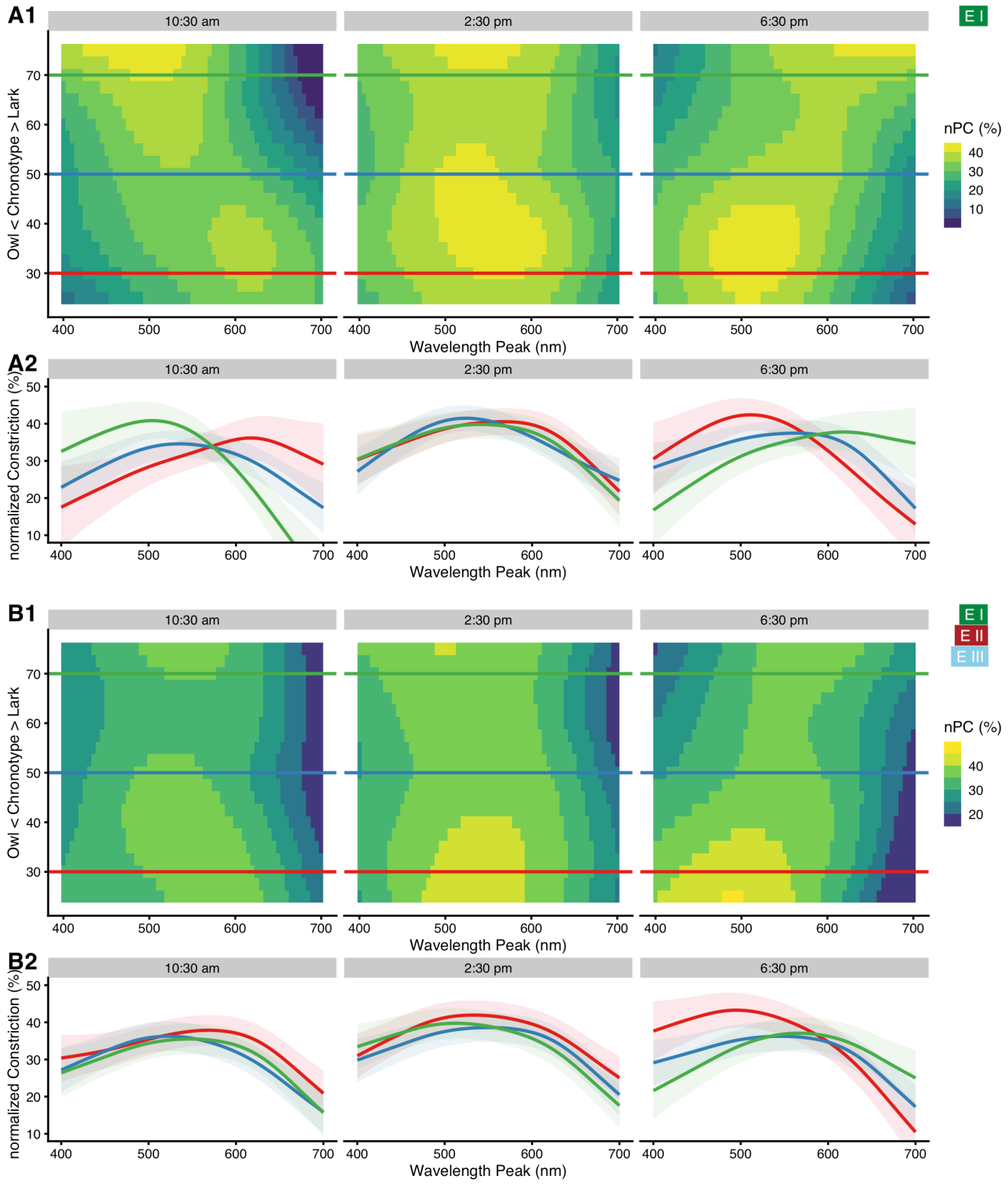

Figure 6-6 Interaction of *wavelength*, *chronotype*, and *time of day*. (A1) False-color graph of model predictions for the nPC's dependence on *wavelength* (x-axis) and *chronotype* (y-axis) for three times of day, when all other predictors (basic model) are held constant at their average. Horizontal lines show where the respective three traces shown in figure part (A2) are taken from. (A2) Model predictions for the nPC vs. wavelength for three chronotypes (trace color), and three times of day. Green traces show *Larks* (CT score = 70), red traces *Owls* (CT score = 30), and

blue traces *Neutral* types (CT score = 50). Ribbons show the 95% confidence interval for the predicted means. (B1/B2) Like (A), but for pooled data across all experiments. See the main text for further details.

6.4.1.5 Other Results

When all significant terms are added to the model – i.e., *the interaction of wavelength and series*, the main effects of *sex* and *age,* and further the *interaction* of *chronotype* with *time of day* and *wavelength* – all model terms remain significant (all $p < 0.001$) except for *irradiance* ($p = 0.31$). More importantly, the predictor-response relationship across the terms is very similar to the descriptions above. One exception is the effect of *age*. When controlling for *chronotype* and *time of day*, nPC is predicted to gradually rise across the whole range from age 18 to 39 (supplemental *Figure S6-6 B*), as opposed to only the range from age 18 to 25 (supplemental *Figure S6-6 A*). This full model was also the best in terms of AIC yet (min ΔAIC = 58). AIC would have been further improved by dropping the main effects of *chronotype* (ΔAIC = 7) or *time of day* (ΔAIC = 40). However, it is not advisable to drop the main effects in the presence of an interaction [60]. Curiously, most of the random *wavelength*-by-participant *smooths* were not significant in this model (61 out of 75). This indicates that the fixed effects above account sufficiently for the interindividual differences in *wavelength* dependency from roughly 80% of participants.

nPC was calculated for the centered and scaled pupil size, as described above in *Materials and methods* (*eq. 1*). When the pupil diameter is not scaled but is centered on the baseline, results show the pupillary constriction in mm instead of in per cent. When pupil diameter is neither scaled nor centered, results show the raw pupil diameter in mm. We explored those two variants of the response variable, but results do not indicate that such scaling changes the model's composition or interpretation (supplemental *Figure S6-9*).

6.4.1.6 Illuminance

To analyze how well each type of illuminance can predict nPC, we constructed several simplified standard linear mixed-effect models according to *eq 4,* with a fixed effect for illuminance, and random intercepts and slopes per participant. Illuminance values were $\log_{10}$ transformed. Nine measures of illuminance were used as described above in *Materials and methods*: photopic illuminance for foveal and ganzfeld stimulation (2° and 10° observer according to *CIE* standards), mesopic and scotopic illuminance, and the *alpha-opically weighted equivalent daylight illuminances* for the five types of photoreceptor. Since the scotopic illuminance and rhodopic equivalent daylight illuminance use the same underlying action spectrum, results on model fitting are identical between these two types of illuminance. Therefore, only results for the scotopic model will be shown in the figures. *Figure 6-7* shows the results for all three experiments together for better comparison. The results for *Experiment I* (*Figure 6-7 A*) show that the photopic (2° and 10°) and especially mesopic functions are much better at predicting nPC ($R^2_{illu} \geq 0.41$) than the commonly used melanopic and rhodopic (viz. scotopic) receptor functions

($R^2_{illu} \leq 0.24$). Of the three cone functions, erythropic and especially chloropic weighing led to good results ($R^2_{illu} \geq 0.42$), whereas cyanopic weighing was the only illuminance type with no support at all by the model ($p = 0.37$, $R^2_{illu} < 0.01$). Results for Experiment II and III are shown in *Figure 6-7 B* and 6-7 *C*, respectively, for better visual comparison across the experiments. Their results are reported below in the respective sections.

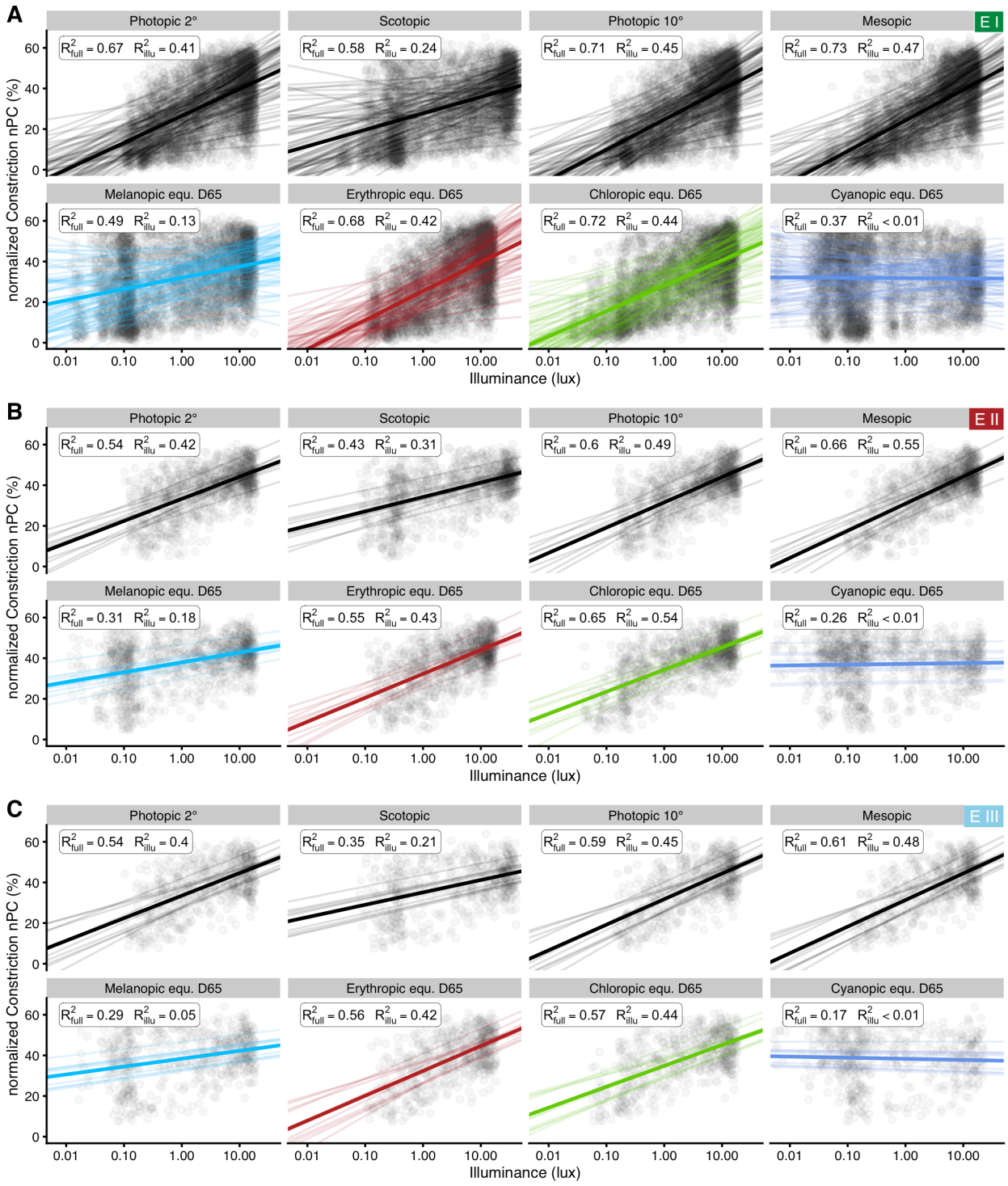

Figure 6-7 Linear mixed-effect model results for nPC's dependency on illuminance. Model predictions for nPC vs. various measures of illuminance. Points show individual data. Thick regression lines show the fixed-effect relationship and thin regression lines random effect variation in slope and intercept by participant. The insets show R^2_{full} for the full model (fixed and random

effects), and, more importantly, a partial R^2_{illu}, i.e. the proportion of variance explained through nPC's relationship with the fixed effect of illuminance. Part (A) shows results for *Experiment I*, (B) for protocols with darkness between light steps in *Experiment II*, and (C) for protocols with thirty seconds of light, followed by nine seconds of darkness in *Experiment III*.

6.4.2 Experiment II

6.4.2.1 Base model results

The results of *Experiment II* for the base model were shown above in *Figure 6-5 B* but are described here. The base model is constructed identically to that in *Experiment I*, with an added factorial predictor for whether there is, or is not, a period of darkness between light steps (referred to as *Dark* in the remainder). There is support for including this factor (ΔAIC = 5). The dependence on *wavelength* shows an inverse-U shaped curve in both cases (*Figure 6-5 B1*). The difference between the two curves is about 13% nPC in the short-wavelength spectrum but almost disappears towards the long wavelengths, above about 600 nm (it is significant below 570 nm at the 5% level). nPC increases slightly with *series* up to step 19 (about 3%) and is steady afterwards (*Figure 6-5 B2*). nPC further increases with *irradiance* ($\beta_{log10(irradiance)}$ = +10.7% ±3.4 SE, *Figure 6-5 B3*). When excluding *irradiance* as a predictor, the shorter wavelengths become less influential; the difference between the curves remains similar (supplemental *Figure S6-15B*). The standard deviation of the random intercept by participant, σ_b^2, was 5.3% in *Experiment II*.

6.4.2.2 Time-course of the wavelength dependency

As stated above in *Materials and methods*, we aggregated the 60Hz-resolution data to mean values over specific periods, i.e., the last five seconds of light, but also created mean values over each one-second period. We used these one-second values to explore how nPC vs. *wavelength* changed over the time course after light onset for each wavelength (referred to as *time*). The results are shown in *Figure 6-8 A1* and *A2* (shown in full in the supplemental *Figures S6-10* and *S6-11*). Note that this implies an oversimplification for the first one or two seconds, where great changes in pupil diameter occur very quickly (cf. *Figure 6-2 B*, *C*, and *D*); the purpose here is to get an overview for the later stages of every light step. nPC decreased over the time course (vertical direction in *Figure 6-8 A1*, horizontal sequence of graphs in *Figure 6-8 A2*). Short wavelengths are especially influential during the first seconds of light onset. Peak nPC also shifts slightly towards lower wavelengths between five and fifteen seconds after onset in the case with darkness between light steps (dashed curve, shift from 525 nm to 500 nm, see also supplemental *Figure S6-10*), but not otherwise (maximum is stationary at 550 nm). nPC increases with *irradiance* ($\beta_{log10(irradiance)}$ = +9.0% ±1.9 SE). When leaving *irradiance* out of the model, differences between the two settings of *Dark* stay mostly the same, whereas nPC sensitivity overall shifts slightly towards higher wavelengths (about 10 to 20 nm; supplemental *Figure S6-12*). Finally, settings with darkness between light steps allow for nPC analysis during the re-dilation phase, known as post-illumination pupil reflex (PIPR,

Figure 6-8 A2 Dark, and Figure 6-8 A2 "21st second or 6th second after lights-off"). Interestingly, re-dilation is slowest for the shortest wavelengths, which is also the case when not controlling for *irradiance (supplemental Figure S6-12)*. Wavelengths above 600 nm were least influential on the PIPR *(Figure 6-8 A2 "21st second or 6th second after lights-off"*). The results for the protocols Long 1 and Long 2 of *Experiment III* are shown in *Figure 6-8 B* for better comparison with *Experiment II*, but are reported further below.

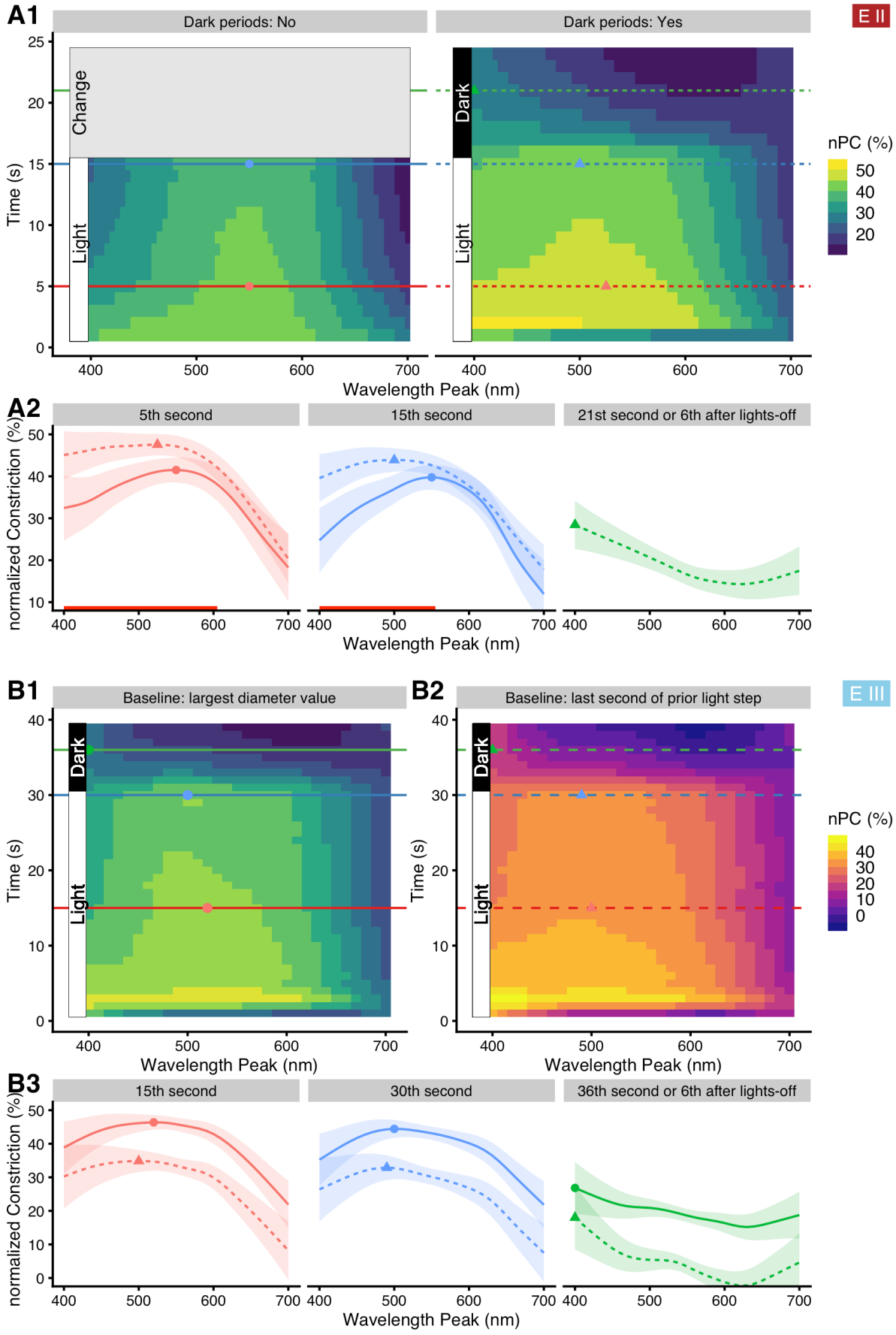

Fig 6-8 Interaction of *wavelength* with *time* in *Experiment II* and *III*. *Time* denotes the time (in seconds) since light onset, or light change to the respective wavelength. (A1) and (A2) show results from *Experiment II*, (B1), (B2), and (B3) those from *Experiment III* for the protocols *Long 1*

and *Long 2*. (A1) False-color graph of model predictions for the nPC's dependence on *wavelength* (x-axis) and *time* (y-axis) for settings with (right panel), or without (left panel), periods of darkness between changes of wavelength. All other predictors are held constant at their average value. Horizontal lines indicate where the respective traces shown in figure part (A2) are taken from; continuous curves refer to the absence of dark periods, dashed curves to their presence; filled circles and triangles mark the wavelength of the respective maximum nPC value of these traces. In the right panel of A1, nPC values after the 15th second (i.e., in the Dark period) show a time-by-wavelength rendition of the post-illumination pupil reflex (PIPR). (A2) Model predictions for nPC vs. wavelength at three points in time. The right panel shows the wavelength dependency of the 6-second PIPR. Ribbons show the 95% confidence interval for the predicted means. Dotted lines with a triangle symbol represent the discontinuous setting with periods of darkness present between light steps; full lines with a filled circle show the continuous setting. The red horizontal line above the x-axis in the two left panels shows where the difference between the two settings is significant at the 0.05 level. (B1) Like (A1 right panel), but for *Experiment III*. Horizontal lines show where the respective traces shown in figure part (B3) are taken from, and points mark the wavelengths of the respective maximum nPC value of these traces. (B2) Like (B1), but with the nPC baseline taken from the last second of the respective previous light step. (B3) Like (A2), but dotted lines and triangles represent the scaling according to (B2), full lines and points according to (B1). The right panel shows the wavelength dependency of the 6-second PIPR.

6.4.2.3 Other dependencies

We tested nPC for an interaction of *wavelength* and *series*, which turned out not significant ($p > 0.18$). An influence of the prior wavelength on nPC was not significant either ($p = 0.37$).

Furthermore, we used the average pupil diameter of the last second before the start of a light step as an alternative baseline value in *eq1*. We explored this variant as the response variable in the *wavelength-by-time* model for protocols using periods of darkness between light steps, where this nPC calculation is a valid alternative. As expected, *series* is no longer significant in this case ($p = 0.31$), since it is accounted for by the respective alternative baseline diameter. Irradiance is not significant either ($p = 0.37$). Otherwise, the model does not seem to behave differently in terms of *wavelength* or *time* (see supplemental *Figure S6-13*), other than that nPC values are, on the average, about 10% lower.

For the protocols having periods of darkness between light steps, the median standard deviation for the pupil diameter at the last second of darkness prior to each light step was 0.37 mm (range 0.21 to 0.95 mm). This was calculated on a by-participant basis, without model fitting.

6.4.2.4 Illuminance

To analyze how well each type of illuminance can predict nPC in those protocols with periods of darkness between light steps, we constructed simplified standard linear mixed-effect models analogous to those used in *Experiment I*. The results were shown above in *Figure 6-7 B* (for comparison to *Experiment I*). As in *Experiment I*, they show

that mesopic weighing predicts nPC best (R^2_{illu} = 0.55). Photopic functions do somewhat less well in comparison (R^2_{illu} = 0.49 for $V_{10}(\lambda)$, and R^2_{illu} = 0.42 for $V(\lambda)$). Melanopic and rhodopic receptor functions work better than in *Experiment I* ($R^2_{illu} \leq 0.31$). Of the three cone functions, chloropic weighing led to the best results (R^2_{illu} = 0.54), with the erythropic function second (R^2_{illu} = 0.43). In contrast, cyanopic weighing was the only illuminance type that had no support by the model at all (p = 0.41, $R^2_{illu} < 0.01$).

6.4.3 Experiment III

6.4.3.1 Base model results

For the analysis of Experiment III, we analyzed nPC results for the protocols *Short 1* and *Short 2* in models separate from those for *Long 1* and *Long 2,* since the two protocol pairs differ conceptually. For those with one second of light followed by thirty seconds of darkness (*Short 1* and *Short 2*), nPC was calculated as the average nPC value of the sixth second after lights-off (or seventh second of the respective light step). The model shows neither support for an effect of *wavelength,* nor for one of *irradiance* (all p > 0.31).

For the two protocols with thirty seconds of light followed by nine seconds of darkness (*Long 1* and *Long 2*), nPC was calculated, as above, as the average nPC value of the last five seconds of light; the results were shown above in *Figure 6-5 C1*. *Wavelength* has support from the model (ΔAIC = 22). The predictor shows an inverted-U shaped curve, with a peak at 500 nm and only slightly lower amplitude at short wavelengths (*Figure 6-5 C1*). The effect of *series* is not significant (p = 0.54) (*Figure 6-5 C2*); nPC does not seem to depend on the stimulus' position in the series when the stimulus duration is extended to thirty seconds. In contrast, nPC increases strongly with *irradiance* ($\beta_{log10(irradiance)}$ = +19.7%, ±4.3 SE). *Irradiance* has support (ΔAIC = 19) as part of the model (*Figure 6-5 C3*). Compared to other estimates of *irradiance*, the effect is rather large. See below for a discussion of a possible overcompensation. When removing *irradiance* as a predictor from the model (supplemental *Figure S6-15C*), the lower wavelengths become far less influential, with results similar to those in *Experiment I* (supplemental *Figure S6-15A*). The standard deviation of the random intercept by participant, σ_b^2, was 5.4% in *Experiment III*.

6.4.3.2 Time-course of the wavelength dependency

Analogous to the analysis in *Experiment II*, we used one-second averaged values in Experiment III to explore how nPC vs. *wavelength* changed over the time course of the light application. The results are shown below in *Figure 6-9* for the protocols *Short 1* and *Short 2*, and were shown above in *Figure 6-8B* for the protocols *Long 1* and *Long 2,* respectively. For the settings with one second of light, followed by thirty seconds of darkness (*Short 1* and *Short 2*), model diagnostics for nPC with the global pupil baseline per protocol were initially problematic, showing heteroscedasticity and skew in the residuals. The skew was eliminated by a logarithmic transformation of nPC and heteroscedasticity was reduced by a logarithmic transformation of *time*. *Time* is the time (in seconds) since

light onset or light change to the respective wavelength. We also analyzed the data using the alternative nPC pupil baseline defined as the average diameter of the last second of the respective previous light step instead of the global baseline diameter taken across all light steps in one protocol. With the alternative baseline, model diagnostics were far more satisfactory compared to the global baseline, and only required logarithmic transformation of *time*, which is why this model is preferred. Both models used *adaptive splines* for accommodating the rapid changes during the first half of the light step compared to almost no changes during the second half. The results are shown in *Figure 6-9 A* and *Figure 6-9 B*, with exemplary sections in *Figure 6-9 C*. Both models predict that shorter wavelengths lead to a speed decrease in pupil re-dilation compared to longer wavelengths. The sixth-second of the PIPR (*Figure 6-9 C*, middle panel) shows a peak constriction at 490 nm for the preferred model, and 520 nm for the standard baseline. At the 15th second (*Figure 6-9 C*, right panel), the peak has disappeared. The effect of *irradiance* is not significant in the preferred model (p = 0.88).

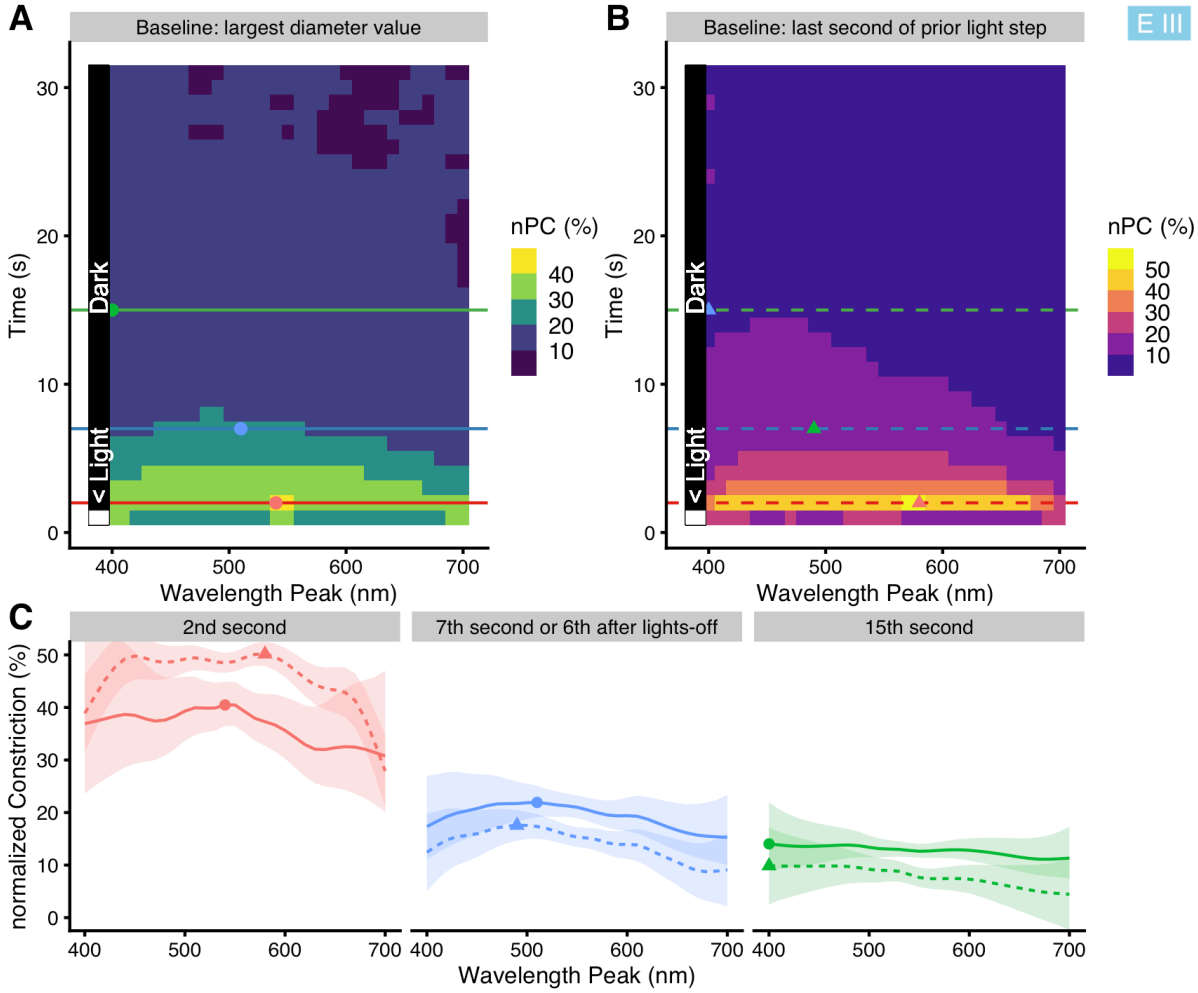

Figure 6-9 Interaction of *wavelength* with *time* in *Experiment III,* for protocols *Short 1* and *Short 2*. *Time* is the time (in seconds) since light onset or light change to the respective wavelength. (A) False-color graph of model predictions for the nPC's dependence on *wavelength* (x-axis) and *time* (y-axis). All other predictors (basic model) are held constant at their average. Horizontal lines show where the respective traces shown in part (C) are taken from, and points mark the wavelengths of the respective maximum nPC value of these traces. (B) Like (A), but with a

different measure of nPC where the nPC baseline is taken as the mean pupil diameter across the last second of the respective previous light step. Model diagnostics are superior to those for the Model in part (A). (C) Model predictions for the nPC vs. wavelength at three points in time after light-step onset: in the 2nd second (red traces), the 7th second (green traces), and the 15th second (blue traces); the latter two cases are also the 6-second PIPR and 14-second PIPR, respectively. Ribbons show the 95% confidence interval for the predicted means. Dotted lines with a triangle represent the scaling according to (B), full lines with a filled circle according to (A).

For the settings with thirty seconds of light followed by nine seconds of darkness (*Long 1* and *Long 2*), model diagnostics for both baseline methods were satisfactory. The results for these models were shown above in *Figure 6-8 B1* and *Figure 6-8 B2*, respectively, with exemplary sections in *Figure 6-8 B3*. Both models predict that shorter wavelengths become more important with *time*, compared to longer wavelengths. With the standard baseline (*Figure 6-8 B1*), peak nPC is at 520 nm after 15 seconds, and at 500 nm at the end of the light application. With the alternative baseline (*Figure 6-8 B2*), peak nPC is at 500 nm after 15 seconds, and at 490 nm at the end of the light application. Re-dilation after lights-off is similar to that in *Experiment II* (*Figure 6-8 A*). nPC increases with *irradiance* (Baseline: largest diameter value; $\beta_{log10(irradiance)}$ = +13.0% ±3.1% SE). When leaving *irradiance* out of the model, nPC sensitivity overall shifts slightly towards higher wavelengths (about 10 to 30 nm; supplemental *Figure S6-14C* and *S6-14D*), similar again to *Experiment II*.

6.4.3.3 Other dependencies

We tested for an influence of the prior wavelength on nPC, which was not significant ($p = 0.68$). For the short protocols, the median standard deviation for the pupil diameter at the last second of darkness prior to each light step was 0.48 mm (range 0.25 to 0.76 mm). For the *Long* protocols, it was 0.49 mm (range 0.32 to 1.26 mm). These values were calculated individually for each participant, without model fitting.

6.4.3.4 Illuminance

To analyze how well each type of illuminance can predict nPC in the *Long* protocols (thirty seconds of light followed by nine seconds of darkness), we constructed simplified standard linear mixed-effect models analogous to those in *Experiment I* and *Experiment II*. The results were shown above in *Figure 6-7 C but are reported here*. As in the other experiments, mesopic weighing predicts nPC best (R^2_{illu} = 0.48). Photopic functions do less well in comparison (R^2_{illu} = 0.45 for $V_{10}(\lambda)$, and R^2_{illu} = 0.40 for $V(\lambda)$). Curiously, melanopic and rhodopic receptor functions are less good predictors than in *Experiment I* or *Experiment II* ($R^2_{illu} \leq 0.21$). Of the three cone functions, chloropic weighing led to the best results (R^2_{illu} = 0.44), with the erythropic function second (R^2_{illu} = 0.42). In contrast, cyanopic weighing was the only illuminance type with no support by the model ($p = 0.24$, $R^2_{illu} < 0.01$).

6.4.4 Pooled data

To gain further insight into the interaction of *wavelength, chronotype,* and *time of day*, we repeated the analysis from *Experiment I* with pooled data from all experiments. Data from protocols *Short 1* and *Short 2* were excluded since these differ conceptually from the others. To partly account for differences between the experiments, we allowed *wavelength* to vary based on experiment type, which is a slight but acceptable oversimplification for *Experiment II* (see above). We further allowed *series* to change, based on the experiment. The interaction effect had strong support (ΔAIC = 163); results were shown above in *Figure 6-6 B*. Compared to the analysis based solely on the results of *Experiment I* (*Figure 6-6 A*), the basic patterns are similar for the evening and the afternoon. Before midday, however, *Larks* do not shift in wavelength sensitivity towards the shorter wavelengths as was the case in Experiment I. Further, the shift towards longer wavelengths for *Owls* is not as strong. Lastly, there is strong support of separate interaction effects (*wavelength, chronotype,* and *time of day)* based on whether or not there are periods of darkness between light steps (ΔAIC = 176), but the resulting model predictions do not lead to any insights beyond what is shown in *Figure 6-6*. Possible reasons for the differences between the models will be discussed in the next section. As a side note, the effect of *irradiance* was estimated to be an increase of nPC of 8.9% per order of magnitude ($\beta_{log10(irradiance)}$ = +8.9% ±1.3 SE) irradiance increase.

6.5 Discussion

6.5.1 Base model results and time-course of the wavelength dependency

Our initial hypothesis was mostly based on findings from McDougal and Gamlin (112) and Gooley et al. (141). For a continuous series of narrowband light steps, lasting 15 seconds each, we expected cones to contribute minimally after 10 seconds [112]. Furthermore, because of the whole series' considerable length (just over 15 minutes), we expected sluggish ipRGC influences to manifest themselves [141]. Therefore, we believed wavelengths between 490 nm to 510 nm to have a considerable effect on normalized pupillary constriction (nPC) ten to fifteen seconds into each light step. However, the results of *Experiment I* do not support this hypothesis (*Figure 6-5 A1*). The peak nPC around 540 nm is close to the peak of the long and middle-wave cone functions (L+M), which suggests strong cone influences. There is further support for an interaction of *wavelength* and *series* in *Experiment I* which indicates a slightly heightened nPC at, and shortly after, reaching the wavelength of peak ipRGC sensitivity, but the effect is small to begin with and disappears over the course of the protocol (supplemental *Figure S6-5*). Compared to other research [24, 50, 112, 135-137, 140, 141], only Alpern and Campbell (136) report similar results (532 nm peak for the 2.5 mm contraction threshold), while most other papers suggest a peak between 480 and 510 nm [24, 50, 112, 135-137, 140, 141], depending on experimental conditions.

There are certain differences and limitations when comparing our results with published literature. Firstly, as stated above, we used continuous light in the first protocols, i.e., participants were pre-adapted to light for all but the very first light step. In the literature, most stimuli are presented singly, with some period of dark adaptation in between [64]. This difference in adaptation also influenced the pupil baseline, as discussed above under *Materials and methods*. Secondly, due to our setup pupil reaction was evaluated at some fixed stimulus intensity, while, in contrast, in most publications stimulus intensity is varied to reach a fixed psychophysiological threshold (e.g., 50% constriction) [135]. Thirdly, we operated in the mesopic stimulus range (see above), a limitation of our light source. Although the stimuli around the ipRGC sensitivity maximum can be considered above the ipRGC-sensitivity threshold as shown above under *Materials and methods*, stimuli of about one degree of magnitude higher intensity would have been desirable to elicit stronger ipRGC reactions [52].Fourthly, differences in *irradiance* between wavelengths required that this variable is included as a predictor in the model, which is relevant in particular for wavelengths at and below 450 nm. Lastly, the long stimulation periods with minor wavelength changes in *Experiment I* made time-dependent confounding influences more likely, e.g., from desensitization or changes in alertness. Therefore, the *series* covariable was included, as the global effect can account for any nonrandom changes across participants over the course of the protocol. Part of the intent of the second and third experiment was thus whether differences in our results from published literature are due to our setup, or due to our protocol, rather than data analysis. Since our initial hypothesis about ipRGC influence on the normalized pupillary constriction (nPC) for a series of narrowband light stimuli did not hold, we aimed to explore several dependencies with the available data and conducted two additional experiments aimed at specific questions arising from our experimental outcomes.

Light-step changes in the first experiment were small, with a wavelength shift of only 5 nm. We set up *Experiment II* to ensure that the wavelength dependency of the first experiment was not some artefact from the near-continuous sweep across the visible spectrum. Results revealed that this was not the case (compare the red trace in *Figure 6-5 B1* to the trace in *Figure 6-5 A1*). More importantly, results showed that short wavelengths had a far stronger influence when the light stimulus was discontinuous between light steps, compared to continuous light (*Figure 6-5 B1*, blue trace compared to the red trace). While the results for discontinuous light, i.e., with short periods of darkness between light steps, suggest a rod rather than an ipRGC influence, they agree far better with published findings [24, 50, 112, 135-137, 140, 141] than those from the first experiment. Regarding the time shift in wavelength dependency throughout each light step, the curve remains centered at around 550 nm with continuous light, but is shifted towards shorter wavelengths with discontinuous light (*Figure 6-8 A2*, full vs. dashed curves). In *Experiment III,* thirty seconds of light were followed by nine seconds of darkness. In this case, the last five seconds of light showed even more influence of short wavelengths than in the previous case (*Figure 6-5 C1*, compared to the cyan trace in *Figure 6-5 B1*),

and the broad peak resembles the behavior shown by Mure et al. (50) for the *0-30 second* condition. The shift in wavelength dependency is also more pronounced in *Experiment III* than in *Experiment II* (*Figure 6-8 B1 and 6-8 B3*, compared to *Figure 6-8 A*).

In summary for our results, the cone influence fades in favor of rod influence for discontinuous series of long-lasting narrowband light steps, agreeing with findings from McDougal and Gamlin (112). However, cone influence does not fade for pre-adapted participants as part of a continuous series of light steps, which to our knowledge has not been reported before. Mure et al. (50) showed changes in wavelength dependency occurring with pre-exposure, but this applied for high-intensity stimuli with several minutes of darkness in between. Joyce et al. (172) showed the effect of short-term light adaptation on the PIPR, but not on the light-adapted pupil itself. The continued bleaching of the sensitive rod photoreceptors might desensitize the rod channel, leaving only the changes in cone input as contributors to nPC. While this mechanism cannot be deduced from our data, it seems a plausible explanation and would result in the shown spectral dependency. It was suggested by McDougal and Gamlin (112), however, that the rod channel remains relevant over minutes of continuous light. Instead, we saw that the spectral dependency of the pupillary reaction to narrowband light is similar to the spectral dependency of polychromatic light [143] when narrowband stimuli are applied under pre-adaption. In vision, interaction effects of rod and cone inputs that depend on the adaptation state of receptors are well known (for a review, see Zele and Cao (173)). In any case, and despite the mesopic experimental conditions, we would have expected some form of ipRGC contribution, which was not apparent, however. Spitschan et al. (174) showed an S-cone opponency to ipRGC input in the pupillary light response, where increasing S-cone stimulation reduced nPC, all other receptor types being stimulated at a constant rate. If cones remain more relevant under pre-adaptation to light compared to prior darkness, as our results suggest, S-cone opponency might help to explain the reduced short-wavelength sensitivity in the presence of relevant ipRGC input to pupil control. IpRGC influence might still be visible in our data, however, as discussed below in *Chronotype and time of day*.

By their presence of a dark period after light stimulation, *Experiment II* and *III* allowed for the analysis of the post-illumination pupil response (PIPR). Surprisingly, the shortest wavelengths led to the PIPR's slowest pupil re-dilation with 15 seconds of prior light in *Experiment II* (*Figure 6-8 A,* supplemental *Figure S6-12*), and even still with thirty seconds of prior light in *Experiment III* (*Figure 6-8 B,* supplemental *Figure S6-14*). The light in the protocols mentioned above was designed to be as continuous as technically possible, leaving only nine seconds of darkness between light steps in the second and third experiment. As can be readily seen in *Figure 6-8*, this was not enough time for the pupil to reach a dark-adapted state. Undoubtedly the absence of full dark adaptation influenced the first seconds of the respective following light step. However, we did not find any systematic influence of the prior wavelength on the last five seconds of the respective following light step. Additionally, after *Experiment I,* the sequences of wavelengths were designed to include large and small light-step differences from across the available

spectrum. Therefore, any effect that the respective previous light step has is not specific to a particular wavelength but is general to the protocol. This can be seen, e.g., in *Figure S6-13C* or *Figure 6-8 B3*. In these figures, the only difference is a shift in the y-axis between using an overall baseline or using a baseline from the last second of the previous light step.

Gamlin et al. (24) reported that a Vitamin-A_1 pigment nomogram with peak sensitivity at 482 nm fitted their data closely for the PIPR of two human subjects after only ten seconds of light. However, when looking at the individual data points for *log relative sensitivity* of the human pupil from that study below 482 nm, i.e., at 452 and 473 nm, their sensitivity does not seem to drop far below that of their closest neighboring data point (493 nm). Park et al. (52) showed that the ipRGC influence is best seen during the sixth second of re-dilation after a one-second light stimulus (compared to a ten-second stimulus in that study). The protocols *Short 1* and *Short 2* in *Experiment III* were constructed accordingly (results shown in *Figure 6-9* and supplemental *Figure S6-14*). We see a peak nPC at around 490 nm, which would fit the ipRGC sensitivity maximum for a young adult [73]. These results agree with a publication by Adhikari et al. (51). That study showed an apparent peak sensitivity between 464 and 508 nm (they fitted a Vitamin-A_1 pigment nomogram with peak sensitivity at 482 nm), with an order of magnitude lower relative sensitivity at the 409-nm wavelength stimulus. After the sixth second in our results, however, sensitivity further shifts towards shorter wavelengths. Thus, our results on the PIPR do not contradict published literature but rather suggest a stronger influence of shorter wavelengths than previously thought, below the ipRGC peak at around 490 nm. A possible mechanism might be an S-cone influence on the pupil [175, 176], which has been shown to influence other ipRGC-dependent effects, such as circadian alignment in mice [36] or, very recently, acute Melatonin-suppression in humans [34]. Circumstances for these additional influences include low light levels and comparatively short stimulus times (less than half an hour), which would fit our setup. The S-cone influence on melanopic effects is not undisputed, however, as Spitschan et al. (177) found no evidence for the influence in acute neuroendocrine and alerting responses. A more far-fetched, but possible, mechanism is the influence of other opsin types in the retina, such as neuropsin (Opn5), which have been found in the retina of vertebrates (for a review see Guido et al. (178).

Regarding the series effect, there seems to be a cumulative effect in *Experiment I* and *II* for the first 18 steps (*Figure 6-5 A2 and 6-5 B2*), where nPC at first increases with each consecutive light step. The downward slope in *Experiment I* then after about five minutes (*Figure 6-5 A2*) might be the result of desensitization, where the small differences in wavelength between light steps are not pronounced enough to counter pupillary escape over time. It can be assumed that changes in arousal, which affect the pupil [179], happen across the timespan of the protocols. In Gooley et al. (141), large fluctuations during the ninety-minute light stimulation can be readily seen. In our study, as far as there is some common change in arousal across the participants over time, this effect is integrated into the series effect by the GAMM. As far as there are individual fluctuations in

arousal over time, the effect on the pupil will be part of the random smooth per participant. In both cases, the effect of arousal cannot be separated from other effects that contribute to the smooth of *series* or the random smooths. In *Experiment II,* wavelength differences between light steps were larger, and nPC after step 18 did not noticeably increase further, nor decrease as in *Experiment I* (*Figure 6-5 B2*). Data analysis for *Experiment I* had suggested an interaction of *series* with *wavelength*. However, further analysis had shown that this effect is of little relevance to the interpretation of the data (supplemental *Figure S6-5*) and does not suggest ipRGC influence as initially assumed in *Materials and methods*. We also found no indication of influences from the prior wavelength to the current wavelength in *Experiment II*.

The estimated effect of *irradiance* varied between experiments and depended on whether five-second (base model) or one-second averages (time-shift model) of nPC were analyzed. While this is plausible insofar as the experiments differ conceptually, it is still worth discussing the estimates, summarized in *Table 6-1*. Except for the *Short* protocols in *Experiment III,* i*rradiance* was a significant predictor in all cases. In the *Short* protocols, the *irradiance* differences between the light steps were seemingly not big enough to influence re-dilation significantly. For the other cases, the estimated value is smallest for *Experiment I,* which is plausible since the changes in *irradiance* between consecutive light steps are the smallest across the experiments. In *Experiment II*, the effect of *irradiance* is similar between the base model and the time-shift model. In *Experiment III*, the estimated effect of *irradiance* for the base model is rather large compared to the other experiments and the time-shift model. The estimate for the time-shift model in *Experiment III* is closer to estimates in *Experiment II*. We believe the estimate for the base model of *Experiment III* to be unlikely high and see no theoretical basis for the large difference to the other estimates. This would mean that the *wavelength* effect of the base model in *Experiment III* overcompensates for *irradiance*. Therefore, the time-shift model is to be preferred to the base model, but the interpretation of *wavelength* as discussed above does not change in a relevant manner (compare *Figure 6-8 B3: 30th second* to *Figure 6-5 C1*). For the model from pooled data of all experiments, estimates for *irradiance* were close to *Experiment II.* Setting the base model in Experiment III aside in favor of the time-shift model (see above), the differences between and within experiments stay broadly the same regardless of the estimated value of *irradiance*, thereby retaining the interpretations above regarding nPC's dependency on *wavelength*.

Table 6-1. Model estimates for *irradiance* across all experiments.

	Base model	Time-shift model
Experiment I	6.5±1.4%	-
Experiment II	10.7±3.4%	9.0±3.4%
Experiment III	19.7±4.3%	13.0±3.1%
Pooled Data	8.9±1.3%	-

Values denote model estimates of $\beta_{log10(irradiance)}$±SE, which indicates the effect of log_{10} transformed irradiance on the normalized pupillary constriction (nPC). The base model uses the average nPC of the last five seconds of light during each light step, the time-shift model uses one-second means of nPC along the time course of each light step.

Finally, regarding the base models, the nPC-by-participant random effect in all three experiments show the large interindividual differences in pupil reaction, even after normalization. These interindividual differences are often remarked in other publications, as summarized by Kelbsch et al. (64). Depending on the experiment, the average nPC is predicted by the model to vary by about 20% between two extreme participant cases (0.025 to 0.975 percentile difference).

6.5.2 Chronotype and time of day

The models from *Experiment I* and pooled data across all experiments strongly suggest the presence of an interaction effect that influences nPC's *wavelength* dependency by an individual's *chronotype* and the measurement's *time of day*. Specifically, early chronotypes, or *Larks*, before noon seem to have a heightened sensitivity to shorter wavelengths (*Figure 6-6 A1* and *B1*). In contrast, late chronotypes, or *Owls*, before noon seem to have a slightly lowered sensitivity to shorter wavelengths. These chronotype-specific differences in sensitivity before noon are called into question by the model constructed from pooled data across the experiments (*Figure 6-6 B1* and *B2*). Both models agree, however, that in the early evening (6:30 pm), the wavelength of maximum sensitivity shifts to longer wavelengths for the *Larks*. For *Owls*, across the day the maximum sensitivity shifts from the longer to the shorter wavelengths, opposite to the behavior in *Larks*. In general, the shifts are predicted to be stronger for the more pronounced or extreme chronotypes, compared to moderate types. For *Neutral* types, the shift is predicted to be minimal. We also see the chronotype bias in *Experiment I* in the daytime scatterplot (*Figure 6-4 B,* the green dots show *Experiment I*), mostly for *Owls* during the first half of the day, which is very likely due to *Owls*' later preferences. We pooled the data across all experiments in the hope to gain more insight from the available data. The pooling adds fifty protocol-runs to the eighty runs of *Experiment I* and leads to a more well-rounded distribution of chronotypes across the day (*Figure 6-4 B,* spread of the dots of all three colors). The pooling also introduces two new dependencies that might influence the interaction and need to be considered. Firstly, *Experiments II* and *III* were conducted decidedly later in the year, compared to *Experiment I* (*Figure 6-4 C*). The thereby introduced general time-shift by the shortened photoperiod should not be too influential according to a recent paper by McHill et al. (180). In that study, the time shift in dim-light melatonin onset was less than half an hour across three months from February to May.

However, the shortened photoperiod might lead to changes in the possible mechanism underlying the interaction effect ([181], see below). Secondly, whether the light stimulus in the experiments is continuous or discontinuous makes a difference in wavelength dependency (*Figure 6-5 B1)*, and likely also with respect to the involved receptor types (see above for the discussion of the base model). Different receptor inputs likely lead to differences in the interaction, which is supported by a model differentiating the interaction of *wavelength, chronotype,* and *time of day* based on whether or not there are periods of darkness between light steps. We slightly prefer the simpler model constructed from *Experiment I*, because while pronounced chronotypes before noon are lacking (*Figure 6-4 B*, green points), it avoids the likely confounding influences from the pooled data mentioned above. It ultimately makes little difference which of the models is preferred, as both indicate the presence of a similar interaction of *chronotype* with *time of day* on the wavelength dependency. The precise nature of this dependency is beyond this study's scope. We checked for possible confounding correlations between *chronotype*, *time of day*, and *age*, all of which did not correlate with one another in any relevant manner. There is also the possibility that we introduced confounding elements into the study design. One could be *alertness*, which is *time-of-day* dependent [182], and, as has already been stated, affects the pupil. However, this dependency on its own would just mean that the *time-of-day* effect, as shown in *Figure 6-5 D3*, were influenced by alertness. Alertness might further influence the interaction of *time of day* with *chronotype*. Yet for alertness to also change the dependency on wavelength would mean changing the underlying retinal neurocircuitry. We are not aware that this is possible. The second confounding option is the effect of prior light exposure in terms of the participants' history of daily light exposure. As the participants arrived in the laboratory approximately thirty minutes before the respective protocol started, they will have *consumed* [183] varying amounts of light on that day. This amount is time-of-day dependent [183] and it is reasonable to assume that it is also depends on chronotype. It is further known that the amount of prior light affects non-visual effects of light, such as melatonin suppression [184], and might also influence the retinal neurocircuitry through the dopaminergic link described further below. In summary, the chronotype effect will have to be approached in a controlled experiment, with measurements for all chronotypes evenly distributed across all times of day while controlling for alertness and prior history of exposure to light, among others.

Circadian effects on the pupil response were reported before and we will discuss two relevant publications in the context of our results. While the focus in those studies is different from ours, we can still compare how their results on circadian ipRGC input line up with our circadian effect. This is under the assumption, that our circadian effect is moderated by ipRGC input, as discussed below. It is further important that, in those studies, the effects of chronotype are adjusted for by looking at participants' internal time or circadian phase, instead of at external time. While this avoids confounding from differences in internal time between participants, it also makes it hard to determine how much of a difference the chronotype signifies. The MEQ, which we used to assess chronotype,

does not describe the participant's phase of entrainment, but rather their time of preference [185]. And while there are correlations between the phase of entrainment and the MEQ score, an exact phase shift cannot be deduced from the score. Therefore, assumed time-shifts between chronotypes in the following section are to be taken tentatively.

Zele et al. (149) showed a circadian response of ipRGC input to the PIPR on eleven participants in a 20–24h laboratory experiment, independent of external light cues. They also investigated circadian changes in the pupil reflex during their ten second light stimulus, but found only growing effects from fatigue owing to the long experiment. IpRGC input was evaluated in that study through the reduction of normalized pupil diameter after lights off (PIPR), compared between a blue and a red narrowband light stimulus (peak wavelength at 488 nm and 610 nm, respectively). The normalized pupil diameter started to decrease about five hours before the evening melatonin onset (DLMO) for the red stimulus, and three hours prior to the DLMO for the blue stimulus, thereby implying a shift in wavelength dependency. The normalized pupil diameter reached its minimum shortly after the DLMO for both wavelengths; the overall period with a reduced pupil diameter lasted longer for the red than the blue stimulus. As mentioned above, any effect on the circadian ipRGC input due to chronotype is not discernible from these results, since the study centered participants' rhythms on their respective points of melatonin onset, thereby eliminating chronotype differences. However, we would expect the effect of chronotype on melatonin onset to be a pure time-shift of a few hours [186]. Translating these findings to our context, we would expect a fixed relationship between nPC curves of comparable wavelengths across the chronotypes, with a general time-shift by about 1.5 to 2 hours between *Owls* and *Neutral* types, and another shift between *Neutral* types and *Larks*. As shown in *Figure 6-10,* our analysis rather suggests a crossed response of nPC depending on wavelength and chronotype (cut-off at 8pm, after which we did not collect data). We thus do not believe that the circadian effect described by Zele et al. (149) is the same as that in our data. Since that study focused on the afternoon and evening, the comparison to our data does not change depending on whether the data from *Experiment I* or the pooled data are used.

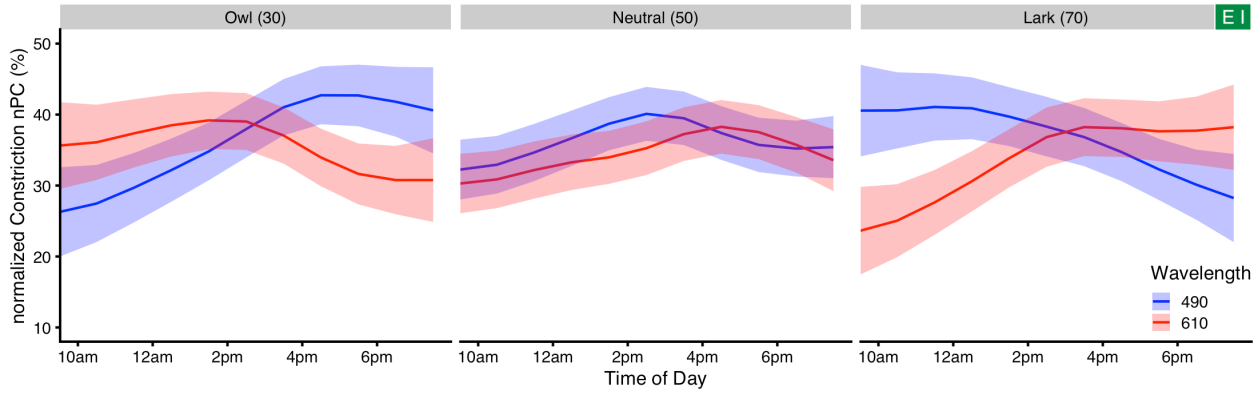

Figure 6-10 Select changes of nPC across the day in *Experiment I*. Model predictions for the nPC vs. time of day for three chronotypes (left to right), and two wavelengths (blue trace 490 nm and red trace 610 nm), that were chosen for comparison with the studies by Zele et al. (149) and Munch et al. (83). Ribbons show the 95% confidence interval for the predicted means.

Another study, by Munch et al. (83), also reported circadian effects on the PIPR. For ten subjects throughout two 12-hour sessions, the 6-second PIPR was assessed after 1-second and after 30-second light stimuli. The authors adjusted the circadian phase in a similar manner to Zele et al. (149). The normalized 6-second post-stimulus pupil size showed a circadian behavior in the short-wavelength, but not the long-wavelength, stimulus. Translating circadian phase and normalized pupil size to our context, nPC for blue stimuli would be highest before noon und decrease afterwards, with *Owls* having a later shift compared to *Larks*. Again, these predictions do not fit our data.

In both of the abovementioned studies, we expect the effect of chronotype to be an effect of time-shift of a few hours [186]. However, our model suggests something different, namely an interaction similar to the so-called synchrony effects of chronotype reported in the context of cognitive performance in education [117, 187], or of physical performance in athletes [188]. Goldstein et al. (117) define chronotype synchrony as the state in which the time of optimal performance is equal to the time of preference of the chronotype, e.g. morning for *Larks* and evening for *Owls*. Our model from *Experiment I* predicts such a heightened sensitivity for short wavelengths at the time of preference for the chronotypes. This connection might even go one step further. It is known that the time-of-day is highly relevant for the magnitude and sign of a circadian phase shift for a given stimulus [16] (for a review of known influences, see Prayag et al. (189)). Furthermore, Roenneberg and Merrow (5) argue that chronotype is not only the result of non-24-hour internal periods but also of the individual's photosensitivity. Following this reasoning, heightened sensitivity to shorter wavelengths at circadian intervals could be part of a reciprocal system to strengthen or even cause a chronotype, rather than being simply a correlation. *Reciprocal* meaning that some mechanism – like an internal period of other than 24h duration – might predetermine a circadian type. Heightened sensitivity to wavelengths for a circadian shift at times of preference (e.g., towards the evening in *Owls*) means one would need more light outside of the preferred time to shift towards a different chronotype. Conversely it would need less light for strengthening the rhythm at the time of preference, thereby solidifying the chronotype. While causation cannot be determined from our study, intraocular mechanisms have been described to allow for such an effect. In general, rod and cone sensitivity follow a circadian rhythm [190, 191], with melatonin and dopamine as key actuators. Furthermore, ipRGCs are intricately and reciprocally connected to dopaminergic amacrine cells (for a review in the context of myopia, where dopamine plays an essential role, see Stone et al. (192)). Through this connection, ipRGCs can attenuate the outer retinal light adaptation in mice [193]. This system is involved in seasonal and circadian regulation of photosensitivity [181]. Other seasonal changes, like that of human color perception [194], might also be connected to this mechanism. Since ipRGC sensitivity is the basis of the mechanism, the shift towards, or away from, the short wavelength spectrum is plausible. Whether the mechanism operates in a chronotype-dependent manner, as shown above, is open for evaluation.

6.5.3 Sex and age

We saw strong support for the model which included *sex* as a predictor. There were no differences in dependence on *wavelength* related to *sex*. However, women were estimated by the model to have a lower average nPC. Chellappa et al. (148), in contrast, found sex differences in light sensitivity. In their study, men showed a stronger response to blue-enriched light in the sleep EEG (NREM sleep slow-wave activity) and for vigilant attention, and had higher brightness perception during blue-enriched light. Men also found blue-enriched light preferable to non-blue-enriched light, contrary to women. The stronger average nPC for men in our study would align with a higher brightness perception for men per se, but unlike in Chellapppa et al.'s study was not limited to short wavelengths. Since men – in general – are more likely to be late chronotypes compared to woman [195], and Chellappa et al. (148) did not mention whether they stratified their sample for chronotype, their reported effect might also have been caused, in part, by a chronotype effect. That study was performed in the late evening, where our interaction effect of chronotype with time of day and wavelength suggests a heightened sensitivity for short wavelengths in *Owls* (see above).

Age was estimated to influence nPC, but there was no indication of an interaction with *wavelength*. The latter agrees with a publication by Rukmini et al. (196), where pupillary responses to short-wavelength compared to long-wavelength light were independent of age (in a comparison of two age groups: 21–30, and ≥50). Depending on whether or not chronotype and time of day were included in our model, nPC was predicted to rise steadily with age (*Figure 6-5 D1,* supplemental *Figure S6-6 A*), or reach a plateau at about age 25 (supplemental *Figure S6-6 B*). According to Rukmini et al. (196), pupillary responses were reduced in older participants. *Age* was also part of the unified model from Watson and Yellott (134) based on data from Winn et al. (197). Winn et al. (197) focused on pupil diameter itself, rather than the (relative) change in diameter, i.e., nPC. The authors calculated the age-dependent pupil-diameter change per log unit stimulus luminance from five illuminance levels (9 to 4400 cd/m²). The resulting regression showed that pupil constriction decreases with age in the photopic range. Conversely, Daneault et al. (155) found no significant age-related differences in pupil constriction, even though pupil size itself decreased with age. Adhikari et al. (198) showed that the relative peak constriction did not change with age, that measure being closely related to our dependent variable nPC. While not significantly correlated with *age*, the trends in their study for both blue and red stimuli show a slight positive slope. In summary, literature reports show a heterogeneous picture of the effect of age on nPC. Our age range was small by design and focused on participants below the age of forty. Accordingly, the effects of *age* in our study were small and appear compatible with any of the studies mentioned above, thereby contributing little for this specific aspect.

6.5.4 Effect sizes

To summarize the unstandardized effect sizes of the various dependencies (*Figure 6-5)*, wavelength clearly shows the biggest effect. nPC changes by about 20% across the

available spectrum in cases of continuous light (*Figure 6-5 A1, B1)* and by more than 30% in cases of discontinuous light (*Figure 6-5 B1, C1)*. The long series of small wavelength changes in *Experiment I* also had a considerable effect, of about 13% (*Figure 6-5 A2*), compared to about 5% for the larger changes in *Experiment II* or no effect for the thirty-second stimulus in *Experiment III*. We already discussed the effect of *irradiance* above. Depending on the model estimate, a 0.5 $\log_{10}$ difference in *irradiance* changes nPC by about 5% (*Figure 6-5 A3, B3, C3*), which is roughly the same influence that *sex* or *age* had in our setup (see *Figure 6-5 D1* for *age*). The estimated main effects of chronotype and time of day amount to about 10% across their respective range. The combined effect of these two covariates and wavelength leads to considerable changes of about 20% nPC *(Figure 6-6 A2*). As this effect has not been reported before, it may be a consequence of the used protocols for continuous light since the effect is far diminished when evaluated across protocols (*Figure 6-6 B2*). This is under the assumption that the effect can be replicated without confounding influences as discussed above.

6.5.5 Illuminance

At present, there are nine distinct measures of illuminance in common use to describe visual and alpha-opic (i.e., single receptor-dependent) effects of light. Scotopic illuminance and rhodopic equivalent daylight illuminance count as two, but both use the same rhodopic action spectrum. Many publications use V(λ)-derived luminance [134] (in cd/m²), but since the spatial stimulus characteristics are unchanged across our experiments (Ganzfeld conditions), luminance and illuminance are interchangeable in terms of comparisons between the types of illuminance. Adrian (138) argued that mesopic weighing was sufficient to explain apparent wavelength-dependency shifts towards the shorter wavelengths (under mesopic conditions). Accordingly, Adrian explained the mechanism behind this shift as purely S-cone and rod-based. We now know that Adrian (138) was incorrect in his assumptions about the sole mechanism and that there is additional input from ipRGCs in the pupillary system, e.g. from the work of Gamlin et al. (24) or Zaidi et al. (140). However, the appeal of the mesopic weighting compared to others is easy to see across all three of our experiments (*Figure 6-7*), where the mesopic illuminance best predicted nPC, thereby considering all cone and rod input. The single-opsin weighting functions for rhodopsin or melanopsin perform far less well in all cases.

In summary, our findings are relevant in the context of arguments made by Spitschan (142) and Zandi et al. (143) about the limited applicability of luminance-based pupil models [134] in the context of ipRGC inputs. At least for our experimental setup of narrowband and mesopic light stimuli of changing wavelength, mesopic weighting was best at predicting pupil constriction. Conventional photopic (il)luminance-based approaches performed still well and, compared to single-opsin based functions, were preferable to predict pupil constriction. Finally, Spitschan et al. (174) reported an S-cone opponency, where the pupil would curiously increase in diameter with increasing stimulation of S-cones. Since our setup did not account for the constant stimulation of all other receptor types as that study did, any opponency effect is expected to be decreased in our study.

The cyanopically weighted equivalent of daylight illuminance (S-cone weighing) was not significantly correlated with nPC in any experiment here. The cause is not known, but the results are compatible to a zero-sum of opposing inputs.

6.6 Conclusion

The spectral dependency of pupillary reactions to narrowband light is well understood for isolated stimuli, but less so for scenarios with preadaptation to light. We looked at the normalized pupillary constriction (nPC) in protocols of narrowband light of periodically changing wavelength and found very little influence of short wavelengths. A second experiment showed that this effect originated in the continuous application of light and that the effect was present over the whole time-course of each wavelength. Our results for continuous narrowband light and literature findings from polychromatic light share a similar wavelength dependency, compared to singularly presented narrowband light. Furthermore, the 6-second post-illumination pupil response (PIPR) to isolated light stimuli, for two out of three durations showed that the slowest re-dilation happens for the shortest wavelengths, well below peak ipRGC sensitivity, implying the presence of different, or at least additional, receptoral influences to the PIPR. Pupillary reactions to isolated light stimuli and the PIPR to short light stimuli behaved very much as would be expected from published literature. This strengthens our belief that our results are valid despite some technical limitations as described above. We further showed that mesopic illuminance was the best measure of illuminance to explain the pupil reaction. We found dependencies of *sex* and *age* on the pupillary response through the exploration of several covariates, but mainly an interaction of *chronotype* and *time of day* with *wavelength*. The interaction effect implies a modulation of wavelength-sensitivity with a heightened sensitivity to shorter wavelengths at the time of chronotype preference. This circadian effect further seems to manifest itself differently, depending on whether light is continuous or discontinuous. The effect could be linked to a mechanism that strengthens an individual's chronotype at the current time of preference, or it could result from chronotype and time-of-day dependent differences in the light history. If the effects are reproducible in a controlled experiment, they might even act as a form of marker for the individual´s chronotype.

6.7 Acknowledgements

We thank Jorge Alberto Gutiérrez Alvarez, Theresa Scherzer, Daniel Philipp Setzensack, and Regina Heiß for their help with data collection as part of their respective thesis work. We thank Moritz Faust for his support on data collection and questionnaire digitalisation. We also thank three anonymous reviewers for their helpful and constructive input to the manuscript.

6.8 Supporting information

All supporting information can be found at https://osf.io/ar2ud/

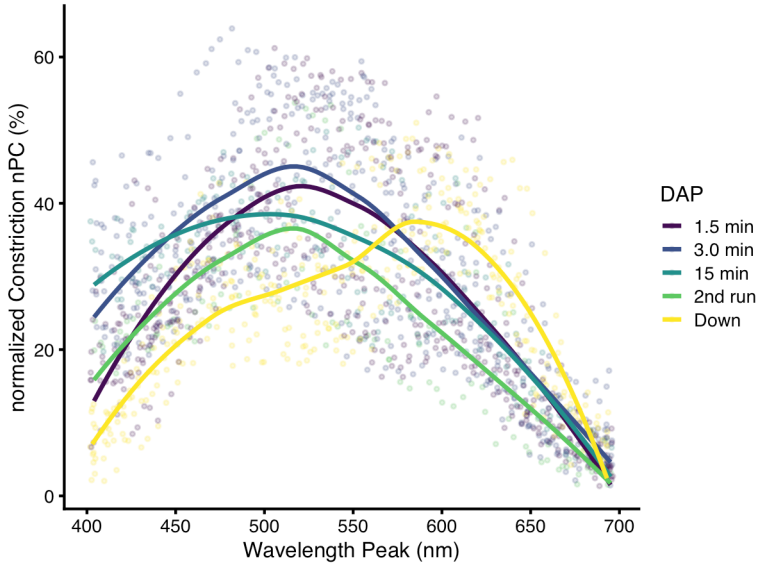

S6-1 Fig. nPC depending on *wavelength* for different dark adaptation periods (DAPs). Traces show the mean, LOESS-smoothed nPC vs. wavelength for two subjects, each repeating all shown protocols three times. DAP varied between 1.5, 3, and 15 minutes (lilac, blue, dark green). For comparison, results of a second, consecutive run (also performed three times, light green) of the first protocol is shown, as is the *Down* protocol (yellow). Points show the nPC values from which the traces were constructed. More information is found in *Materials and methods*.

S6-2 Zip File. R-Markdown script results for calculating nPC from measurement data. Zip file containing nine html files with results from R-Markdown scripts. The scripts are one each for the nine protocols used across the experiments. Since the raw measurement data are not part of the provided supplements, we included one exemplary result file for each protocol instead of the script itself. These html files show the code, as well as the output for the example participant.

S6-3 Microsoft Excel File. Irradiance measurements and illuminance values for the range of light stimuli. Microsoft Excel file containing two worksheets. The worksheet 'Measurements' contains the irradiance measurements in a resolution of 1 nm. The worksheet 'Illuminance' contains all types of illuminance values described in the main text and irradiance. All displayed values are based on spectral irradiance measurements with a field-of-view restriction according to the CIE S 026 standard [73]. In our case, these measurements are 24% lower than those of the unobstructed sensor diffusor.

S6-4 Zip File. R-Markdown script used for statistical analysis and graphics generation. Zip file containing several files necessary to replicate the statistical analysis and generation of graphics. Besides some external tables, an R-function file, and three pictures to mark the respective experiment in graphs, the zip file consists of nine R-Markdown scripts. One of these is used to set up the data prior to analysis. The necessary

data can be downloaded from the *Open Science Framework* [157]. Five of the R-Markdown files are for analysis of *Experiment I, II, III Short, III Long*, and the pooled data. The eighth file is for graphics generation. The second-to-last file takes a sample of ten random participants from the first experiment for every protocol and builds the base model from this subset. This sample analysis is to show that the main dependencies of *wavelength* and *series* can come from a smaller sample. An html file with the same file name shows an example. The last file is for calculating estimates for prereceptoral filtering and using those estimates to calculate irradiance and photon density values from the spectral irradiance measurements.

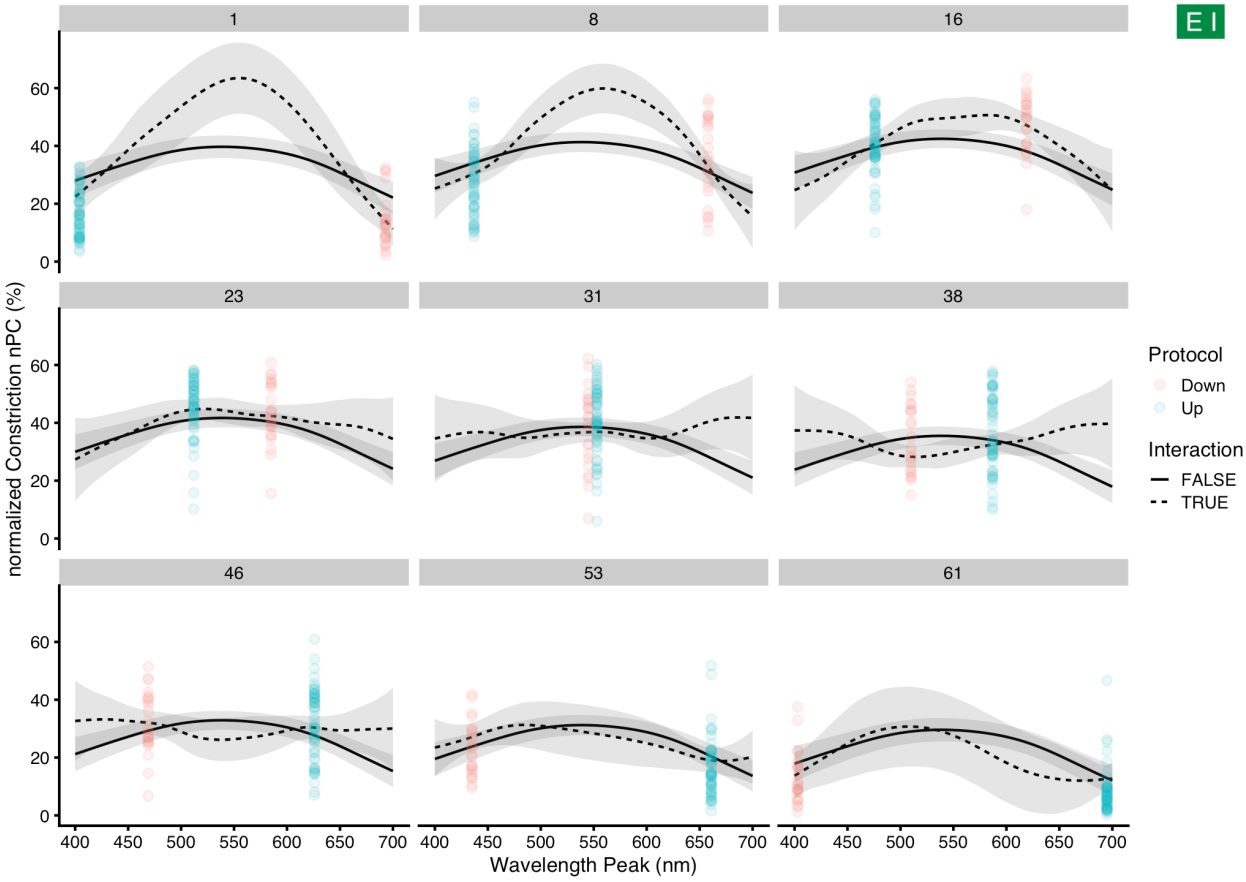

S6-5 Fig. nPC depending on wavelength with and without interaction in *Experiment I*. Model prediction for models with (dashed lines), and without an interaction effect (solid lines) of *wavelength* and *series,* across the series. The number above each plot indicates the series number. Colored dots represent raw nPC values at the respective series number and wavelength, their color indicates the respective protocol. The positions of points on the x-axis indicate where changes between the two models (lines) should be evaluated. For the model with the interaction effect, it seems as though nPC is increased after reaching the ipRGC peak sensitivity (at about 490 nm for a young adult), but not strongly and not for long.

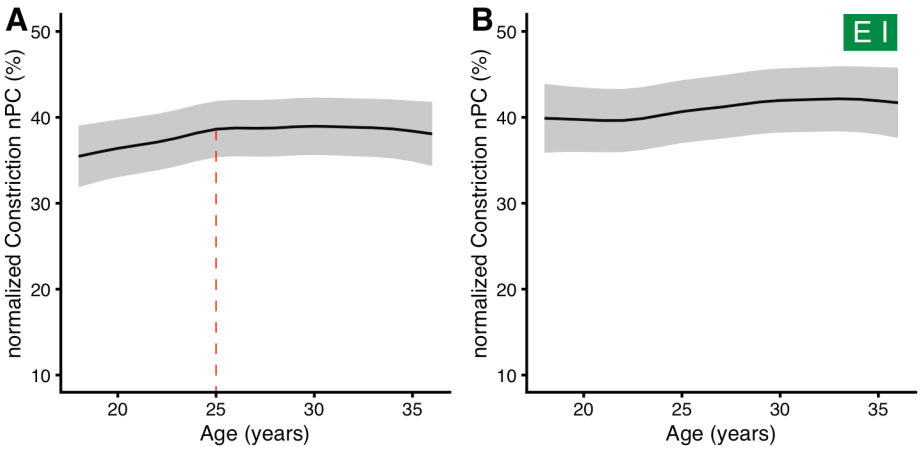

S6-6 Fig Influence of *age* in *Experiment I*. (A) Model predictions how nPC depends on *age*, when all other predictors (basic model) are held constant at an average level. (B) Like (A), but for the model with all other dependencies in *Experiment I* included. Here, *age* seems to affect nPC with a more continuous rise over the age range.

S6-7 Fig. GIF Animation of nPC depending on *wavelength*, *time of day*, and *chronotype* in *Experiment I*. Model predictions show time-of-day values at half-hour points from 8:30 am to 7:30 pm. Left: False-color model predictions for hourly nPC values depending on *wavelength* (x-axis) and *chronotype* (y-axis), when all other predictors (basic model) are held constant at an average level. Horizontal lines show where the traces from the right image are taken from. Right: Model predictions for hourly nPC values depending on wavelength for three chronotypes: *Larks* (green traces, CT score 70), *Owls* (red traces, CT score 30), and *Neutral* types (blue traces, CT score 50). Ribbons show the 95% confidence interval for the predicted mean values.

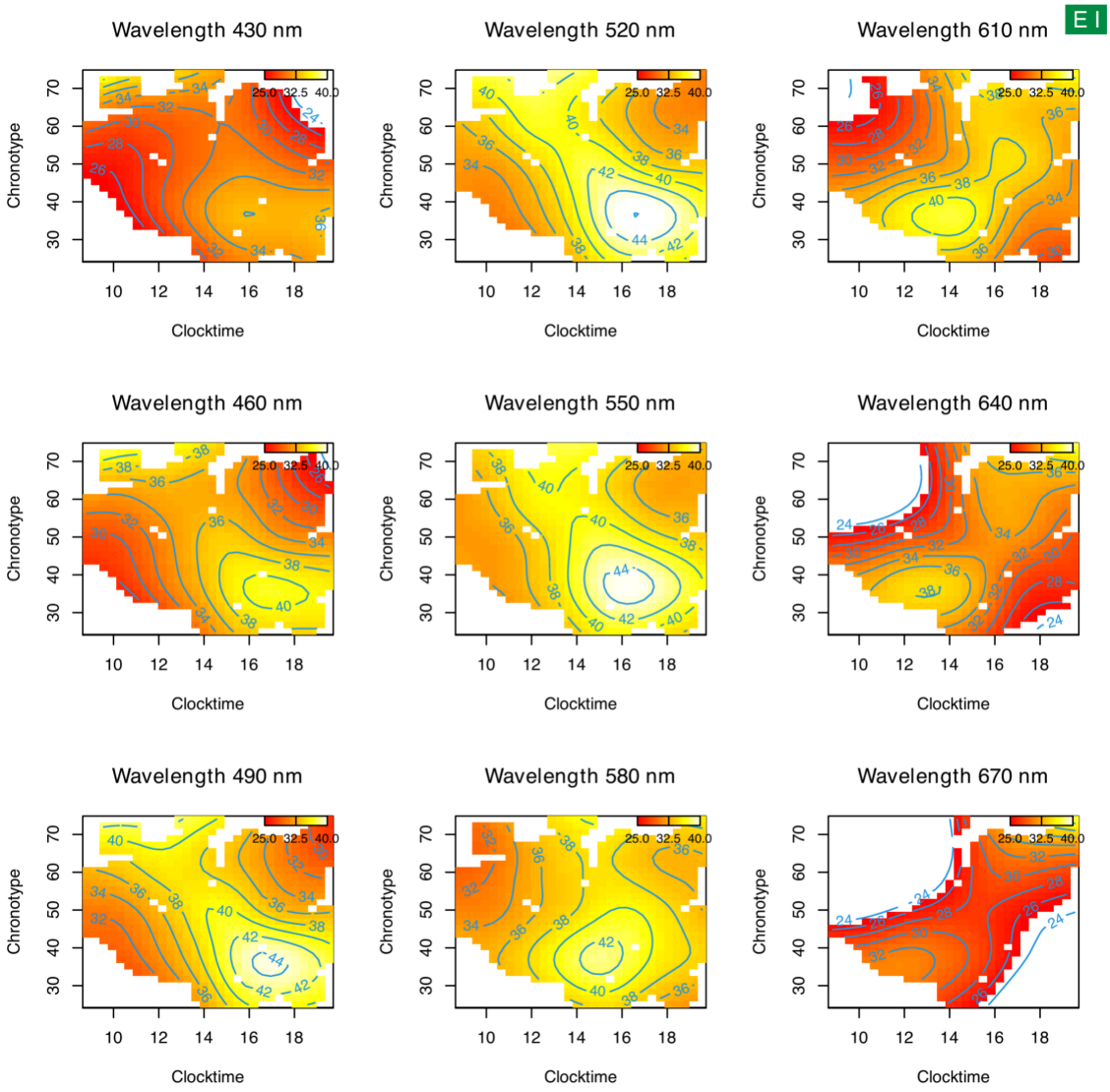

S6-8 Fig. nPC depending on *wavelength*, *time of day*, and *chronotype* in *Experiment I*. False-color contour-line graphs of nPC model predictions for several wavelengths between 430 and 670 nm (color scale shown in the inset at the upper right corner of each plot). All plots are scaled equally. Each plot visualizes nPC depending on *time of day* (clock time in 24h values, x-axis) and *chronotype* (higher values are morning types, lower values evening types). Plots were created with the *vis.gam()* function in R, with the *too.far* argument set to 0.1. The *too.far* argument excludes grid points from the plot, when points are not represented by variable combinations close enough to actual data. Thereby, *too.far* is a measure of accepted extrapolation, scaled from 0 to 1.

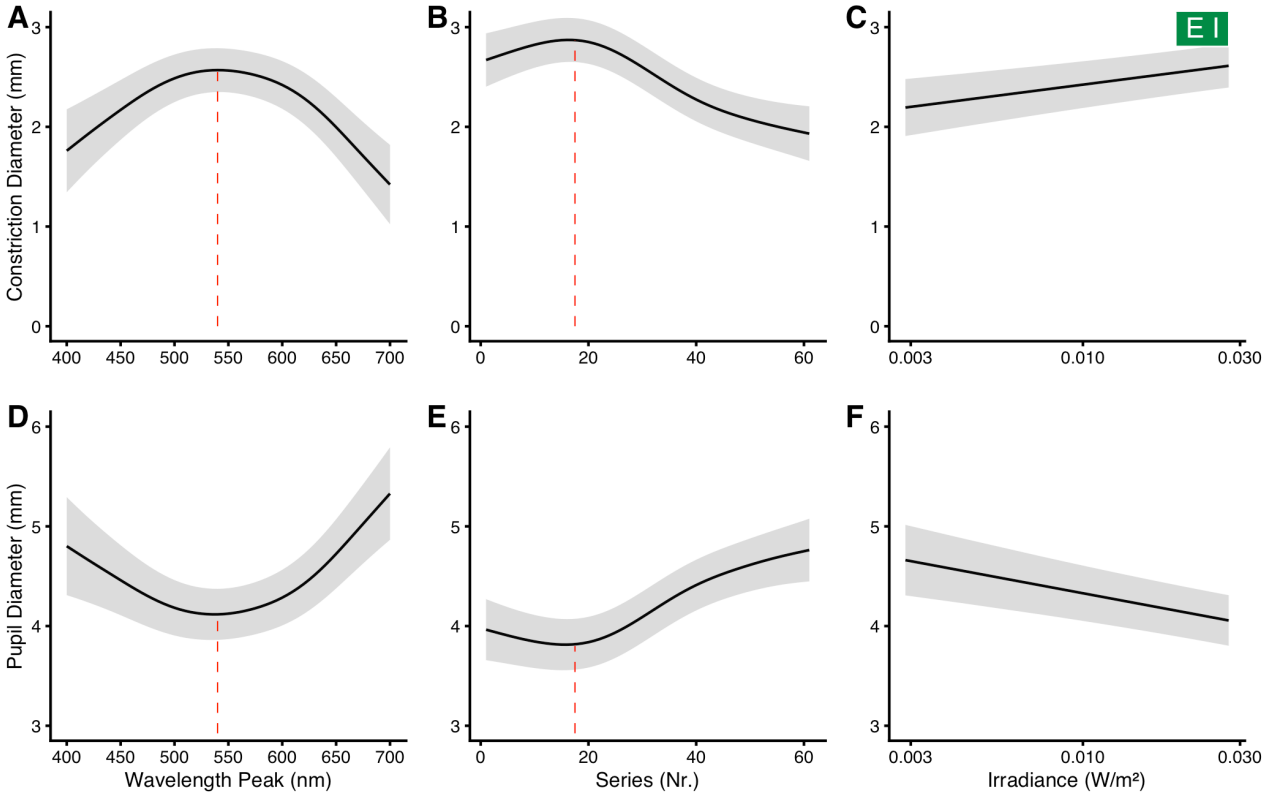

S6-9 Fig. Basic model predictions for unscaled changes in pupil diameter, and raw pupil diameter, in *Experiment I*. Model predictions for response variables other than nPC, versus three main predictors (*wavelength, series,* and *irradiance*), when all other predictors are held constant at their average level. Traces show the model prediction for the mean, ribbons its 95% confidence interval. Red dotted lines show particular predictor values for the plotted relationship. (A / D) Response vs. stimulus peak wavelength. (B / E) Response vs. series number of light steps. (C) Response vs. stimulus irradiance. The x-axis scaling reflects the logarithmic transformation of irradiance.

S6-10 Fig. GIF Animation of normalized pupillary constriction (nPC) depending on *wavelength* and *time* in *Experiment II*. Left: False-color model predictions for nPC depending on *wavelength* (x-axis) and *time* (y-axis), for settings with, or without, periods of darkness between wavelength steps. All other predictors are held constant at an average level. Horizontal lines show where the traces from the right image are taken from. Right: Model predictions for the nPC vs. *wavelength* over *time*. Ribbons show the 95% confidence interval for the predicted means. Blue lines represent the setting when periods of darkness are present between light steps, red lines when not. The red horizontal line above the x-axis shows where the difference between the two settings is significant (5% level).

S6-11 Zip File. Html file with 3-D visualizations of normalized pupillary constriction (nPC) depending on *wavelength* and *time* in *Experiment II*. The zip file contains three files. One html file with a scalable and rotatable diagram of nPC (denoted as “Amplitude”) vs. wavelength and *time*. An html viewer, or browser with support for html widgets, is

needed. The other two files are snapshots from the html file for each condition of *Dark*. Color mapping is according to the z-axis (nPC) for better visibility.

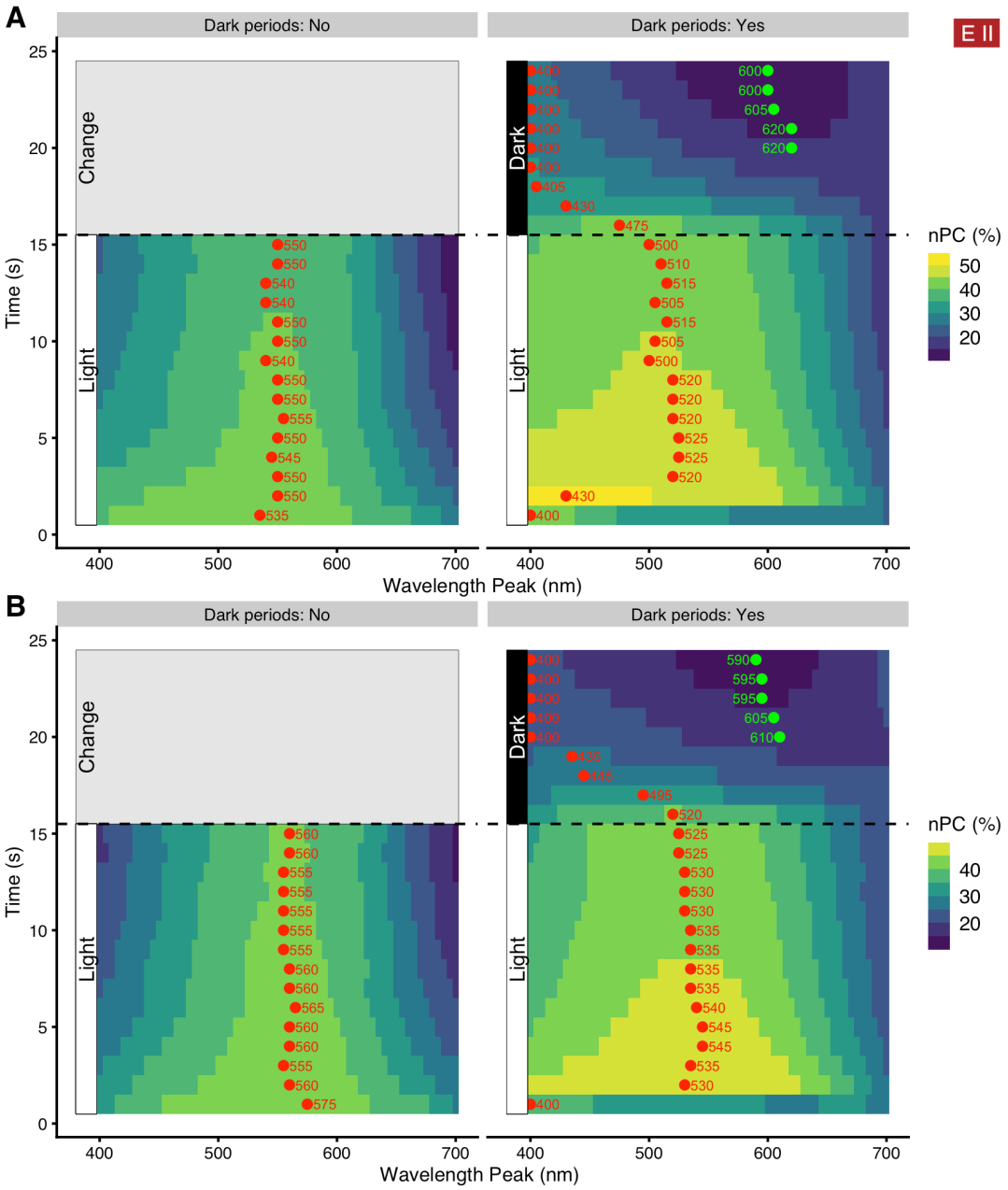

S6-12 Fig. Interaction of *wavelength* with *time* in *Experiment II*. (A) False-color graph of model predictions for the nPC's dependence on *wavelength* (x-axis) and *time* (y-axis) for settings with, or without, periods of darkness between wavelength steps. All other predictors (basic model) are held constant at their average. Red dots show the peak nPC value for each second, the value right next to it the respective peak wavelength. Green dots and values show the respective trough for nPC. The trough is at 700 nm where green dots are not shown. (B) Like (A), but for the model without *irradiance* as predictor.

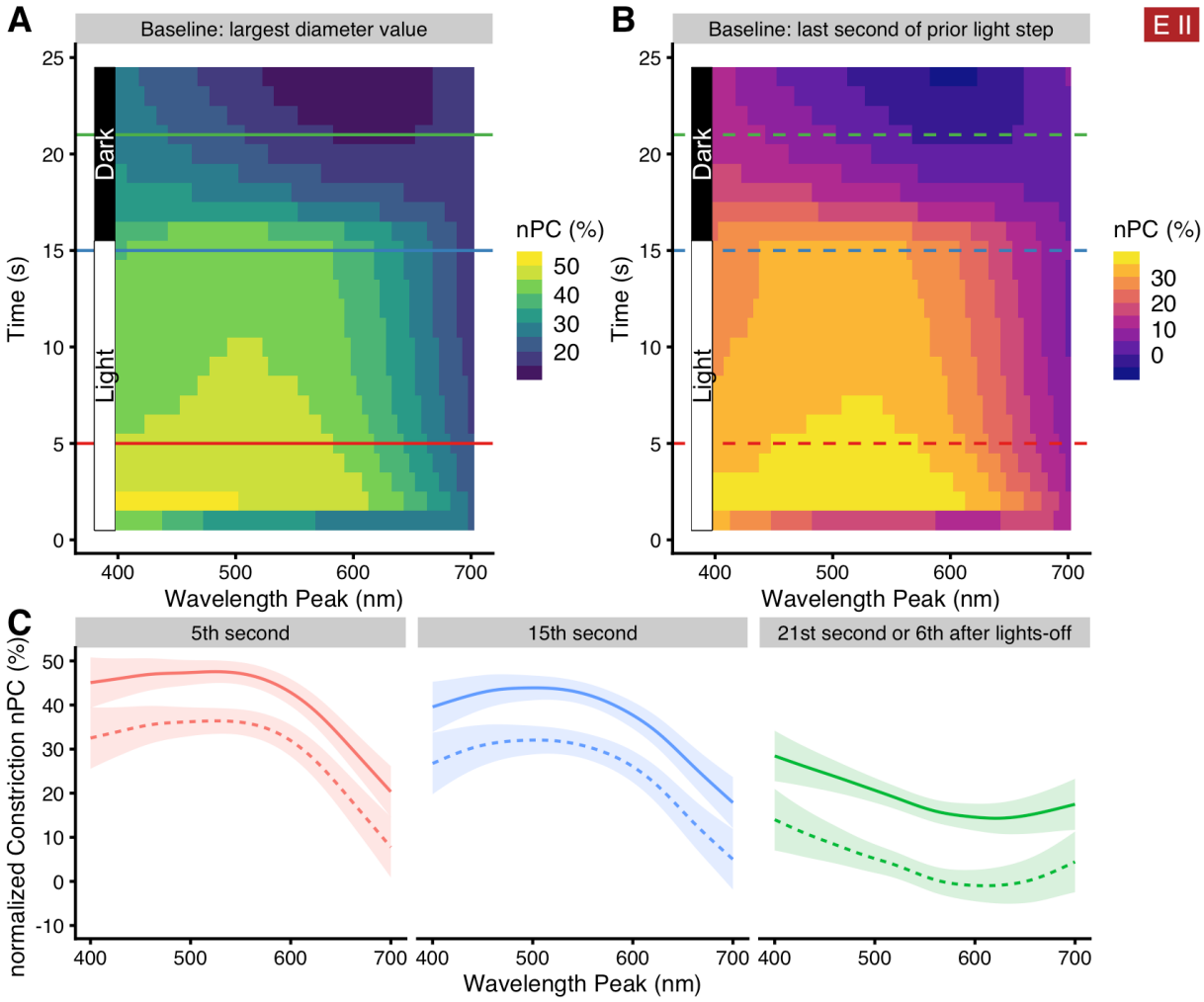

S6-13 Fig. Interaction of *wavelength* with *time* in *Experiment II,* for protocols with darkness between light steps. (A) False-color graph of model predictions for the nPC's dependence on *wavelength* (x-axis) and *time* (y-axis). All other predictors (basic model) are held constant at their average. Horizontal lines show where the respective traces shown in part (C) are taken from. (B) Same as in (A) except that the baseline for nPC calculation (*eq1*) is taken from the last second of the respective previous light step. (B) The graph serves to check whether and how the single baseline value per protocol (shown in A) changes the model prediction. (C) Model predictions for the nPC vs. wavelength at three points in time after light step onset: in the 5th second (red), 15th second (blue), and 21st second (green); the latter case is also the sixth seconds after lights-off. Ribbons show the 95% confidence interval for the predicted means. Full lines represent nPC values when baseline pupil values are taken from each protocol's largest pupil diameter, dotted lines when baseline pupil values are taken from the last second of the respective prior wavelength-step.

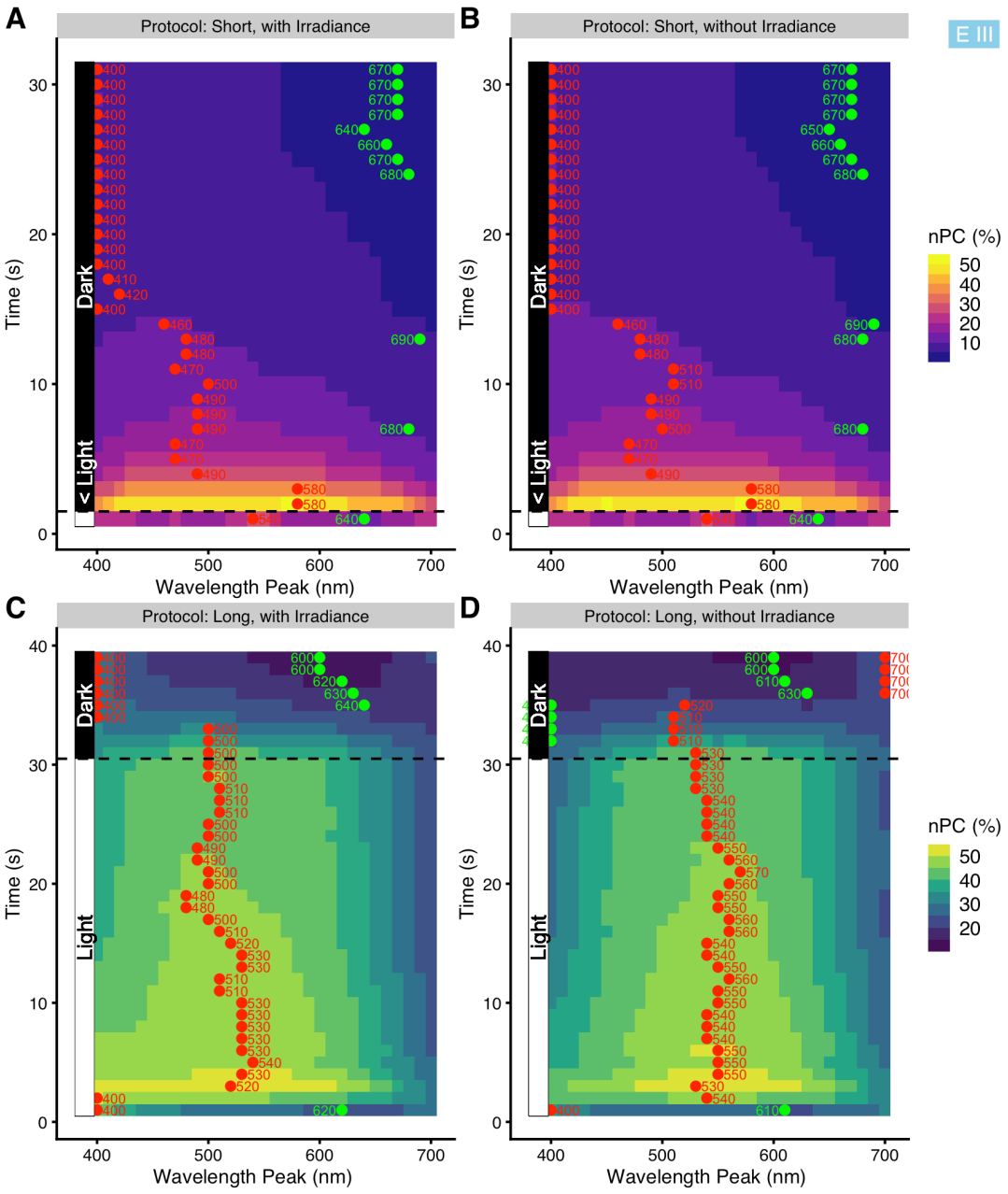

S6-14 Fig. Interaction of *wavelength* with *time* in *Experiment III*, for models with, or without, irradiance as predictor. (A) False-color graph of model predictions for the nPC's dependence on *wavelength* (x-axis) and *time* (y-axis) for the protocols with one second of light, followed by thirty seconds of darkness, and with *irradiance* as the predictor. All other predictors (basic model) are held constant at their average. Red dots show the peak nPC value for each second, the value right next to it the respective peak wavelength. Green dots and values show the respective trough for nPC. The trough is at 700 nm where green dots are not shown (e.g. between 2 and 30 seconds). The baseline for nPC calculation (*eq1*) is taken from the last second of the respective previous light step, since this baseline led to a preferable model in terms of model diagnostics. (B) Like (A), but for the model without *irradiance* as the predictor. (C) Like (A), but for protocols with thirty seconds of light, followed by nine seconds of darkness with irradiance as

a predictor. The baseline for nPC is as described in *Materials and methods*. (D) Like (C), but for the model without *irradiance* as the predictor.

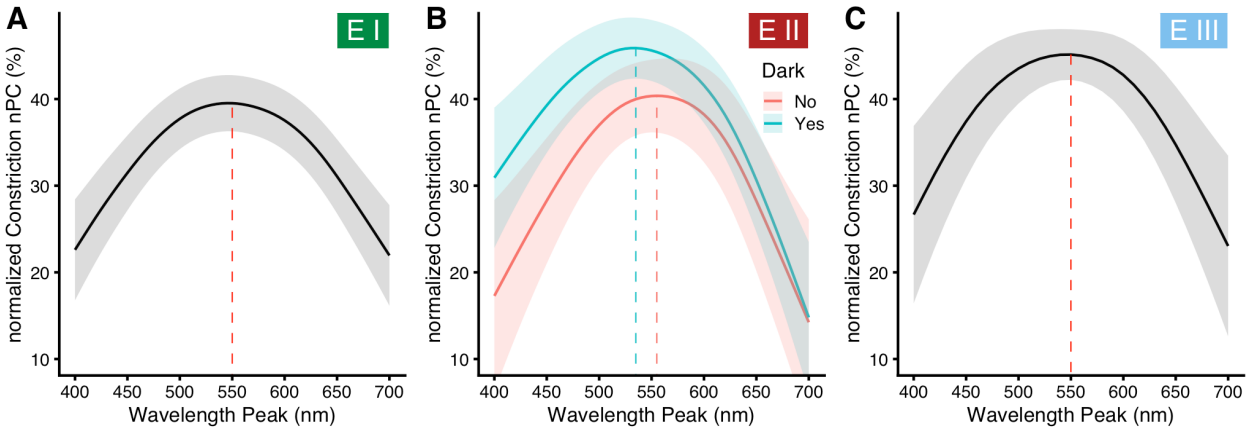

S6-15 Fig. Model predictions for models without *irradiance* as a predictor. Normalized pupillary constriction (nPC) as depending on *wavelength*, when all other predictors are held at an average, constant level. Traces show the model prediction for the mean, ribbons its 95% confidence interval. Dotted lines show the respective peak. (A) through (C) show dependencies in *Experiment I*, *II*, and *III*, respectively. They can be compared to the model results which include irradiance in *Fig 5 A1*, *B1*, and *C1*.

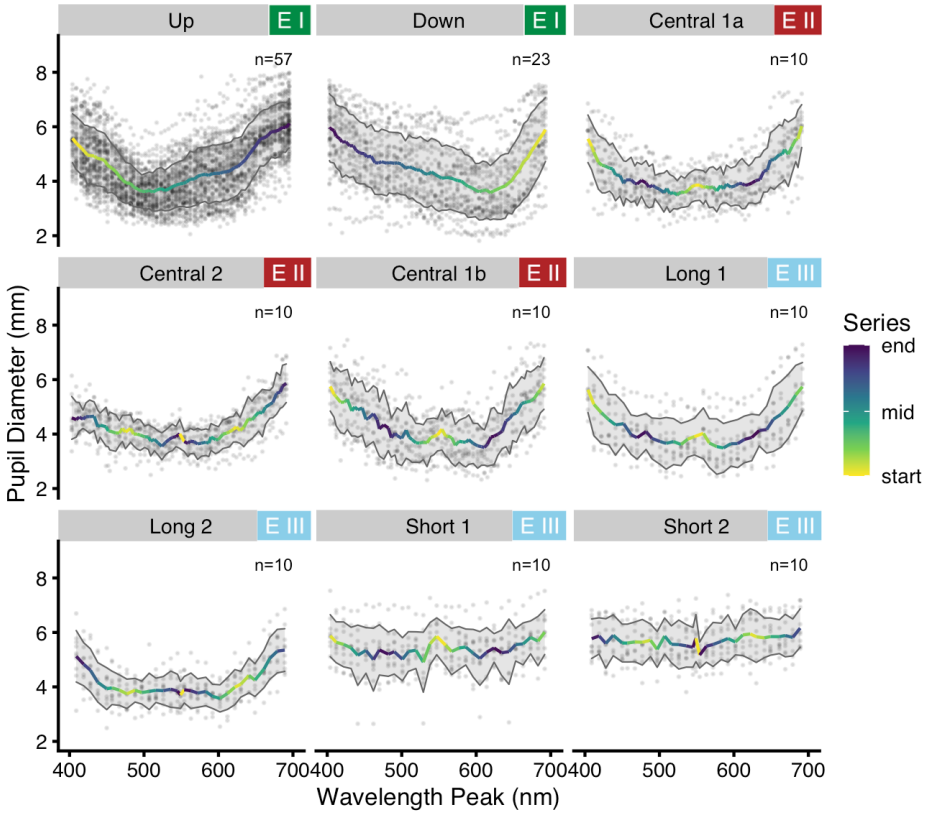

S6-16 Fig. Experimental data. (A) Pupil diameter plotted against wavelength, for each of the nine protocols. The color scale shows at which point in the series a specific wavelength was presented; light yellow represents early in the series. For all but the *Short*

protocols, points represent the average nPC during the respective last five seconds of a light step. In the two *Short* protocols, points represent the average nPC during the sixth second after lights-off (or sevenths second after lights-on). Traces show the mean nPC, ribbons its standard deviation. The number in the upper right corner of each plot shows the corresponding sample size.

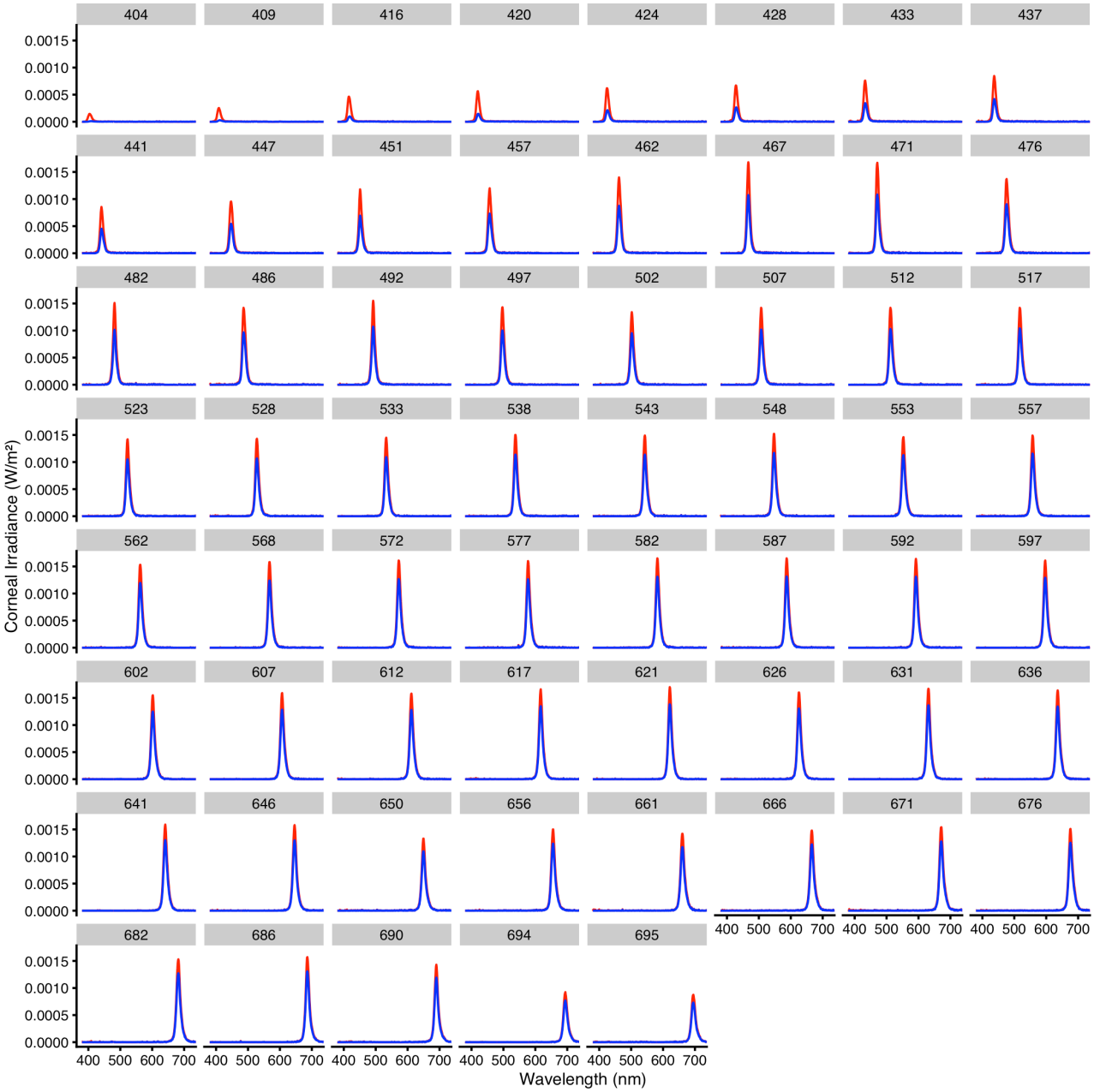

S6-17 Fig. Plot of the 61 spectral distributions shown in Fig 1A. Corneal irradiance (W/m²) vs. wavelength, labelled by wavelengths peaks (404–695 nm) above each sub-graph. The x-axis on the bottommost plots and the y-axis on the left apply to all plots in their respective row and column. Blue and red traces show the spectral measurements with and without an estimate of prereceptoral filtering, respectively. Wavelength peaks above each plot state the peak for the raw stimulus measurement. All displayed values are based on spectral irradiance measurements with a field-of-view restriction according to the CIE *S 026* standard [73]. In our case, these measurements are 24% lower than those of the unobstructed sensor diffusor.

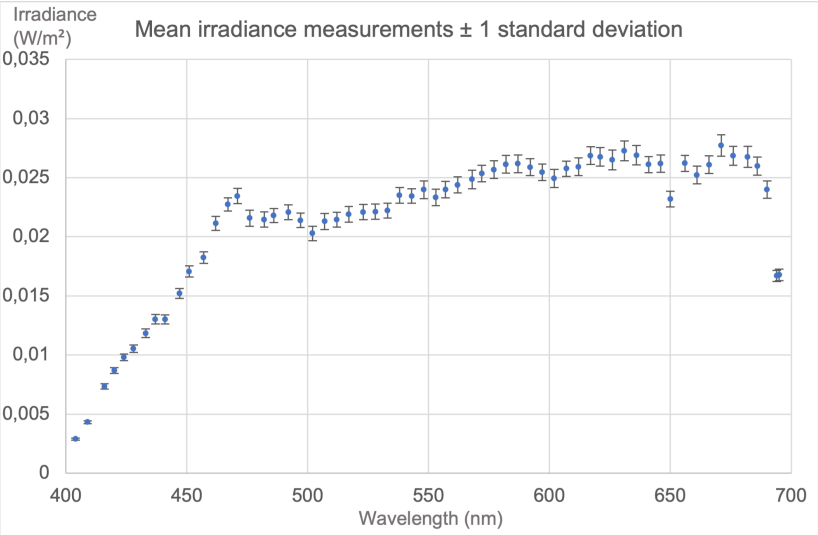

S6-18 Fig. Mean irradiance and standard deviation. Corneal irradiance (W/m²) against wavelength for all wavelength peaks, with their respective standard deviation across multiple measurements. All displayed values are based on spectral irradiance measurements with a field-of-view restriction according to the CIE *S 026* standard [73]. In our case, these measurements are 24% lower than those of the unobstructed sensor diffusor.

7. References

1. Wolfe JM, Kluender KR, Levi DM, Bartoshuk LM, Herz RS, Klatzky RL, et al. Sensation and perception. Second Ed. Sunderland, MA, US: Sinauer Associates; 2017.

2. Roenneberg T, Foster RG. Twilight Times: Light and the Circadian System. Photochemistry and Photobiology. 1997;66(5):549-61. doi: 10.1111/j.1751-1097.1997.tb03188.x.

3. Palm D, Uzoni A, Simon F, Fischer M, Coogan A, Tucha O, et al. Evolutionary conservations, changes of circadian rhythms and their effect on circadian disturbances and therapeutic approaches. Neurosci Biobehav Rev. 2021;128:21-34. Epub 2021/06/09. doi: 10.1016/j.neubiorev.2021.06.007. PubMed PMID: 34102148.

4. Aschoff J. Circadian rhythms in man. Science. 1965;148(3676):1427-32.

5. Roenneberg T, Merrow M. Entrainment of the human circadian clock. Cold Spring Harb Symp Quant Biol. 2007;72:293-9. Epub 2008/04/19. doi: 10.1101/sqb.2007.72.043. PubMed PMID: 18419286.

6. Challet E, Pévet P. Interactions between photic and nonphotic stimuli to synchronize the master circadian clock in mammals. Front Biosci. 2003;8:s246-57. Epub 20030501. doi: 10.2741/1039. PubMed PMID: 12700025.

7. Knoop M, Stefani O, Bueno B, Matusiak B, Hobday R, Wirz-Justice A, et al. Daylight: What makes the difference? Lighting Research & Technology. 2019;0(0):1477153519869758. doi: 10.1177/1477153519869758.

8. Pilorz V, Helfrich-Forster C, Oster H. The role of the circadian clock system in physiology. Pflugers Arch. 2018;470(2):227-39. Epub 20180104. doi: 10.1007/s00424-017-2103-y. PubMed PMID: 29302752.

9. Welsh DK, Takahashi JS, Kay SA. Suprachiasmatic nucleus: cell autonomy and network properties. Annu Rev Physiol. 2010;72:551-77. Epub 2010/02/13. doi: 10.1146/annurev-physiol-021909-135919. PubMed PMID: 20148688; PubMed Central PMCID: PMCPMC3758475.

10. Kalsbeek A, Palm IF, La Fleur SE, Scheer FA, Perreau-Lenz S, Ruiter M, et al. SCN outputs and the hypothalamic balance of life. J Biol Rhythms. 2006;21(6):458-69. Epub 2006/11/17. doi: 10.1177/0748730406293854. PubMed PMID: 17107936.

11. Hattar S, Liao HW, Takao M, Berson DM, Yau KW. Melanopsin-containing retinal ganglion cells: architecture, projections, and intrinsic photosensitivity. Science. 2002;295(5557):1065-70. Epub 2002/02/09. doi: 10.1126/science.1069609. PubMed PMID: 11834834; PubMed Central PMCID: PMCPMC2885915.

12. Berson DM, Dunn FA, Takao M. Phototransduction by retinal ganglion cells that set the circadian clock. Sci. 2002;295(5557):1070-3. doi: 10.1126/science.1067262.

13. Lucas RJ, Peirson SN, Berson DM, Brown TM, Cooper HM, Czeisler CA, et al. Measuring and using light in the melanopsin age. Trends Neurosci. 2014;37(1):1-9. Epub 2013/11/30. doi: 10.1016/j.tins.2013.10.004. PubMed PMID: 24287308; PubMed Central PMCID: PMCPMC4699304.

14. Brainard GC, Hanifin JP, Greeson JM, Byrne B, Glickman G, Gerner E, et al. Action Spectrum for Melatonin Regulation in Humans: Evidence for a Novel Circadian Photoreceptor. The Journal of Neuroscience. 2001;21(16):6405-12. doi: 10.1523/jneurosci.21-16-06405.2001.

15. Thapan K, Arendt J, Skene DJ. An action spectrum for melatonin suppression: evidence for a novel non-rod, non-cone photoreceptor system in humans. The Journal of Physiology. 2001;535(1):261-7. doi: 10.1111/j.1469-7793.2001.t01-1-00261.x.

16. Khalsa SBS, Jewett ME, Cajochen C, Czeisler CA. A phase response curve to single bright light pulses in human subjects. J Physiol. 2003;549(3):945-52. doi: 10.1113/jphysiol.2003.040477.

17. Vandewalle G, Gais S, Schabus M, Balteau E, Carrier J, Darsaud A, et al. Wavelength-dependent modulation of brain responses to a working memory task by daytime light exposure. Cereb Cortex. 2007;17(12):2788-95. Epub 2007/04/04. doi: 10.1093/cercor/bhm007. PubMed PMID: 17404390.

18. Vandewalle G, Schmidt C, Albouy G, Sterpenich V, Darsaud A, Rauchs G, et al. Brain responses to violet, blue, and green monochromatic light exposures in humans: prominent role of blue light and the brainstem. PLoS One. 2007;2(11):e1247. Epub 2007/11/29. doi: 10.1371/journal.pone.0001247. PubMed PMID: 18043754; PubMed Central PMCID: PMCPMC2082413.

19. Cajochen C, Munch M, Kobialka S, Krauchi K, Steiner R, Oelhafen P, et al. High sensitivity of human melatonin, alertness, thermoregulation, and heart rate to short wavelength light. J Clin Endocrinol Metab. 2005;90(3):1311-6. Epub 2004/12/09. doi: 10.1210/jc.2004-0957. PubMed PMID: 15585546.

20. Lockley SW, Evans EE, Scheer FAJL, Brainard GC, Czeisler CA, Aeschbach D. Short-Wavelength sensitivity for the direct effects of light on alertness, vigilance, and the waking electroencephalogram in humans. Sleep. 2006;29(2):161-8. doi: 10.1093/sleep/29.2.161.

21. Mills PR, Tomkins SC, Schlangen LJ. The effect of high correlated colour temperature office lighting on employee wellbeing and work performance. J Circadian Rhythms. 2007;5:2. Epub 2007/01/16. doi: 10.1186/1740-3391-5-2. PubMed PMID: 17217543; PubMed Central PMCID: PMCPMC1779263.

22. aan het Rot M, Benkelfat C, Boivin DB, Young SN. Bright light exposure during acute tryptophan depletion prevents a lowering of mood in mildly seasonal women. European Neuropsychopharmacology. 2008;18(1):14-23. doi: 10.1016/j.euroneuro.2007.05.003.

23. Viola AU, James LM, Schlangen LJ, Dijk DJ. Blue-enriched white light in the workplace improves self-reported alertness, performance and sleep quality. Scand J Work Environ Health. 2008;34(4):297-306. Epub 2008/09/26. doi: 10.5271/sjweh.1268. PubMed PMID: 18815716.

24. Gamlin PD, McDougal DH, Pokorny J, Smith VC, Yau KW, Dacey DM. Human and macaque pupil responses driven by melanopsin-containing retinal ganglion cells. Vision Res. 2007;47(7):946-54. Epub 2007/02/27. doi: 10.1016/j.visres.2006.12.015. PubMed PMID: 17320141; PubMed Central PMCID: PMCPMC1945238.

25. Gaston KJ, Bennie J, Davies TW, Hopkins J. The ecological impacts of nighttime light pollution: a mechanistic appraisal. Biol Rev Camb Philos Soc. 2013;88(4):912-27. Epub 20130408. doi: 10.1111/brv.12036. PubMed PMID: 23565807.

26. Kolberg E, Pallesen S, Hjetland G, Nordhus I, Thun E, Flo-Groeneboom E. Insufficient melanopic equivalent daylight illuminance in nursing home dementia units across seasons and gaze directions. Lighting Research & Technology. 2021;0(0):1477153521994539. doi: 10.1177/1477153521994539.

27. Foster RG. Sleep, circadian rhythms and health. Interface Focus. 2020;10(3):20190098. Epub 2020/05/10. doi: 10.1098/rsfs.2019.0098. PubMed PMID: 32382406; PubMed Central PMCID: PMCPMC7202392.

28. Rea MS, Bierman A, Figueiro MG, Bullough JD. A new approach to understanding the impact of circadian disruption on human health. J Circadian Rhythms. 2008;6:7. Epub 2008/05/31. doi: 10.1186/1740-3391-6-7. PubMed PMID: 18510756; PubMed Central PMCID: PMCPMC2430544.

29. Blask DE, Brainard GC, Dauchy RT, Hanifin JP, Davidson LK, Krause JA, et al. Melatonin-depleted blood from premenopausal women exposed to light at night stimulates growth of human breast cancer xenografts in nude rats. Cancer Res. 2005;65(23):11174-84. Epub 2005/12/03. doi: 10.1158/0008-5472.CAN-05-1945. PubMed PMID: 16322268.

30. Lemmer B, editor Importance of Circadian Rhythms for Regulation of the Cardiovascular System - Studies in Animal and Man. 2006 International Conference of the IEEE Engineering in Medicine and Biology Society; 2006 30 Aug.-3 Sept. 2006.

31. Plitnick B, Figueiro M, Wood B, Rea M. The effects of red and blue light on alertness and mood at night. Light Res Technol. 2010;42(4):449-58. doi: 10.1177/1477153509360887.

32. Brown TM. Melanopic illuminance defines the magnitude of human circadian light responses under a wide range of conditions. J Pineal Res. 2020:e12655. Epub 2020/04/06. doi: 10.1111/jpi.12655. PubMed PMID: 32248548.

33. Do MT, Yau KW. Intrinsically photosensitive retinal ganglion cells. Physiol Rev. 2010;90(4):1547-81. Epub 2010/10/21. doi: 10.1152/physrev.00013.2010. PubMed PMID: 20959623; PubMed Central PMCID: PMCPMC4374737.

34. Brown TM, Thapan K, Arendt J, Revell VL, Skene DJ. S-cone contribution to the acute melatonin suppression response in humans. J Pineal Res. 2021:e12719. Epub 2021/01/30. doi: 10.1111/jpi.12719. PubMed PMID: 33512714.

35. Nagare R, Rea MS, Plitnick B, Figueiro MG. Effect of white light devoid of "Cyan" spectrum radiation on nighttime melatonin suppression over a 1-h exposure duration. J Biol Rhythms. 2019;34(2):195-204. Epub 2019/03/02. doi: 10.1177/0748730419830013. PubMed PMID: 30821188; PubMed Central PMCID: PMCPMC6699625.

36. Mouland JW, Martial F, Watson A, Lucas RJ, Brown TM. Cones support alignment to an inconsistent world by suppressing mouse circadian responses to the blue colors associated with twilight. Curr Biol. 2019;29(24):4260-7 e4. Epub 2019/12/18. doi: 10.1016/j.cub.2019.10.028. PubMed PMID: 31846668; PubMed Central PMCID: PMCPMC6926481.

37. Griefahn B, Künemund C, Bröde P, Mehnert P. The validity of a German version of the Morningness-Eveningness-Questionnaire developed by Horne and Ostberg. Somnologie (Berl). 2001;5(2):71-80. doi: 10.1046/j.1439-054X.2001.01149.x.

38. Kantermann T, Sung H, Burgess HJ. Comparing the Morningness-Eveningness Questionnaire and Munich ChronoType Questionnaire to the Dim Light Melatonin Onset. J Biol Rhythms. 2015;30(5):449-53. Epub 20150804. doi: 10.1177/0748730415597520. PubMed PMID: 26243627; PubMed Central PMCID: PMCPMC4580371.

39. Zauner J, Plischke H, Stijnen H, Schwarz UT, Strasburger H. Influence of common lighting conditions and time-of-day on the effort-related cardiac response. PloS One. 2020;15(10). doi: 10.1371/journal.pone.0239553.

40. Lasauskaite R, Cajochen C. Influence of lighting color temperature on effort-related cardiac response. Biol Psychol. 2018;132:64-70. Epub 2017/11/15. doi: 10.1016/j.biopsycho.2017.11.005. PubMed PMID: 29133144.

41. Bates D, Mächler M, Bolker B, Walker S. Fitting linear mixed-effects models using lme4. J Stat Softw. 2015;67(1). doi: 10.18637/jss.v067.i01.

42. Obayashi K, Saeki K, Kurumatani N. Ambient Light Exposure and Changes in Obesity Parameters: A Longitudinal Study of the HEIJO-KYO Cohort. J Clin Endocrinol Metab. 2016;101(9):3539-47. Epub 2016/07/08. doi: 10.1210/jc.2015-4123. PubMed PMID: 27383113.

43. Esaki Y, Obayashi K, Saeki K, Fujita K, Iwata N, Kitajima T. Effect of evening light exposure on sleep in bipolar disorder: A longitudinal analysis for repeated measures in the APPLE cohort. Australian & New Zealand Journal of Psychiatry. 2020;0(0):0004867420968886. doi: 10.1177/0004867420968886. PubMed PMID: 33118369.

44. Lok R, Zerbini G, Gordijn MCM, Beersma DGM, Hut RA. Gold, silver or bronze: circadian variation strongly affects performance in Olympic athletes. Sci Rep. 2020;10(1):16088. Epub 2020/10/10. doi: 10.1038/s41598-020-72573-8. PubMed PMID: 33033271.

45. Druijff-van de Woestijne GB, McConchie H, de Kort YAW, Licitra G, Zhang C, Overeem S, et al. Behavioural biometrics: Using smartphone keyboard activity as a proxy for rest-activity patterns. J Sleep Res. 2021:e13285. Epub 2021/03/06. doi: 10.1111/jsr.13285. PubMed PMID: 33666298.

46. Kaifie A, Reugels M, Kraus T, Kursawe M. The pupillary light reflex (PLR) as a marker for the ability to work or drive - a feasibility study. J Occup Med Toxicol. 2021;16(1):39. Epub 2021/09/09. doi: 10.1186/s12995-021-00330-2. PubMed PMID: 34493308; PubMed Central PMCID: PMCPMC8422642.

47. Plischke H, Linek M, Zauner J. The opportunities of biodynamic lighting in homes for the elderly. Current Directions in Biomedical Engineering. 2018;4(1):123-6. doi: 10.1515/cdbme-2018-0031.

48. Zauner J, Plischke H. Designing Light for Night Shift Workers: Application of Nonvisual Lighting Design Principles in an Industrial Production Line. Applied Sciences. 2021;11(22). doi: 10.3390/app112210896.

49. Zauner J, Plischke H, Strasburger H. Spectral dependency of the human pupillary light reflex. Influences of pre-adaptation and chronotype. PLoS ONE. 2021;Accepted November 2nd, 2021. doi: 10.1371/journal.pone.0253030.

50. Mure LS, Cornut PL, Rieux C, Drouyer E, Denis P, Gronfier C, et al. Melanopsin bistability: a fly's eye technology in the human retina. PLoS One. 2009;4(6):e5991. Epub 2009/06/25. doi: 10.1371/journal.pone.0005991. PubMed PMID: 19551136; PubMed Central PMCID: PMCPMC2695781.

51. Adhikari P, Zele AJ, Feigl B. The post-illumination pupil response (PIPR). Invest Ophthalmol Vis Sci. 2015;56(6):3838-49. Epub 2015/06/13. doi: 10.1167/iovs.14-16233. PubMed PMID: 26066752.

52. Park JC, Moura AL, Raza AS, Rhee DW, Kardon RH, Hood DC. Toward a clinical protocol for assessing rod, cone, and melanopsin contributions to the human pupil response. Invest Ophthalmol Vis Sci. 2011;52(9):6624-35. Epub 2011/07/12. doi: 10.1167/iovs.11-7586. PubMed PMID: 21743008; PubMed Central PMCID: PMCPMC3175993.

53. Kankipati L, Girkin CA, Gamlin PD. The post-illumination pupil response is reduced in glaucoma patients. Invest Ophthalmol Vis Sci. 2011;52(5):2287-92. Epub 2011/01/08. doi: 10.1167/iovs.10-6023. PubMed PMID: 21212172; PubMed Central PMCID: PMCPMC3080733.

54. Maynard ML, Zele AJ, Feigl B. Melanopsin-mediated post-illumination pupil response in early age-related macular degeneration. Invest Ophthalmol Vis Sci. 2015;56(11):6906-13. Epub 2015/10/28. doi: 10.1167/iovs.15-17357. PubMed PMID: 26505464.

55. Ba-Ali S, Brondsted AE, Andersen HU, Jennum P, Lund-Andersen H. Pupillary light responses in type 1 and type 2 diabetics with and without retinopathy. Acta Ophthalmol. 2020. Epub 2020/01/17. doi: 10.1111/aos.14348. PubMed PMID: 31943805.

56. You S, Hong JH, Yoo J. Analysis of pupillometer results according to disease stage in patients with Parkinson's disease. Sci Rep. 2021;11(1):17880. Epub 2021/09/11. doi: 10.1038/s41598-021-97599-4. PubMed PMID: 34504251; PubMed Central PMCID: PMCPMC8429555.

57. Roecklein K, Wong P, Ernecoff N, Miller M, Donofry S, Kamarck M, et al. The post illumination pupil response is reduced in seasonal affective disorder. Psychiatry Res. 2013;210(1):150-8. Epub 2013/07/03. doi: 10.1016/j.psychres.2013.05.023. PubMed PMID: 23809464; PubMed Central PMCID: PMCPMC3795919.

58. Rukmini AV, Milea D, Gooley JJ. Chromatic pupillometry methods for assessing photoreceptor health in retinal and optic nerve diseases. Front Neurol. 2019;10:76. Epub 2019/02/28. doi: 10.3389/fneur.2019.00076. PubMed PMID: 30809186; PubMed Central PMCID: PMCPMC6379484.

59. de Zeeuw J, Papakonstantinou A, Nowozin C, Stotz S, Zaleska M, Hadel S, et al. Living in Biological Darkness: Objective Sleepiness and the Pupillary Light Responses Are Affected by Different Metameric Lighting Conditions during Daytime. J Biol Rhythms. 2019;34(4):410-31. Epub 20190602. doi: 10.1177/0748730419847845. PubMed PMID: 31156018; PubMed Central PMCID: PMCPMC6637815.

60. Wood S. Generalized Additive Models: An Introduction with R, Second Edition. Boca Raton: CRC Press, Taylor & Francis Group; 2017.

61. Pedersen EJ, Miller DL, Simpson GL, Ross N. Hierarchical generalized additive models in ecology: an introduction with mgcv. PeerJ. 2019;7:e6876. Epub 2019/06/11. doi: 10.7717/peerj.6876. PubMed PMID: 31179172; PubMed Central PMCID: PMCPMC6542350.

62. Sóskuthy M. Generalised additive mixed models for dynamic analysis in linguistics: a practical introduction. arXiv: 1703.05339v1 [stat.AP]; 2017.

63. Simpson GL. Modelling palaeoecological time series using generalised additive models. Front Ecol Evol. 2018;6. doi: 10.3389/fevo.2018.00149.

64. Kelbsch C, Strasser T, Chen Y, Feigl B, Gamlin PD, Kardon R, et al. Standards in Pupillography. Front Neurol. 2019;10:129. Epub 2019/03/12. doi: 10.3389/fneur.2019.00129. PubMed PMID: 30853933; PubMed Central PMCID: PMCPMC6395400.

65. Mohawk JA, Green CB, Takahashi JS. Central and peripheral circadian clocks in mammals. Annu Rev Neurosci. 2012;35:445-62. Epub 2012/04/10. doi: 10.1146/annurev-neuro-060909-153128. PubMed PMID: 22483041; PubMed Central PMCID: PMCPMC3710582.

66. Lucassen EA, Coomans CP, van Putten M, de Kreij SR, van Genugten JH, Sutorius RP, et al. Environmental 24-hr cycles are essential for health. Curr Biol. 2016;26(14):1843-53. Epub 2016/07/19. doi: 10.1016/j.cub.2016.05.038. PubMed PMID: 27426518.

67. Boivin DB, Duffy JF, Kronauer RE, Czeisler CA. Dose-response relationships for resetting of human circadian clock by light. Nature. 1996;379(6565):540-2. doi: 10.1038/379540a0.

68. Zeitzer JM, Dijk DJ, Kronauer R, Brown E, Czeisler C. Sensitivity of the human circadian pacemaker to nocturnal light: melatonin phase resetting and suppression. The Journal of physiology. 2000;526 Pt 3(Pt 3):695-702. doi: 10.1111/j.1469-7793.2000.00695.x. PubMed PMID: 10922269.

69. Dijk DJ, Archer SN. Light, sleep, and circadian rhythms: together again. PLoS Biol. 2009;7(6):e1000145. Epub 2009/06/24. doi: 10.1371/journal.pbio.1000145. PubMed PMID: 19547745; PubMed Central PMCID: PMCPMC2691600.

70. Chellappa SL, Gordijn MCM, Cajochen C. Chapter 7 - Can light make us bright? Effects of light on cognition and sleep. In: Van Dongen HPA, Kerkhof GA, editors. Prog Brain Res. 190: Elsevier; 2011. p. 119-33.

71. Bailes HJ, Lucas RJ. Human melanopsin forms a pigment maximally sensitive to blue light (lambdamax approximately 479 nm) supporting activation of G(q/11) and G(i/o) signalling cascades. Proc Biol Sci. 2013;280(1759):20122987. Epub 2013/04/05. doi: 10.1098/rspb.2012.2987. PubMed PMID: 23554393; PubMed Central PMCID: PMCPMC3619500.

72. Schmidt TM, Chen SK, Hattar S. Intrinsically photosensitive retinal ganglion cells: many subtypes, diverse functions. Trends Neurosci. 2011;34(11):572-80. Epub 2011/08/06. doi: 10.1016/j.tins.2011.07.001. PubMed PMID: 21816493; PubMed Central PMCID: PMCPMC3200463.

73. CIE. CIE S 026/E:2018. CIE system for metrology of optical radiation for ipRGC-influenced responses of light. In: CIE, editor. CIE S 026/E:2018. Vienna: CIE; 2018.

74. Pachito DV, Eckeli AL, Desouky AS, Corbett MA, Partonen T, Rajaratnam SM, et al. Workplace lighting for improving alertness and mood in daytime workers. Cochrane Database Syst Rev. 2018;3:CD012243. Epub 2018/03/03. doi: 10.1002/14651858.CD012243.pub2. PubMed PMID: 29498416; PubMed Central PMCID: PMCPMC6494162.

75. Obrist PA. The cardiovascular-behavioral interaction—as it appears today. Psychophysiology. 1976;13(2):95-107. doi: 10.1111/j.1469-8986.1976.tb00081.x.

76. Brehm JWa, Self EA. The intensity of motivation. Annu Rev Psychol. 1989;40(1):109-31. doi: 10.1146/annurev.ps.40.020189.000545. PubMed PMID: 2648973.

77. André N, Audiffren M, Baumeister RF. An integrative model of effortful control. Front Syst Neurosci. 2019;13. doi: 10.3389/fnsys.2019.00079.

78. Wright RA, Kirby LD. Effort determination of cardiovascular response: An integrative analysis with applications in social psychology. Adv Exp Soc Psychol. 33: Academic Press; 2001. p. 255-307.

79. Prayag AS, Jost S, Avouac P, Dumortier D, Gronfier C. Dynamics of non-visual responses in humans: as fast as lightning? Front Neurosci. 2019;13:126. Epub 2019/03/21. doi: 10.3389/fnins.2019.00126. PubMed PMID: 30890907; PubMed Central PMCID: PMCPMC6411922.

80. Scholkmann F, Hafner T, Metz AJ, Wolf M, Wolf U. Effect of short-term colored-light exposure on cerebral hemodynamics and oxygenation, and systemic physiological activity. Neurophotonics. 2017;4(4):045005. Epub 2017/11/29. doi: 10.1117/1.NPh.4.4.045005. PubMed PMID: 29181427; PubMed Central PMCID: PMCPMC5695650.

81. Billman GE. The LF/HF ratio does not accurately measure cardiac sympatho-vagal balance. Front Physiol. 2013;4:26. Epub 2013/02/23. doi: 10.3389/fphys.2013.00026. PubMed PMID: 23431279; PubMed Central PMCID: PMCPMC3576706.

82. McIntyre IM, Norman TR, Burrows GD, Armstrong SM. Human melatonin response to light at different times of the night. Psychoneuroendocrinology. 1989;14(3):187-93. doi: 10.1016/0306-4530(89)90016-4.

83. Munch M, Leon L, Crippa SV, Kawasaki A. Circadian and wake-dependent effects on the pupil light reflex in response to narrow-bandwidth light pulses. Invest Ophthalmol Vis Sci. 2012;53(8):4546-55. Epub 2012/06/07. doi: 10.1167/iovs.12-9494. PubMed PMID: 22669721.

84. Blatter K, Cajochen C. Circadian rhythms in cognitive performance: Methodological constraints, protocols, theoretical underpinnings. Physiol Behav. 2007;90(2):196-208. doi: 10.1016/j.physbeh.2006.09.009.

85. Faul F, Erdfelder E, Lang A-G, Buchner A. G*Power 3: A flexible statistical power analysis program for the social, behavioral, and biomedical sciences. Behavior Research Methods. 2007;39(2):175-91. doi: 10.3758/BF03193146.

86. DIN. DIN EN 12464-1:2011-08. Light and lighting - Lighting of work places - Part 1: Indoor work places. DIN EN 12464-1:2011-08. Berlin: Beuth publishing company; 2011.

87. Bellia L, Pedace A, Fragliasso F. Indoor lighting quality: Effects of different wall colours. Light Res Technol. 2017;49(1):33-48. doi: 10.1177/1477153515594654.

88. Spitschan M, Woelders T. The Method of Silent Substitution for Examining Melanopsin Contributions to Pupil Control. Front Neurol. 2018;9:941. Epub 2018/12/13. doi: 10.3389/fneur.2018.00941. PubMed PMID: 30538662; PubMed Central PMCID: PMCPMC6277556.

89. Sherwood A, Allen MT, Fahrenberg J, Kelsey RM, Lovallo WR, van Doornen LJP. Methodological guidelines for impedance cardiography. Psychophysiology. 1990;27(1):1-23. doi: 10.1111/j.1469-8986.1990.tb02171.x.

90. Akerstedt T, Gillberg M. Subjective and objective sleepiness in the active individual. Int J Neurosci. 1990;52(1-2):29-37. Epub 1990/05/01. doi: 10.3109/00207459008994241. PubMed PMID: 2265922.

91. Kaida K, Takahashi M, Akerstedt T, Nakata A, Otsuka Y, Haratani T, et al. Validation of the Karolinska sleepiness scale against performance and EEG variables. Clin Neurophysiol. 2006;117(7):1574-81. Epub 2006/05/09. doi: 10.1016/j.clinph.2006.03.011. PubMed PMID: 16679057.

92. Cajochen C. Alerting effects of light. Sleep Med Rev. 2007;11(6):453-64. Epub 2007/10/16. doi: 10.1016/j.smrv.2007.07.009. PubMed PMID: 17936041.

93. Mueller ST, Piper BJ. The Psychology Experiment Building Language (PEBL) and PEBL test battery. J Neurosci Methods. 2014;222:250-9. Epub 2013/11/26. doi: 10.1016/j.jneumeth.2013.10.024. PubMed PMID: 24269254; PubMed Central PMCID: PMCPMC3897935.

94. Sternberg S. High-speed scanning in human memory. Science. 1966;153(3736):652-4. doi: 10.1126/science.153.3736.652.

95. Hart SG, Staveland LE. Development of NASA-TLX (Task Load Index): results of empirical and theoretical research. In: Hancock PA, Meshkati N, editors. Advances in Psychology. 52: North-Holland; 1988. p. 139-83.

96. Lozano DL, Norman G, Knox D, Wood BL, Miller BD, Emery CF, et al. Where to B in dZ/dt. Psychophysiology. 2007;44(1):113-9. Epub 2007/01/24. doi: 10.1111/j.1469-8986.2006.00468.x. PubMed PMID: 17241147.

97. Berntson GG, Lozano DL, Chen YJ, Cacioppo JT. Where to Q in PEP. Psychophysiology. 2004;41(2):333-7. Epub 2004/03/23. doi: 10.1111/j.1469-8986.2004.00156.x. PubMed PMID: 15032999.

98. Savitzky A, Golay MJE. Smoothing and differentiation of data by simplified least squares procedures. Anal Chem. 1964;36(8):1627-39. doi: 10.1021/ac60214a047.

99. Press WH, Teukolsky SA, Vetterling WT, Flannery BP. Numerical Recipes 3rd Edition: The Art of Scientific Computing: Cambridge University Press; 2007.

100. Debski TT, Zhang Y, Jennings JR, Kamarck TW. Stability of cardiac impedance measures: Aortic opening (B-point) detection and scoring. Biol Psychol. 1993;36(1):63-74. doi: 10.1016/0301-0511(93)90081-I.

101. McCubbin JA, Richardson JE, Langer AW, Kizer JS, Obrist PA. Sympathetic neuronal function and left ventricular performance during behavioral stress in humans: the relationship between plasma catecholamines and systolic time intervals. Psychophysiology. 1983;20(1):102-10. doi: 10.1111/j.1469-8986.1983.tb00910.x.

102. Wallace AG, Mitchell JH, Skinner NS, Sarnoff SJ. Duration of the phases of left ventricular systole. Circ Res. 1963;12(6):611-9. doi: doi:10.1161/01.RES.12.6.611.

103. Schächinger H, Weinbacher M, Kiss A, Ritz R, Langewitz W. Cardiovascular indices of peripheral and central sympathetic activation. Psychosom Med. 2001;63(5):788-96. PubMed PMID: 00006842-200109000-00012.

104. R Core Team. R: a language and environment for statistical computing. Vienna, Austria: R Foundation for Statistical Computing; 2017.

105. Barr DJ, Levy R, Scheepers C, Tily HJ. Random effects structure for confirmatory hypothesis testing: keep it maximal. J Mem Lang. 2013;68(3). Epub 2014/01/10. doi: 10.1016/j.jml.2012.11.001. PubMed PMID: 24403724; PubMed Central PMCID: PMCPMC3881361.

106. Selya AS, Rose JS, Dierker LC, Hedeker D, Mermelstein RJ. A practical guide to calculating Cohen's f(2), a measure of local effect size, from PROC MIXED. Front Psychol. 2012;3:111. Epub 2012/04/25. doi: 10.3389/fpsyg.2012.00111. PubMed PMID: 22529829; PubMed Central PMCID: PMCPMC3328081.

107. Sheskin DJ. Handbook of Parametric and Nonparametric Statistical Procedures, Fifth Edition. Boca Raton: CRC Press; 2011.

108. Christensen RHB. Ordinal - regression models for ordinal data. 2019.

109. Allen M, Poggiali D, Whitaker K, Marshall TR, Kievit RA. Raincloud plots: a multi-platform tool for robust data visualization. Wellcome Open Res. 2019;4:63. Epub 2019/05/10. doi: 10.12688/wellcomeopenres.15191.1. PubMed PMID: 31069261; PubMed Central PMCID: PMCPMC6480976.

110. Hart SG. Nasa-Task Load Index (NASA-TLX); 20 years later. Proceedings of the Human Factors and Ergonomics Society Annual Meeting. 2006;50(9):904-8. doi: 10.1177/154193120605000909.

111. Figueiro MG, Sahin L, Wood B, Plitnick B. Light at night and measures of alertness and performance: implications for shift workers. Biol Res Nurs. 2016;18(1):90-100. Epub 2015/02/24. doi: 10.1177/1099800415572873. PubMed PMID: 25697165.

112. McDougal DH, Gamlin PD. The influence of intrinsically-photosensitive retinal ganglion cells on the spectral sensitivity and response dynamics of the human pupillary light reflex. Vision Res. 2010;50(1):72-87. Epub 2009/10/24. doi: 10.1016/j.visres.2009.10.012. PubMed PMID: 19850061; PubMed Central PMCID: PMCPMC2795133.

113. van Eekelen APJ, Houtveen JH, Kerkhof GA. Circadian variation in cardiac autonomic activity: reactivity measurements to different types of stressors. Chronobiol Int. 2004;21(1):107-29. doi: 10.1081/CBI-120027983.

114. Holmes AL, Burgess HJ, McCulloch K, Lamond N, Fletcher A, Dorrian J, et al. Daytime cardiac autonomic activity during one week of continuous night shift. J Hum Ergol (Tokyo). 2001;30(1-2):223-8. doi: 10.11183/jhe1972.30.223.

115. Carrington M, Walsh M, Stambas T, Kleiman J, Trinder J. The influence of sleep onset on the diurnal variation in cardiac activity and cardiac control. J Sleep Res. 2003;12(3):213-21. doi: 10.1046/j.1365-2869.2003.00364.x.

116. Oldham MA, Ciraulo DA. Bright light therapy for depression: a review of its effects on chronobiology and the autonomic nervous system. Chronobiol Int. 2014;31(3):305-19. Epub 2014/01/09. doi: 10.3109/07420528.2013.833935. PubMed PMID: 24397276; PubMed Central PMCID: PMCPMC5403163.

117. Goldstein D, Hahn CS, Hasher L, Wiprzycka UJ, Zelazo PD. Time of day, intellectual performance, and behavioral problems in morning versus evening type adolescents: is there a synchrony effect? Pers Individ Dif. 2007;42(3):431-40. doi: 10.1016/j.paid.2006.07.008. PubMed PMID: 17268574.

118. Krauchi K, Wirz-Justice A. Circadian rhythm of heat production, heart rate, and skin and core temperature under unmasking conditions in men. Am J Physiol Regul Integr Comp Physiol. 1994;267(3):R819-R29. doi: 10.1152/ajpregu.1994.267.3.R819. PubMed PMID: 8092328.

119. Satish U, Mendell MJ, Shekhar K, Hotchi T, Sullivan D, Streufert S, et al. Is CO2 an indoor pollutant? Direct effects of low-to-moderate CO2 concentrations on human decision-making performance. Environ Health Perspect. 2012;120(12):1671-7. doi: doi:10.1289/ehp.1104789.

120. Seppanen O, Fisk WJ, Lei QH, editors. Effect of temperature on task performance in office environment. Conference: 5th International Conference on Cold ClimateHeating, Ventilating and Air Conditioning, Moscow, Russia, May 21-24,2006; 2006: ; Ernest Orlando Lawrence Berkeley NationalLaboratory, Berkeley, CA (US).

121. Goodman SN. Of P-values and Bayes: a modest proposal. Epidemiology. 2001;12(3):295-7. doi: 10.1097/00001648-200105000-00006. PubMed PMID: 11337600.

122. Richter M, Friedrich A, Gendolla GH. Task difficulty effects on cardiac activity. Psychophysiology. 2008;45(5):869-75. Epub 2008/07/31. doi: 10.1111/j.1469-8986.2008.00688.x. PubMed PMID: 18665860.

123. Richter M, Gendolla GH. The heart contracts to reward: monetary incentives and preejection period. Psychophysiology. 2009;46(3):451-7. Epub 2009/02/20. doi: 10.1111/j.1469-8986.2009.00795.x. PubMed PMID: 19226305.

124. Silvestrini N, Gendolla GH. Beta-adrenergic impact underlies the effect of mood and hedonic instrumentality on effort-related cardiovascular response. Biol Psychol. 2011;87(2):209-17. Epub 2011/03/09. doi: 10.1016/j.biopsycho.2011.02.017. PubMed PMID: 21382436.

125. Sikka G, Hussmann GP, Pandey D, Cao S, Hori D, Park JT, et al. Melanopsin mediates light-dependent relaxation in blood vessels. Proc Natl Acad Sci U S A. 2014;111(50):17977-82. Epub 2014/11/19. doi: 10.1073/pnas.1420258111. PubMed PMID: 25404319; PubMed Central PMCID: PMCPMC4273372.

126. Stern M, Broja M, Sansone R, Grone M, Skene SS, Liebmann J, et al. Blue light exposure decreases systolic blood pressure, arterial stiffness, and improves endothelial function in humans. Eur J Prev Cardiol. 2018;25(17):1875-83. Epub 2018/09/11. doi: 10.1177/2047487318800072. PubMed PMID: 30196723.

127. Revell VL, Arendt J, Fogg LF, Skene DJ. Alerting effects of light are sensitive to very short wavelengths. Neurosci Lett. 2006;399(1-2):96-100. Epub 2006/02/24. doi: 10.1016/j.neulet.2006.01.032. PubMed PMID: 16490309.

128. Chellappa SL, Steiner R, Blattner P, Oelhafen P, Götz T, Cajochen C. Non-visual effects of light on melatonin, alertness and cognitive performance: can blue-

enriched light keep us alert? PLOS ONE. 2011;6(1):e16429. doi: 10.1371/journal.pone.0016429.

129. Laszewska K, Goroncy A, Weber P, Pracki T, Tafil-Klawe M. Influence of the spectral quality of light on daytime alertness levels in humans. Adv Cogn Psychol. 2018;14:192-208. doi: 10.5709/acp-0250-0.

130. DIN. DIN SPEC 67600:2013-04. Biologically effective illumination - Design guidelines. DIN SPEC 67600:2013-04. Berlin: Beuth Publishing Company; 2013.

131. CIE position statement - proper light at the proper time [Internet]. Vienna: CIE; 2019. Available from: http://cie.co.at/publications/position-statement-non-visual-effects-light-recommending-proper-light-proper-time-2nd (last viewed 24.11.2021)

132. McDougal DH, Gamlin PD. Autonomic Control of the Eye. Comprehensive Physiology2014. p. 439-73.

133. Szabadi E. Functional Organization of the Sympathetic Pathways Controlling the Pupil: Light-Inhibited and Light-Stimulated Pathways. Front Neurol. 2018;9:1069. Epub 2019/01/09. doi: 10.3389/fneur.2018.01069. PubMed PMID: 30619035; PubMed Central PMCID: PMCPMC6305320.

134. Watson AB, Yellott JI. A unified formula for light-adapted pupil size. J Vis. 2012;12(10):12. Epub 2012/09/27. doi: 10.1167/12.10.12. PubMed PMID: 23012448.

135. Wagman IH, Gullberg JE. The relationship between monochromatic light and pupil diameter. The low intensity visibility curve as measured by pupillary measurements. Am J Physiol. 1942;137(4):769-78. doi: 10.1152/ajplegacy.1942.137.4.769.

136. Alpern M, Campbell FW. The spectral sensitivity of the consensual light reflex. J Physiol. 1962;164(3):478-507. doi: 10.1113/jphysiol.1962.sp007033. PubMed PMID: 14012269.

137. Bouma H. Size of the static pupil as a function of wave-length and luminosity of the light incident on the human eye. Nat. 1962;193(4816):690-1. doi: 10.1038/193690a0.

138. Adrian W. Spectral sensitivity of the pupillary system. Clin Exp Optom. 2003;86(4):235-8. doi: 10.1111/j.1444-0938.2003.tb03111.x.

139. Lucas RJ, Douglas RH, Foster RG. Characterization of an ocular photopigment capable of driving pupillary constriction in mice. Nat Neurosci. 2001;4(6):621-6. doi: 10.1038/88443.

140. Zaidi FH, Hull JT, Peirson SN, Wulff K, Aeschbach D, Gooley JJ, et al. Short-wavelength light sensitivity of circadian, pupillary, and visual awareness in humans lacking an outer retina. Curr Biol. 2007;17(24):2122-8. Epub 2007/12/18. doi: 10.1016/j.cub.2007.11.034. PubMed PMID: 18082405; PubMed Central PMCID: PMCPMC2151130.

141. Gooley JJ, Ho Mien I, St Hilaire MA, Yeo SC, Chua EC, van Reen E, et al. Melanopsin and rod-cone photoreceptors play different roles in mediating pupillary light responses during exposure to continuous light in humans. J Neurosci. 2012;32(41):14242-53. Epub 2012/10/12. doi: 10.1523/JNEUROSCI.1321-12.2012. PubMed PMID: 23055493; PubMed Central PMCID: PMCPMC3515688.

142. Spitschan M. Photoreceptor inputs to pupil control. J Vis. 2019;19(9):5. Epub 2019/08/16. doi: 10.1167/19.9.5. PubMed PMID: 31415056; PubMed Central PMCID: PMCPMC6699792.

143. Zandi B, Klabes J, Khanh TQ. Prediction accuracy of L- and M-cone based human pupil light models. Sci Rep. 2020;10(1):10988. Epub 2020/07/06. doi: 10.1038/s41598-020-67593-3. PubMed PMID: 32620793.

144. Rao F, Chan AHS, Zhu XF. Effects of photopic and cirtopic illumination on steady state pupil sizes. Vision Res. 2017;137:24-8. Epub 2017/07/10. doi: 10.1016/j.visres.2017.02.010. PubMed PMID: 28688906.

145. Bonmati-Carrion MA, Hild K, Isherwood C, Sweeney SJ, Revell VL, Skene DJ, et al. Relationship between human pupillary light reflex and circadian system status. PLoS One. 2016;11(9):e0162476. Epub 2016/09/17. doi: 10.1371/journal.pone.0162476. PubMed PMID: 27636197; PubMed Central PMCID: PMCPMC5026360.

146. Adhikari P, Zele AJ, Thomas R, Feigl B. Quadrant field pupillometry detects melanopsin dysfunction in glaucoma suspects and early glaucoma. Sci Rep. 2016;6:33373. Epub 2016/09/14. doi: 10.1038/srep33373. PubMed PMID: 27622679; PubMed Central PMCID: PMCPMC5020729.

147. Feigl B, Zele AJ, Fader SM, Howes AN, Hughes CE, Jones KA, et al. The post-illumination pupil response of melanopsin-expressing intrinsically photosensitive retinal ganglion cells in diabetes. Acta Ophthalmol. 2012;90(3):e230-4. Epub 2011/09/03. doi: 10.1111/j.1755-3768.2011.02226.x. PubMed PMID: 21883986.

148. Chellappa SL, Steiner R, Oelhafen P, Cajochen C. Sex differences in light sensitivity impact on brightness perception, vigilant attention and sleep in humans. Sci Rep. 2017;7(1):14215. Epub 2017/10/29. doi: 10.1038/s41598-017-13973-1. PubMed PMID: 29079823; PubMed Central PMCID: PMCPMC5660221.

149. Zele AJ, Feigl B, Smith SS, Markwell EL. The circadian response of intrinsically photosensitive retinal ganglion cells. PLoS One. 2011;6(3):e17860. Epub 2011/03/23. doi: 10.1371/journal.pone.0017860. PubMed PMID: 21423755; PubMed Central PMCID: PMCPMC3056772.

150. Lanthony P. The desaturated panel D-15. Doc Ophthalmol. 1978;46(1):185-9. doi: 10.1007/BF00174107.

151. Ishihara S. Tests for colour-blindness. Tokyo: Kanehara Shuppan Co., LTD.; 1972.

152. Simmons JP, Nelson LD, Simonsohn U. False-positive psychology: undisclosed flexibility in data collection and analysis allows presenting anything as significant. Psychol Sci. 2011;22(11):1359-66. Epub 2011/10/19. doi: 10.1177/0956797611417632. PubMed PMID: 22006061.

153. Dacey DM, Liao H-W, Peterson BB, Robinson FR, Smith VC, Pokorny J, et al. Melanopsin-expressing ganglion cells in primate retina signal colour and irradiance and project to the LGN. Nature. 2005;433(7027):749-54. doi: 10.1038/nature03387.

154. Schneider CA, Rasband WS, Eliceiri KW. NIH Image to ImageJ: 25 years of image analysis. Nat Methods. 2012;9(7):671-5. doi: 10.1038/nmeth.2089.

155. Daneault V, Vandewalle G, Hebert M, Teikari P, Mure LS, Doyon J, et al. Does pupil constriction under blue and green monochromatic light exposure change with age? J Biol Rhythms. 2012;27(3):257-64. Epub 2012/06/02. doi: 10.1177/0748730412441172. PubMed PMID: 22653894; PubMed Central PMCID: PMCPMC5380439.

156. Iadanza E, Goretti F, Sorelli M, Melillo P, Pecchia L, Simonelli F, et al. Automatic detection of genetic diseases in pediatric age using pupillometry. IEEE Access. 2020;8:34949-61. doi: 10.1109/access.2020.2973747.

157. Supporting Information to this publication in the Open Science Framework Database [Internet]. 2021. Available from: https://osf.io/ar2ud/

158. CIE. ISO/CIE 11664-1:2019(E). Colorimetry — Part 1: CIE standard colorimetric observers. ISO/CIE 11664-1:2019(E). Vienna: CIE; 2019.

159. CIE. CIE 165:2005. CIE 10 Degree photopic photometric observer. CIE 165:2005. Vienna: CIE; 2005.

160. Lang D. Human Centric Lighting. Daylight-Related Metrics as prerequisite for assessment of light quality and for lighting design 2016. Available from: http://lightingforpeople.eu/2016/wp-content/uploads/2016/10/Day-light-related-metrics-for-human-centric-lighting.pdf (last viewed 24.11.2021).

161. CIE. ISO 23539:2005(E) / CIE S 010/E:2004. Photometry - the CIE system of physical photometry. ISO 23539:2005(E) / CIE S 010/E:2004. Vienna: CIE; 2004.

162. DIN. DIN 5031-2:1982:03. Optical radiation physics and illuminating engineering; evaluation of radiation by different detectors. DIN 5031-2:1982:03. Berlin: Beuth publishing company; 1982.

163. DIN. DIN 5031-3:1982:03. Optical radiation physics and illuminating engineering; quantities, symbols and units of illuminating engineering. DIN 5031-3:1982:03. Berlin: Beuth publishing company; 1982.

164. CIE. CIE TN 004:2016. The use of terms and units in photometry - implementation of the CIE system for mesopic photometry. CIE TN 004:2016. Vienna: CIE; 2016.

165. Lund D, Marshall J, Mellerio J, Okuno T, Schulmeister K, Sliney D, et al., editors. A computerized approach to transmission and absorption characteristics of the human eye. CIE; 2012.

166. Hastie T, Tibshirani R. Generalized additive models. Statist Sci. 1986;1(3):297-310. doi: 10.1214/ss/1177013604.

167. Hastie T, Tibshirani R. Generalized additive models for medical research. Stat Methods Med Res. 1995;4(3):187-96. doi: 10.1177/096228029500400302. PubMed PMID: 8548102.

168. Ringer RVC, Allison M.; Larson, Adam M.; Loschky, Lester C. Crowding in natural scenes. Iperception. 2021.

169. Wood SN, Pya N, Säfken B. Smoothing parameter and model selection for general smooth models. J Am Stat Assoc. 2017;111(516):1548-63. doi: 10.1080/01621459.2016.1180986.

170. Xu R. Measuring explained variation in linear mixed effects models. Stat Med. 2003;22(22):3527-41. Epub 2003/11/06. doi: 10.1002/sim.1572. PubMed PMID: 14601017.

171. Veitch JA, Knoop M. CIE TN 011:2020. What to document and report in studies of ipRGC-influenced responses to light. CIE TN 011:2020. Vienna: CIE; 2020.

172. Joyce DS, Feigl B, Zele AJ. The effects of short-term light adaptation on the human post-illumination pupil response. Invest Ophthalmol Vis Sci. 2016;57(13):5672-80. Epub 2016/10/27. doi: 10.1167/iovs.16-19934. PubMed PMID: 27784072.

173. Zele AJ, Cao D. Vision under mesopic and scotopic illumination. Front Psychol. 2014;5:1594. Epub 2015/02/07. doi: 10.3389/fpsyg.2014.01594. PubMed PMID: 25657632; PubMed Central PMCID: PMCPMC4302711.

174. Spitschan M, Jain S, Brainard DH, Aguirre GK. Opponent melanopsin and S-cone signals in the human pupillary light response. Proc Natl Acad Sci U S A. 2014;111(43):15568-72. Epub 2014/10/15. doi: 10.1073/pnas.1400942111. PubMed PMID: 25313040; PubMed Central PMCID: PMCPMC4217411.

175. Lee SK, Sonoda T, Schmidt TM. M1 intrinsically photosensitive retinal ganglion cells integrate rod and melanopsin inputs to signal in low light. Cell Rep.

2019;29(11):3349-55 e2. Epub 2019/12/12. doi: 10.1016/j.celrep.2019.11.024. PubMed PMID: 31825819; PubMed Central PMCID: PMCPMC6951432.

176. Patterson SS, Kuchenbecker JA, Anderson JR, Neitz M, Neitz J. A color vision circuit for non-image-forming vision in the primate retina. Curr Biol. 2020. Epub 2020/02/23. doi: 10.1016/j.cub.2020.01.040. PubMed PMID: 32084404.

177. Spitschan M, Lazar R, Yetik E, Cajochen C. No evidence for an S cone contribution to acute neuroendocrine and alerting responses to light. Curr Biol. 2019;29(24):R1297-R8. Epub 2019/12/18. doi: 10.1016/j.cub.2019.11.031. PubMed PMID: 31846672; PubMed Central PMCID: PMCPMC6926470.

178. Guido ME, Marchese NA, Rios MN, Morera LP, Diaz NM, Garbarino-Pico E, et al. Non-visual opsins and novel photo-detectors in the vertebrate inner retina mediate light responses within the blue spectrum region. Cell Mol Neurobiol. 2020. Epub 2020/11/25. doi: 10.1007/s10571-020-00997-x. PubMed PMID: 33231827.

179. Morad Y, Lemberg H, Yofe N, Dagan Y. Pupillography as an objective indicator of fatigue. Curr Eye Res. 2000;21(1):535-42. Epub 2000/10/18. PubMed PMID: 11035533.

180. McHill AW, Sano A, Hilditch CJ, Barger LK, Czeisler CA, Picard R, et al. Robust stability of melatonin circadian phase, sleep metrics, and chronotype across months in young adults living in real-world settings. J Pineal Res. 2021:e12720. Epub 2021/02/02. doi: 10.1111/jpi.12720. PubMed PMID: 33523499.

181. Okimura K, Nakane Y, Nishiwaki-Ohkawa T, Yoshimura T. Photoperiodic regulation of dopamine signaling regulates seasonal changes in retinal photosensitivity in mice. Sci Rep. 2021;11(1):1843. Epub 2021/01/21. doi: 10.1038/s41598-021-81540-w. PubMed PMID: 33469071; PubMed Central PMCID: PMCPMC7815869.

182. Dijk D-J, Duffy JF, Czeisler CA. Circadian and sleep/wake dependent aspects of subjective alertness and cognitive performance. Journal of Sleep Research. 1992;1(2):112-7. doi: 10.1111/j.1365-2869.1992.tb00021.x.

183. Webler FS, Spitschan M, Foster RG, Andersen M, Peirson SN. What is the 'spectral diet' of humans? Curr Opin Behav Sci. 2019;30:80-6. Epub 2019/08/23. doi: 10.1016/j.cobeha.2019.06.006. PubMed PMID: 31431907; PubMed Central PMCID: PMCPMC6701986.

184. Rufiange M, Beaulieu C, Lachapelle P, Dumont M. Circadian light sensitivity and rate of retinal dark adaptation in indoor and outdoor workers. J Biol Rhythms. 2007;22(5):454-7. Epub 2007/09/19. doi: 10.1177/0748730407305375. PubMed PMID: 17876066.

185. Roenneberg T. Having Trouble Typing? What on Earth Is Chronotype? J Biol Rhythms. 2015;30(6):487-91. Epub 2015/10/09. doi: 10.1177/0748730415603835. PubMed PMID: 26446872.

186. Roenneberg T. What is chronotype? Sleep Biol Rhythms. 2012;10(2):75-6. doi: 10.1111/j.1479-8425.2012.00541.x.

187. Martinez-Lozano N, Barraco GM, Rios R, Ruiz MJ, Tvarijonaviciute A, Fardy P, et al. Evening types have social jet lag and metabolic alterations in school-age children. Sci Rep. 2020;10(1):16747. Epub 2020/10/09. doi: 10.1038/s41598-020-73297-5. PubMed PMID: 33028896; PubMed Central PMCID: PMCPMC7541646.

188. Facer-Childs E, Brandstaetter R. The impact of circadian phenotype and time since awakening on diurnal performance in athletes. Curr Biol. 2015;25(4):518-22. Epub 2015/02/03. doi: 10.1016/j.cub.2014.12.036. PubMed PMID: 25639241.

189. Prayag AS, Munch M, Aeschbach D, Chellappa SL, Gronfier C. Light modulation of human clocks, wake, and sleep. Clocks Sleep. 2019;1(1):193-208. Epub

2020/04/29. doi: 10.3390/clockssleep1010017. PubMed PMID: 32342043; PubMed Central PMCID: PMCPMC7185269.

190. Danilenko KV, Plisov IL, Cooper HM, Wirz-Justice A, Hebert M. Human cone light sensitivity and melatonin rhythms following 24-hour continuous illumination. Chronobiol Int. 2011;28(5):407-14. Epub 2011/07/05. doi: 10.3109/07420528.2011.567425. PubMed PMID: 21721856.

191. Besharse J, Dunis D. Methoxyindoles and photoreceptor metabolism: activation of rod shedding. Sci. 1983;219(4590):1341-3. doi: 10.1126/science.6828862.

192. Stone RA, Pardue MT, Iuvone PM, Khurana TS. Pharmacology of myopia and potential role for intrinsic retinal circadian rhythms. Exp Eye Res. 2013;114:35-47. Epub 2013/01/15. doi: 10.1016/j.exer.2013.01.001. PubMed PMID: 23313151; PubMed Central PMCID: PMCPMC3636148.

193. Prigge CL, Yeh PT, Liou NF, Lee CC, You SF, Liu LL, et al. M1 ipRGCs influence visual function through retrograde signaling in the retina. J Neurosci. 2016;36(27):7184-97. Epub 2016/07/08. doi: 10.1523/JNEUROSCI.3500-15.2016. PubMed PMID: 27383593; PubMed Central PMCID: PMCPMC4938862.

194. Welbourne LE, Morland AB, Wade AR. Human colour perception changes between seasons. Curr Biol. 2015;25(15):R646-7. Epub 2015/08/05. doi: 10.1016/j.cub.2015.06.030. PubMed PMID: 26241135.

195. Fischer D, Lombardi DA, Marucci-Wellman H, Roenneberg T. Chronotypes in the US - Influence of age and sex. PLoS One. 2017;12(6):e0178782. Epub 2017/06/22. doi: 10.1371/journal.pone.0178782. PubMed PMID: 28636610; PubMed Central PMCID: PMCPMC5479630.

196. Rukmini AV, Milea D, Aung T, Gooley JJ. Pupillary responses to short-wavelength light are preserved in aging. Sci Rep. 2017;7:43832. Epub 2017/03/08. doi: 10.1038/srep43832. PubMed PMID: 28266650; PubMed Central PMCID: PMCPMC5339857.

197. Winn B, Whitaker D, Elliott DB, Phillips NJ. Factors affecting light-adapted pupil size in normal human subjects. Investigative Ophthalmology & Visual Science. 1994;35(3):1132-7.

198. Adhikari P, Pearson CA, Anderson AM, Zele AJ, Feigl B. Effect of age and refractive error on the melanopsin mediated post-illumination pupil response (PIPR). Sci Rep. 2015;5:17610. Epub 2015/12/02. doi: 10.1038/srep17610. PubMed PMID: 26620343; PubMed Central PMCID: PMCPMC4664956.

Danksagung

Ich danke in chronologischer Reihenfolge:

Mathias Wambsganß, der mich buchstäblich „ins Licht“ geführt hat. Seine Begeisterung für das Thema in allen seinen Facetten ist ansteckend und wird vermutlich nur durch seine beispiellose Integrität und dem Drang übertroffen, den Grund aller Dinge aufzuspüren. Mit diesen Eigenschaften motivierte und unterstützte er einige meiner wichtigsten Lebensentscheidungen und ich bin dankbar, einen solchen Freund, Arbeitskollegen, und Lehrer zu haben. Durch und mit ihm kam es auch zum ersten Planungsprojekt für Licht und Gesundheit, bei dem ich das Feuer fing, einen Schritt tiefer zu gehen.

Herbert Plischke, der sich meinem früheren *Ich* als Planungsingenieur angenommen und die Faszination für die menschliche Biologie geschürt hat. Ich danke ihm nicht nur für seine Anleitung in den letzten sechs Jahren, sondern auch für seine Ruhe in schwierigen Situationen, seine Begeisterung für das Thema (ich sehe ein Muster), und für seine inspirierende Leichtigkeit mit dem aus einem schier endlosen See des Wissens und der Erfahrung schöpft. Er hat mir ermöglicht diese Dissertation zu schreiben und war mir zu allen Zeiten ein wertvoller Gesprächspartner. Es bereitet mir immer Freude mit ihm zusammen zu arbeiten.

Hans Strasburger, der mir nicht nur Doktorvater war, sondern neue Welten erschlossen hat. Durch ihn habe ich eine Faszination und Freude an der Statistik entwickelt, die ich vorher nicht für möglich gehalten hätte. Sein tiefer Wissensschatz verbunden mit anekdotischer Leichtigkeit (ich empfehle jedem die Bücher „Der Hund der Eier legt“ und „The Lady Tasting Tea“) waren mir eine große Hilfe bei der Erschließung dieses Themas und auch für alle Unterstützung in den Themen der Psychologie und Wahrnehmung bin ich sehr dankbar. Hans hinterfragte in unseren Gesprächen treffsicher alle „weichen“ Stellen und ließ keine meiner unspezifischen Aussagen zu, bis er zum Kern vorgedrungen war. Für diese Präzision im Denken und im Schreiben bin ich ihm sehr dankbar, denn sie hat sicherlich diese Arbeit und - so hoffe ich - auch mich für das Wesentliche geschärft und belastbarer gemacht.

Nicht in chronologischer Reihenfolge, sondern außer Konkurrenz, danke ich meiner Frau, Eva Zauner. Sie hat mir nicht nur den Rücken in schwierigen Momenten freigehalten, sondern ist mir auch ein wertvoller Sparringspartner in allen Dingen. Ohne sie wäre diese Arbeit nicht die Gleiche und meine Zeit beim Erstellen bei weitem trauriger verlaufen. Ihre gelegentlich subtilen, gelegentlich unmissverständlichen Hinweise, nicht nur über die Bedeutung von Tageslicht zu schreiben, sondern gefälligst auch selbst nach Stunden am PC das Tageslicht zu erleben, haben sicherlich zu meinem robusten circadianen Rhythmus beigetragen.

Abschließend danke ich meinen Eltern Franziska und Michael. Was mir diese beiden Lehrer in all ihrer Gegensätzlichkeit mitgegeben haben, ist mir ein fester Halt in allen Dingen.